https://doi.org/10.15388/vu.thesis.911
https://orcid.org/0009-0000-5054-5445

VILNIUS UNIVERSITY
CENTER FOR PHYSICAL SCIENCES AND TECHNOLOGY

Ashutosh Sharma

Spectroscopic Study of the Planet-Host Stars

DOCTORAL DISSERTATION

Natural Sciences,
Physics (N 002)

VILNIUS 2026

This dissertation was prepared between 2020 and 2025 at Vilnius University, Faculty of Physics, Institute of Theoretical Physics and Astronomy.

Academic Supervisor:

Dr. Edita Stonkutė (Vilnius University, Natural Sciences, Physics, N 002)

Defence Council:

Chairman – Prof. Habil. Dr. Gediminas Gaigalas (Vilnius University, Natural Sciences, Physics, N 002)

Members –

Dr. Vidas Dobrovolskas (Vilnius University, Natural Sciences, Physics, N 002)

Dr. Marius Maskoliūnas (Vilnius University, Natural Sciences, Physics, N 002)

Habil. Dr. Tamara Mishenina (Odesa National University, Natural Sciences, Physics, N 002)

Prof. Dr. Leonid Piliugin (Vilnius University, Natural Sciences, Physics, N 002)

The dissertation shall be defended at a public meeting of the Dissertation Defence Panel at 11:00 on May 4, 2026 in the National Center for Physical Sciences and Technology, Room A101. Address: Saulėtekio al. 3, LT–10257, Vilnius, Lithuania Tel. +370 5 2234637; email tfai@tfai.vu.lt

https://doi.org/10.15388/vu.thesis.911
https://orcid.org/0009-0000-5054-5445

VILNIAUS UNIVERSITETAS
FIZINIŲ IR TECHNOLOGIJOS MOKSLŲ CENTRAS

Ashutosh Sharma

Spektroskopinis žvaigždžių su planetomis tyrimas

DAKTARO DISERTACIJA

Gamtos mokslai,
Fizika (N 002)

VILNIUS 2026

Disertacija rengta 2020 – 2025 metais Vilniaus universiteto Fizikos fakulteto Teorinės fizikos ir astronomijos institute.

Mokslinis vadovas:

Dr. Edita Stonkutė (Vilniaus universitetas, gamtos mokslai, fizika, N 002)

Gynimo taryba:

Pirmininkas – prof. habil. dr. Gediminas Gaigalas (Vilniaus universitetas, gamtos mokslai, fizika, N 002)

Nariai –

Dr. Vidas Dobrovolskas (Vilniaus universitetas, gamtos mokslai, fizika, N 002)

Dr. Marius Maskoliūnas (Vilniaus universitetas, gamtos mokslai, fizika, N 002)

Habil. dr. Tamara Mishenina (Odesos nacionalinis universitetas, gamtos mokslai, fizika, N 002)

Prof. dr. Leonid Piliugin (Vilniaus universitetas, gamtos mokslai, fizika, N 002)

Disertacija ginama viešame Gynimo tarybos posėdyje 2026 m. gegužės mėn. 04 d. 11 val. Nacionalinio fizinių ir technologijos mokslų centro posėdžių salėje A101. Adresas: Saulėtekio al. 3, LT–10257, Vilnius, Lietuva Tel. +370 5 2234637; el. paštas tfai@tfai.vu.lt

Contents

Acronyms and abbreviations **8**

Problem statement and relevance of the research topic **9**

Main aims and tasks **12**

Scientific novelty and statements for defence **14**

Publications related to this thesis **16**

Contributions by the author **18**

1 Introduction **19**
1.1 Importance of studying planet-host stars 19
1.1.1 Stellar abundances as tracers of planet formation . . . 21
1.1.2 Volatile and α-elements in shaping planetary systems . 24
1.1.3 Neutron-capture element abundances 26
1.1.4 Element condensation temperature 27
1.2 From formation to discovery: understanding exoplanets 28

2 Data and methodology **30**
2.1 Sample selection, observations and data reduction 30
2.2 Comparison sample 31
2.3 Stellar atmospheric parameters 32
2.4 Elemental abundance analysis 35
2.4.1 CNO and Mg, Si abundances 36
2.4.2 Abundances of neutron-capture elements 38
2.4.3 (Non)-local thermodynamic equilibrium effects 40
2.4.4 Uncertainty analysis 44
2.5 Stellar kinematics and ages 50
2.6 Planets in our sample 56

3 Implications of light elements in planet-host stars **60**
3.1 [(C; N; O)/Fe] abundance trends with [Fe/H] 60
3.2 [(Mg; Si)/Fe] abundance trends with [Fe/H] 65
3.3 C/O, N/O, and Mg/Si ratios in planet-host stars 66
3.3.1 Metallicity trends and comparison to non-hosts 67
3.3.2 Low mass vs high mass planet hosts: Statistical tests . 68

3.4 Evolutionary effects in giants: Combined C+N+O abundances 71

4 Heavy elements in planet-host stars: *n*-capture species 74
4.1 The first *s*-process peak. The light *s*-process elements Sr, Y, Zr 74
4.2 The second *s*-process peak 76
4.2.1 The heavy *s*-process elements Ba, La, Ce 77
4.2.2 The mixed-process elements Pr and Nd 78
4.3 The *r*-process dominated element Eu 79
4.4 Statistical tests 79

5 [Y/Mg] as age indicator 84

6 Δ[El/H]-$T_{\rm cond}$ trends 86

7 Chemical signatures and planet properties 93
7.1 Stellar chemistry versus planet mass relation 93
7.1.1 CNO and α-elements 94
7.1.2 *n*-capture elements 98
7.2 Stellar age as a function of planet mass 103

8 Summary, conclusions and future outlook 105

9 Acknowledgements 113

Santrauka (Summary in Lithuanian) 114

References 145

A Appendix 164

Curriculum Vitae 167

Acronyms and Abbreviations

Term	Abbreviation
Atmospheric Remote-sensing Infrared Exoplanet Large-survey	ARIEL
Asymptotic giant branch	AGB
Condensation Temperature	$T_{\rm cond}$
Continuous viewing zone	CVZ
Gaia Data release 3	EDR3
European Southern Observatory	ESO
European Extremely Large Telescope	E-ELT
Gaia-ESO survey	GES
Hyperfine structure	HFS
Interstellar medium	ISM
Isotopic splitting	IS
Model Atmospheres with Radiative and Convective Scheme	MARCS
Molėtai Astronomical Observatory	MAO
Local thermodynamic equilibrium	LTE
Local standard of rest	LSR
(Non)-local thermodynamic equilibrium	NLTE
Planet-hosting stars	PHS
Planetary Transits and Oscillations of stars	PLATO
Radial velocity	RV
Signal-to-noise ratio	S/N
Thick-to-thin disc probability ratio	TD/D
Transiting Exoplanet Survey Satellite	TESS
Very Large Telescope	VLT
Vilnius University Echelle Spectrograph	VUES

Problem statement and relevance of the research topic

The discovery of thousands of exoplanets in the last few decades has revolutionised our understanding of planetary systems and challenged traditional models of planet formation and evolution. There is growing evidence that the composition of host stars plays a fundamental role in shaping the characteristics of their planets. Since planets form from protoplanetary disks surrounding young stars, the chemical composition of these stars is intrinsically linked to the composition and internal structure of their planetary companions. Consequently, the precise and homogeneous determination of stellar atmospheric parameters and chemical abundances plays a crucial role in the study of planetary systems.

Despite the importance of stellar composition in shaping planetary architectures, several key questions remain unanswered. How do specific elemental abundances correlate with the occurrence and properties of exoplanets? Do stars with different planetary masses exhibit systematic differences in their chemical profiles? What are the roles of volatile and refractory elements in the planet formation process? How do stellar and planetary characteristics such as age, mass, and Galactic kinematics influence these chemical signatures?

Several studies have successfully linked stellar chemistry and the occurrence of planets. It is well established that stars with giant planets tend to be more metal-rich than stars without planets (Gonzalez 1997; Santos et al. 2001; Fischer & Valenti 2005). However, for stars hosting smaller planets (e.g., super-earths and neptunes), the dependence on metallicity appears weaker or absent (Ghezzi et al. 2010; Sousa et al. 2011; Buchhave et al. 2012). More recent works have extended these studies to other elements beyond Fe, including volatile and refractory elements, which are key to planetary structure and composition (Delgado Mena et al. 2010; Mishenina et al. 2016; Suárez-Andrés et al. 2016, 2017, and more).

Of particular interest are the elemental ratios such as C/O and Mg/Si. Theoretical studies suggest that these ratios influence the condensation chemistry in protoplanetary disks, affecting the mineralogy of terrestrial planets and the volatile content of gas giants (Madhusudhan et al. 2012; Thiabaud et al. 2015). It has been observed that C/O < 0.8 favors silicate-dominated rocky planets (Brewer & Fischer 2016), while Mg/Si determines the proportion of pyroxene to olivine that dominates a planet's mantle (Santos et al. 2015). However, the statistical significance and reproducibility of such findings remain under discussion, as large homogeneous datasets are still limited.

At the same time, signatures of planet formation may also manifest as differences in the elemental abundance patterns between planet-hosting stars and their comparison counterparts. Studies have reported trends between elemental abundances and condensation temperatures, suggesting that some of the heavier, refractory elements were locked away in planetesimals during the early stages of planet formation (Meléndez et al. 2009; Ramírez et al. 2010). In Sun-like stars, a depletion of refractory elements has been interpreted as a possible chemical fingerprint of rocky planet formation (González Hernández et al. 2013; Liu et al. 2020), although other works suggest that such abundance patterns could be due to Galactic chemical evolution or dust-gas segregation in the star-forming environment (Adibekyan et al. 2014; Nissen 2015).

The situation becomes even more complex when considering *n*-capture elements produced through slow and rapid neutron-capture processes. These elements have diverse nucleosynthetic origins and timescales, including contributions from low- and intermediate-mass AGB stars (*s*-process; (Busso et al. 2001), massive stars and core-collapse supernovae (*r*-process), and neutron-star mergers (e.g., Pian et al. 2017; Côté et al. 2018). Some studies have explored the abundances of Ba, La, and Eu in planet-hosting stars (e.g., Delgado Mena et al. 2018; Mishenina et al. 2016; Swastik et al. 2022). The trends observed often vary with stellar mass, age, and Galactic location, indicating that multiple processes influence these abundances. The so-called "Barium puzzle" (Reddy & Lambert 2017), the observation of unusually high [Ba/Fe] in young clusters without corresponding enhancements in other *s*-process elements, suggests that our understanding of neutron-capture processes and their timescales is still incomplete. Such and other unexplained abundance patterns in planet-hosting stars highlight the need for more detailed studies of the full range of heavy elements.

Another major challenge is the limitations of existing datasets. Many earlier studies of planet hosts suffer from small sample sizes, inconsistent methods, or limited spectral resolution. These limitations make it difficult to separate intrinsic chemical patterns related to planet formation from broader Galactic trends. In this context, high-resolution and homogeneous analyses of well-characterized samples are essential for minimising systematic uncertainties and enabling meaningful comparisons. Furthermore, combining chemical abundances with stellar ages, Galactic kinematics, and orbital properties provides a richer, more complete picture of how planets form and evolve around different stars in the Galaxy.

This thesis addresses several of these challenges by investigating the detailed chemical composition of a large and homogeneous sample of F-, G-, and K-type stars with confirmed planets in the northern hemisphere. A primary motivation of this work is to investigate whether the abundances of planet-host stars carry intrinsic signatures of planet formation or primarily reflect broader Galactic chemical evolution. The thesis is based on a compilation of three peer-reviewed papers published during the course of my PhD (listed in section: Publications related to this thesis), each focusing on several elemental groups and their connection to planetary systems.

Paper I (Tautvaišienė et al. 2022) analysed the abundances of C, N, O, Mg, and Si, as well as the C/O and Mg/Si abundance ratios in a sample of 25 bright planet-hosting stars located in the northern TESS continuous viewing zone. This study established a homogeneous reference framework for investigating key elements relevant to both stellar chemistry and planetary composition.

Paper II (Sharma et al. 2024) expanded this analysis to a larger sample of 149 stars with confirmed planetary systems, retaining the same elemental set (C, N, O, Mg, and Si) in order to examine abundance trends across a broader stellar population and to evaluate their potential implications for planet formation and mineralogy.

Finally, Paper III (Sharma et al. 2025) extended the sample to 160 stars by including 11 additional stars, and incorporated a detailed investigation of nine neutron-capture elements (Sr, Y, Zr, Ba, La, Ce, Nd, Pr, and Eu). This allowed the thesis to explore whether neutron-capture element abundances exhibit systematic trends in planet-hosting stars and to place these patterns in the broader context of Galactic chemical evolution.

Main aims and tasks

The main aim of this thesis is to study the star-planet connection by investigating the chemistry of stellar atmospheres of planet-hosting stars and to understand if and how stellar abundances influence the formation and evolution of planetary systems. By conducting a homogeneous and high-resolution spectroscopic analysis of a carefully selected sample of F-, G-, and K-type stars with confirmed exoplanets, this work aims to identify possible correlations between stellar elemental abundances and key planetary parameters such as mass, and orbital characteristics.

To achieve this aim, several major tasks were carried out during the course of this work. A representative sample of bright stars hosting planets was compiled from the NASA Exoplanet Archive and TESS catalogue. The stars were observed using the high-resolution Vilnius University Echelle Spectrograph mounted on the 1.65 m Ritchey-Chrétien telescope located at the Molėtai Astronomical Observatory in Lithuania. A carefully matched control sample of stars without detected planets, observed and analysed using the same instrument and methodology in previous studies, was used to enable robust statistical comparisons.

Following observations and spectral processing, the main atmospheric parameters (effective temperature, $T_{\rm eff}$; surface gravity, $\log g$; microturbulence velocity, $v_{\rm t}$; and metallicity $[{\rm Fe/H}]$) were determined using the classical equivalent width method, supported by the DAOSPEC and MOOG codes. These parameters serve as the foundation for a detailed abundance analysis. Precise chemical abundances of C, N, O, Mg, and Si were determined using synthetic spectrum fitting and carefully selected atomic and molecular lines. The analysis was later extended to include a set of 9 neutron-capture elements (Sr, Y, Zr, Ba, La, Ce, Nd, Pr, and Eu).

The abundance ratios C/O, N/O, and Mg/Si were computed for all stars and analysed in relation to their metallicity, and evolutionary state. These ratios are important in studying the star-planet connection as they provide insights into the formation of planets and can help us to determine the likely structure and composition of exoplanets. The study also examined how the abundance differences between our stars with planets and their comparison counterparts (Δ[El/H]) vary as a function of elemental condensation temperature, providing insights into possible chemical signatures of planet formation, such as the sequestration of refractory elements into rocky bodies.

A key objective was to statistically investigate potential links between stellar chemistry and planetary properties by analysing correlations between elemental abundances and planetary mass across both dwarf and giant hosts. This includes applying rigorous statistical tests, such as the Kolmogorov-Smirnov and Anderson-Darling analyses, to determine whether specific elements or abundance ratios exhibit distinct behaviours in stars hosting high-mass versus low-mass planets. Through this approach, the study aimed to identify chemical patterns that may serve as prerequisites for the formation of different classes of exoplanets.

This dissertation is structured into eight chapters. Chapter 1 provides the scientific background and motivation for this work, introducing the fundamentals of high-resolution stellar spectroscopy and discussing the importance of studying planet-host stars through their detailed chemical abundances. Chapter 2 describes the observational material and methodology, including sample selection, spectroscopic observations, determination of stellar atmospheric parameters, and the procedures adopted for deriving elemental abundances, stellar ages, and kinematics. Chapter 3 focuses on the behaviour of light elements (C, N, O, Mg, Si) in planet-host stars, analysing their trends with metallicity and comparing them with stars without detected planets. Chapter 4 extends the analysis to heavy, *n*-capture elements, discussing their production channels, observed abundance-metallicity patterns, comparisons to non-hosts, and statistical analysis of such comparisons. Chapter 5 investigates the age-chemistry relations, particularly the [Y/Mg] ratio as a stellar clock, while Chapter 6 examines condensation temperature trends and their possible connection to planet formation processes. Chapter 7 links stellar chemical signatures to planetary properties, focusing on relations between stellar abundances and planetary masses. Finally, Chapter 8 summarises the main conclusions and outlines prospects for future studies, highlighting how detailed spectroscopic analyses of planet-host stars can advance our understanding of exoplanetary systems in the era of ongoing and upcoming large surveys.

Scientific novelty and statements for defence

The scientific novelty of this research lies in the homogeneous and precise abundance analysis of both light elements (C, N, O, Mg, and Si) and neutron-capture elements (Sr, Y, Zr, Ba, La, Ce, Pr, Nd, and Eu) in 160 bright planet-hosting stars located in the Northern Hemisphere. These stars, many of which are potential targets for missions like ARIEL and PLATO, among others, offer long-term scientific value for studies of stellar evolution and planetary system formation. The work employs synthetic spectrum fitting techniques and consistent model atmospheres across all stars, ensuring high accuracy and comparability. One of the main scientific advancements of this work is the first-time homogeneous determination of neutron-capture element abundances for the majority of these stars. Additionally, the work applies non-LTE corrections for Mg, Sr, Y, Ba, and Eu, thereby significantly improving the reliability of derived abundances.

The thesis uniquely combines stellar chemical data with planetary properties, Galactic kinematics, and stellar ages, providing new observational constraints on the star-planet connection. In addition, by analysing abundance differences relative to condensation temperatures, the study explores potential chemical signatures linked to rocky planet formation processes. These results are systematically compared with a well-matched control sample of stars without detected planets, enabling statistically robust conclusions about planet-related chemical anomalies.

Statements for Defence

The following statements summarises the original scientific contributions and key findings of this doctoral dissertation, which are hereby presented for defense:

1. Dwarf planet hosts show lower [C/Fe] and [O/Fe] at super-solar metallicities, but no differences at sub-solar [Fe/H]. Giant hosts display broadly similar CNO trends with comparison stars, though planet hosts have slightly lower carbon abundance at given [Fe/H]. C/O and N/O ratios increase with [Fe/H] and without significant host-non-host differences in dwarfs, while giants we see the reduced mean C/O ratios in host stars compared to the comparison sample. [Mg/Fe] and [Si/Fe] are enhanced in planet-hosting stars, especially at low metallicity, while Mg/Si ratios are lower and statistically distinct in high-mass planet systems.

2. [C/Fe], [N/Fe], and [O/Fe] ratios in dwarfs show weak negative correla-

tions, while in giants, [C/Fe], [N/Fe], and [O/Fe] exhibit positive correlations toward higher planet masses. C/O and N/O ratios increase weakly with planet mass in dwarfs, whereas in giants, they exhibit stronger trends, with C/O decreasing and N/O increasing toward higher planetary masses. Mg and Si increase with planet mass; Mg/Si shows an overall negative trend.

3. A(C+N+O) in giant stars increases with [Fe/H], consistent with Galactic chemical evolution, and shows no significant correlation with planet mass. No significant host-non-host difference is detected overall, though within the thin disc subsample, statistical tests and bootstrap resampling suggest a possible distinction between the two populations.

4. Neutron-capture element abundances in planet-hosting stars largely follow Galactic chemical evolution trends, with light s-process elements (Sr, Y, Zr) generally increasing toward lower metallicities, most strongly for Zr. For second-peak elements, flat [Ba/Fe] or rising [La/Fe], [Ce/Fe] trends are observed at low [Fe/H], with planet hosts overabundant in La and Ce. Heavier elements (Pr, Nd) and the r-process element Eu increase toward lower metallicities.

5. Sr, Y, and Ba display no clear trends with planet mass, while Zr shows a weak positive correlation, especially in dwarfs. In giants, La, Ce, Pr, and Nd exhibit moderate positive correlations with planet mass, and Eu shows a weaker, similar trend, though these patterns may be partly influenced by Galactic chemical evolution effects.

6. A differential analysis of Δ[El/H]-$T_{\rm cond}$ slopes shows that planet-hosting stars are systematically enriched in refractory elements relative to carefully matched control sample, producing positively skewed slope distributions. This signature weakens in dwarfs. When compared to stellar or planetary properties, metal-rich and multiplanet systems suggests subtle planet-formation imprints on stellar abundances.

Publications related to this thesis

- **Chemical Composition of Bright Stars in the Northern Hemisphere: Star-Planet Connection**
  Tautvaišienė, G.; Mikolaitis, Š.; Drazdauskas, A.; Stonkutė, E.; Minkevičiūtė, R.; Pakštienė, E.; Kjeldsen, H.; Brogaard, K.; Chorniy, Y.; von Essen, C.; Grundahl, F.; Ambrosch, M.; Bagdonas, V.; **Sharma, A.**; Viscasillas Vázquez, C. (2022)
  The Astrophysical Journal Supplement Series, Volume 259, Number 2
  https://doi.org/10.3847/1538-4365/ac50b5

- **Chemical composition of planetary hosts: C, N, and α-element abundances**
  Sharma, A.; Stonkutė, E.; Drazdauskas, A.; Minkevičiūtė, R.; Mikolaitis, Š.; Tautvaišienė, G.; Narbuntas, T. (2024)
  Astronomy & Astrophysics, Volume 691, A160
  https://doi.org/10.1051/0004-6361/202451889

- **Chemical composition of planetary hosts: II. Abundances of neutron-capture elements**
  Sharma, A.; Stonkutė, E.; Drazdauskas, A.; Minkevičiūtė, R.; Mikolaitis, Š. ; Tautvaišienė, G.; Jonauskaitė, U. (2025)
  Astronomy & Astrophysics, Volume 701, A153
  https://doi.org/10.1051/0004-6361/202555466

Scientific talks delivered by the author

- **Probing the C, N, O, and α-element abundances in planet-harbouring stars through high-resolution spectroscopy**
  Conference: "When stars meet planets: exploiting high-resolution observations. A conference in honour of Raffaele Gratton". July 22-26, 2024. Sexten, Italy

- **Probing the light element ratios in planet-host stars**
  Conference: "45th Lithuanian National Physics Conference". October 25-27, 2023. Vilnius, Lithuania

- **Spectroscopic study of the planet-host stars.**
  Europlanet Summer School 2023 "Space missions: ground-based observations and science communication". August 8-18, 2023. Molėtai, Lithuania

- **Probing the C/O and Mg/Si elemental ratios in planet-harbouring stars**
  Conference: "Europlanet Telescope Network: Exoplanets". June 19-23, 2023. Bratislava, Slovakia

Contributions by the author

The research presented in this thesis was carried out by the author during the course of his PhD studies and is based on three peer-reviewed scientific publications. The author served as the lead and corresponding author of two of these publications (Paper II and Paper III) and as a contributing co-author of Paper I. In Paper I, the author contributed to the section investigating the star-planet connection. In particular, the author was responsible for compiling the corresponding planetary parameters from the NASA Exoplanet Archive and analysing the correlations for the subsample of planet-host stars. For Papers II and III, the author led all major stages of the research. These included conducting the stellar observations, analysing Galactic kinematics and stellar ages, performing complete spectroscopic analysis, and compiling planetary parameters from the NASA Exoplanet Archive. The author independently derived elemental abundances for all investigated elements, calculated elemental abundance ratios (e.g. C/O, N/O, and Mg/Si), and carried out statistical analyses, including Kolmogorov-Smirnov and Anderson-Darling tests. The author further interpret abundance trends as functions of metallicity, planet mass and element condensation temperature. In addition, the author performed a homogeneous comparison between planet-hosting stars and a control sample of stars without detected planets, thereby placing the chemical abundance results within a broader evolutionary context. All figures and tables presented in Papers II and III were prepared by the author. The author also drafted the manuscripts, and managed all correspondence and revisions throughout the peer-review process.

1 Introduction

The study of planets outside the Solar System has undergone a dramatic transformation since the first confirmed detections around a pulsar (Wolszczan & Frail 1992) and a solar-type star (Mayor & Queloz 1995). From a few pioneering discoveries, the field has rapidly evolved into one of the most dynamic branches of astrophysics. Thanks to ground-based radial velocity programs and space missions such as Kepler (Borucki et al. 2010) and the Transiting Exoplanet Survey Satellite (TESS) (Rinehart et al. 2015), over 6 000 exoplanets have been confirmed so far[1], with discoveries accelerating as next-generation facilities come online (e.g. Planetary Transits and Oscillations of stars, PLATO: Rauer et al. 2024; Atmospheric Remote-sensing Infrared Exoplanet Large-survey, ARIEL: Tinetti et al. 2022; ground-based European Extremely Large Telescope, E-ELT; de Zeeuw et al. 2014). These planets orbit a wide variety of stars distributed across diverse Galactic environments. The expanding exoplanet catalogue has not only confirmed the presence of planetary systems but has also unveiled their remarkable diversity in terms of mass, orbital architecture, and chemical composition. As the number of known exoplanets continues to increase, the research focus has progressively shifted from detection to the statistical characterisation of planetary populations, investigating the diversity of their properties and searching for the underlying mechanisms of planet formation and evolution (see e.g. Udry & Santos (2007); Winn & Fabrycky (2015)).

1.1 Importance of studying planet-host stars

The formation of planets is fundamentally shaped by the physical and chemical properties of the protoplanetary disk from which they emerge. Since such disks are direct by-products of star formation, the initial conditions of a planetary system are intrinsically linked to the chemical composition of its host star. Consequently, stellar abundance studies provide a powerful window into the environments where planets form. Theoretical studies have shown that connecting exoplanet properties with the chemistry of their host stars is key to explaining the formation and

[1] https://exoplanetarchive.ipac.caltech.edu/

evolution of planetary systems (see e.g., Madhusudhan et al. 2012; Unterborn & Panero 2019; Dorn et al. 2019; Bitsch & Battistini 2020; Mah & Bitsch 2023). This forms the central hypothesis behind the 'star-planet chemical connection', which proposes that planet-host stars not only govern their systems through gravitational and radiative influence but also retain, in their photospheres, the chemical signatures of the natal environments of their planets. As such, stellar parameters represent essential constraints for planet formation models and provide a foundation for understanding the diversity of planetary system architectures across the Galaxy.

Our motivation in this study is to investigate whether the presence and nature of planets are reflected in subtle chemical signatures imprinted in the atmospheres of their host stars. To this end, we have initiated a high-resolution spectroscopic survey targeting a homogeneous and well-characterised sample of bright ($V \leq 8.5$ mag) F-, G-, and K-type stars with confirmed planetary companions. For this stellar sample, we have precisely determined main atmospheric parameters and conducted a uniform abundance analysis of both light and heavy elements. Our goal is to investigate potential correlations between elemental abundance patterns and planetary properties, such as planet type and mass. In particular, we aim to determine whether stars with planets differ chemically from their non-host counterparts, beyond the well-established trend of higher overall metallicity in planet-hosting stars (hereafter referred to as PHS). This research goes beyond just studying stars as it bridges the study of stellar nucleosynthesis, planetary formation theories, and Galactic evolution. Moreover, it supports the goals of upcoming space missions that aim to study exoplanet atmospheres and interiors by providing a stellar context for interpreting planetary compositions. In short, the better we understand stars, the better we understand the planets that form around them and possibly, the conditions that could make those planets habitable. The motivation for this thesis is therefore rooted in a fundamental question in modern astrophysics: What can the stars tell us about the origins and characteristics of their planets?

1.1.1 Stellar abundances as tracers of planet formation

One of the earliest and most firmly established results in exoplanet research is the correlation between stellar metallicity and the likelihood of hosting giant planets. Since the pioneering works by Gonzalez (1997), Santos et al. (2001), and Fischer & Valenti (2005), numerous surveys have confirmed that metal-rich stars are more likely to harbour giant planets. This "planet-metallicity correlation" is naturally explained within the core-accretion model of planet formation, in which higher metallicities promote the rapid formation of planetesimals, accelerating the growth of planetary cores to the critical mass required for the subsequent accretion of gas envelopes. However, this correlation does not extend uniformly to all types of planets. Studies have shown that low-mass planets (super-Earths and Neptunes) are observed across a much broader range of stellar metallicities, including sub-solar values. Statistical analyses reveal that their occurrence rate depends more weakly, if at all, on metallicity, indicating that smaller planets can form efficiently even in relatively metal-poor environments (e.g. Ghezzi et al. 2010; Sousa et al. 2011; Buchhave et al. 2012). This dichotomy between giant and low-mass planets highlights the sensitivity of formation pathways to the initial solid budget in discs.

The search for deeper chemical fingerprints in stars has expanded beyond bulk metallicity to focus on individual elemental abundances and abundance ratios. Recent advancements in high-resolution spectroscopy, combined with the homogeneous analysis of large stellar samples, have significantly improved our ability to measure these abundances with precision and consistency. Instruments like the Vilnius University Echelle Spectrograph (Jurgenson et al. 2016) have facilitated detailed and uniform spectroscopic studies of PHS. Within this framework, many chemical elements have been studied, from light elements such as carbon, nitrogen, oxygen, magnesium and silicon to heavy elements such as strontium, yttrium, and barium. These elements not only serve as tracers of Galactic chemical evolution but also directly influence protoplanetary disk chemistry and the interior composition of the forming planets.

Stellar spectroscopy is a fundamental tool in modern astrophysics, allowing astronomers to probe the physical and chemical properties of stars by analysing the light they emit. Absorption lines form when atoms

or ions in the stellar photosphere absorb photons and transition from lower to higher energy levels. Each chemical element and its ionisation states, is characterised by a unique set of allowed electronic transitions, giving rise to a distinctive pattern of spectral lines. These patterns act as fingerprints, allowing us to identify the presence of different elements and ions in the stellar atmosphere. The strength and profile of each line depend on the number of atoms in the relevant state, the temperature and pressure of the gas, and the probability of the transition occurring, governed by the oscillator strength or $\log gf$ value (Gray 2005).

The formation of spectral lines is described by the radiative transfer equation, which governs the propagation of radiation through a medium that both absorbs and emits photons (Mihalas 1978). In its one-dimensional, plane-parallel form, the radiative transfer equation can be written as:

$$\frac{dI_\nu}{d\tau_\nu} = I_\nu - S_\nu \tag{1}$$

where I_ν is the specific intensity, τ_ν is the optical depth at frequency ν, and S_ν is the source function. In stellar atmosphere models assuming local thermodynamic equilibrium (LTE), the source function is given by the Planck function, $S_\nu = B_\nu(T)$, where T is the local temperature.

To interpret spectral lines quantitatively, the radiative transfer equation must be solved using a model atmosphere. In many cases, the assumption of LTE is made, meaning that the atomic level populations are set by the local temperature and follow the Boltzmann and Saha distributions. The Boltzmann distribution describes the relative populations of atomic energy levels,

$$\frac{n_i}{n_j} = \frac{g_i}{g_j} \exp\left(-\frac{[E_i - E_j]}{kT}\right), \tag{2}$$

where n_i/n_j are the number density of atoms in level i and j, g_i/g_j are the statistical weights, E_i/E_j are the excitation energies, k is the Boltzmann constant and T is the temperature. The ionisation balance between successive ionisation stages is governed by the Saha equation,

$$\frac{n_{j+1}}{n_j} = \frac{2}{n_e}\left(\frac{2\pi m_e kT}{h^2}\right)^{3/2} \frac{U_{j+1}(T)}{U_j(T)} \exp\left(-\frac{\chi_j}{kT}\right), \tag{3}$$

where n_j/n_{j+1} are the number densities of two successive ionisation stages, n_e is the electron density, χ_j is the ionisation potential, m_e is the electron mass, h is Planck's constant, and U_j/U_{j+1} are the corresponding partition functions.

While LTE provides a practical and widely used approximation, it may break down in low-density or radiation-dominated regions of stellar atmospheres, where radiative transitions dominate over collisions. In such cases, non-local thermodynamic equilibrium (NLTE) calculations are required to accurately model level populations and line strengths (Asplund 2005; Mashonkina et al. 2011; Lind & Amarsi 2024; Bergemann & Hoppe 2025).

Accurate modeling of line formation also depends heavily on high-quality atomic data, including wavelengths, excitation potentials, oscillator strengths, and damping constants. These values are typically sourced from databases such as VALD (Piskunov et al. 1995) and NIST (Kramida et al. 2023). Errors in these parameters can propagate into significant uncertainties in abundance determinations. For certain elements, especially those with complex electronic structures or odd atomic numbers, hyperfine splitting and isotopic shifts can alter line shapes and must be included in the synthesis (McWilliam 1998; Sneden et al. 2002).

The depth at which a spectral line forms within the stellar atmosphere varies with the strength, opacity, and excitation potential of the line. Generally, weak lines form deeper in the photosphere where the temperature is higher, while strong or saturated lines form higher up. This depth sensitivity allows us to probe different layers of a star's atmosphere and study vertical gradients in temperature, velocity fields, and chemical composition (Gray 2005). In evolved or active stars, this capability is particularly valuable for understanding convection, chromospheric activity, or mass loss processes. Together, these phenomena make spectral line formation a complex but powerful diagnostic of stellar atmospheres. When interpreted through accurate models, spectral lines allow for precise measurements of stellar parameters and chemical abundances. These measurements, in turn, support a wide range of research, from calibrating stellar evolution models to reconstructing Galactic chemical history and exploring the conditions under which planetary systems emerge.

1.1.2 Volatile and α-elements in shaping planetary systems

Beyond the widely discussed role of stellar metallicity, the abundances of individual volatile and α-elements provide crucial information about the physical and chemical processes that link stars and planets. Elements such as carbon, nitrogen, and oxygen are not only central to stellar and Galactic chemical evolution, but they also play an essential role in determining the formation pathways and compositions of planets (see e.g., Bitsch & Battistini 2020; Bitsch & Mah 2023). Their relative abundances and ratios determine the distribution of condensates in protoplanetary disks, shaping both the efficiency of volatile delivery and the chemistry of planetary atmospheres. Several studies have reported that the carbon-to-oxygen (C/O) and nitrogen-to-oxygen (N/O) ratios could affect whether planets form inside or outside major "snow lines" of various carbon, nitrogen, and oxygen-bearing molecules (Öberg et al. 2011; Schneider & Bitsch 2021; Ohno & Fortney 2023). α-elements such as magnesium and silicon are equally significant in planet formation studies, as these elements govern the mineralogy of planetary interiors (Chachan et al. 2023). The magnesium-to-silicon ratio (Mg/Si), in particular, governs the relative proportions of silicate minerals, such as olivine and pyroxene, in a rocky planet's mantle (Bond et al. 2010). This ratio, therefore, has direct implications for the planet's mineralogy, geodynamics, and potential habitability. Deviations from the solar Mg/Si ratio are expected to result in planets with different mineralogies and internal structures.

Empirical studies of volatile and α-elements abundances in planet hosts have been the subject of numerous high-resolution spectroscopic investigations. Carbon and oxygen have been analysed in several large samples of stars with and without planets (Ecuvillon et al. 2004b, 2006; Delgado Mena et al. 2010, 2021; Nissen et al. 2014; Suárez-Andrés et al. 2017, 2018; Mishenina et al. 2021; Unni et al. 2022), while nitrogen has been studied in a smaller number of works due to the observational challenges posed by its weak spectral features (Ecuvillon et al. 2004a; Suárez-Andrés et al. 2016; Biazzo et al. 2022). Magnesium and silicon have also been investigated in the works of Gonzalez (2009); Adibekyan et al. (2012a).

Despite this extensive literature, significant uncertainties remain in the investigation of these elements. Results are often sensitive to

the size and composition of the stellar samples analysed, with smaller datasets sometimes leading to inconclusive or contradictory interpretations. Furthermore, deriving precise CNO abundances is intrinsically difficult as both atomic and molecular lines can yield inconsistent results (see e.g. Ecuvillon et al. 2004a; Nissen et al. 2014). Moreover, departures from local thermodynamic equilibrium (LTE) and the influence of three-dimensional atmospheric structures can strongly affect abundance determinations (Amarsi et al. 2022).

Even with these challenges, observational progress has led to important insights. For carbon, early works using small samples and atomic features found no significant differences between planet-hosting stars and their comparison counterparts (Ecuvillon et al. 2004b, 2006). Suárez-Andrés et al. (2017) studied carbon using a larger sample of solar-type stars and the CH band molecular feature at 4300 Å and found that planet hosts are carbon-rich when compared to comparison stars. More recently, Delgado Mena et al. (2021) found that low-mass planet hosts may exhibit systematically higher [C/Fe] values at sub-solar metallicities, while no enhancement is seen at higher metallicities.

For oxygen, similar indications of higher abundances in low-mass planet hosts have been reported, but the results remain inconclusive due to substantial measurement uncertainties and the difficulty of analysing weak or blended oxygen lines (Delgado Mena et al. 2021; Biazzo et al. 2022).

Nitrogen remains the least studied among the light elements in planet-host stars, largely because its accessible spectral features are confined to the near-UV or weak CN bands. One of the most detailed efforts so far was the work by Suárez-Andrés et al. (2016) for 42 solar-type hosts. Their results suggested a possible increase in [N/Fe] for stars with low-mass planets, followed by a roughly constant behaviour for more massive planet hosts; however, the limited number of stars prevented any robust statistical conclusions.

For α-elements, observations suggest that planet-hosting stars may display systematically higher Mg and Si abundance patterns compared to stars without planets, particularly in the thick disk (e.g. Adibekyan et al. 2012a), where these enhancements can compensate for lower iron content during planet formation (e.g. see Bashi & Zucker 2019).

Thiabaud et al. (2015) showed that the Mg/Si ratio in planets tends to mirror that of their host stars. Such observations emphasise the direct link between α-element abundances and planetary composition.

1.1.3 Neutron-capture element abundances

Beyond volatile and α-elements, the abundances of heavier species produced through neutron-capture processes provide further insight into the environments where planets originate. These elements are created when nuclei capture free neutrons, and the outcome depends on whether the capture happens more quickly than a subsequent beta decay (Burbidge et al. 1957). The synthesis of these elements can be distinguished in two main pathways. The *s*-process which occurs during helium-core and carbon-shell burning in massive stars or in the asymptotic giant branch (AGB) phases of low- and intermediate-mass stars (Karakas & Lattanzio 2014; Cseh et al. 2022). This gives rise to the characteristic peaks in the abundance of certain nuclei, notably strontium, yttrium, and zirconium (first *s*-process peak) as well as barium, lanthanum, cerium, praseodymium, and neodymium (second *s*-process peak). By contrast, the *r*-process is proposed to be linked to more energetic events such as supernovae explosions and neutron-star mergers (Cowan et al. 2021, and references therein), and contributes to the production of elements like europium (Travaglio et al. 1999; Bisterzo et al. 2014; Prantzos et al. 2020).

These elements are essential tracers of Galactic chemical evolution and the nucleosynthetic yields of both massive and low-mass stars. At the same time, they may also carry signatures relevant to planet formation. Initial studies suggested that planet-hosting stars may be enriched in *n*-capture elements compared to non-hosts. Bond et al. (2008), for example, found that stars with planets exhibited overabundances in several *s*- and *r*-process species relative to a control sample, with differences up to 0.1 dex. The study concluded that the chemical anomalies in planetary host stars result from the normal Galactic chemical evolution processes. However, subsequent investigations have reported more complex behavior, particularly regarding barium. da Silva et al. (2015) identified anomalous Ba abundances that could not be easily explained, while Mishenina et al. (2016) found an underabundance of Ba in stars

with planets. Similarly, Delgado Mena et al. (2018) found a deficiency of Ba in stars hosting low-mass planets, highlighting the complexity of interpreting such trends and the importance of accounting for underlying stellar population differences.

1.1.4 Element condensation temperature

Elemental abundance signatures may also be linked to planet formation through correlations with condensation temperature ($T_{\rm cond}$). The condensation temperature represents the temperature at which a particular element or compound transitions from the gas phase to the solid phase in a protoplanetary disk, thereby determining whether it is incorporated into dust and planetary material. Elements with high $T_{\rm cond}$ (refractories such as Fe, Mg, Si, and Zr) tend to condense at temperatures typically above $\sim$1200 K, while volatile elements (such as C, N, and O) condense at much lower temperatures, typically below 200 K.

Correlations between stellar abundance differences and $T_{\rm cond}$ when compared to stellar analogues and often expressed as slopes in Δ[El/H] versus $T_{\rm cond}$ have been interpreted as potential chemical signatures of planet formation, where refractory material becomes locked into terrestrial planets or planetesimals, depleting the stellar photosphere of these elements. Conversely, enrichment in refractories could indicate accretion of rocky material onto the stellar surface (see e.g. Meléndez et al. 2009; Adibekyan et al. 2016; Yun et al. 2024). This raises the important question of whether *n*-capture elements, many of which are refractory, exhibit similar trends and thus play a role in shaping planetary systems.

Recent work has therefore aimed to establish whether there are systematic differences in volatile and refractory element abundances between stars with and without planets, and whether these abundances correlate with planetary parameters such as mass and multiplicity (e.g. Mishenina et al. 2016; Delgado Mena et al. 2018; Swastik et al. 2022; da Silva et al. 2024). In addition, by investigating condensation temperature trends across volatile and refractory species, studies have begun to explore whether such patterns reflect underlying planet-formation processes.

1.2 From formation to discovery: understanding exoplanets

Understanding how planets form in protoplanetary discs through mechanisms such as core accretion or gravitational disc instability directly informs which kind of planetary systems we expect to find, while the sensitivities and biases of our detection methods determine which of these worlds are actually discovered. Subsequent advances in observational programs and instrumentation, from precision Doppler spectrographs to wide-field transit surveys and dedicated space missions, have transformed exoplanetary studies from a field of isolated discoveries into one of population-level statistics (Fischer et al. 2014; Borucki et al. 2010; Ricker et al. 2015).

These data reveal a remarkable diversity of planetary systems, enabling theoretical models to be tested across a wide range of masses and orbital separations. While the core-accretion paradigm remains the dominant framework for forming most planets (Pollack et al. 1996; Mordasini et al. 2009), alternative channels such as disc instability and core-assisted gas collapse are increasingly invoked to explain massive companions at wide separations (Boss 1997; Nayakshin 2017).

Planet formation is a complex, multi-stage process that links the evolution of protoplanetary discs to the architecture of planetary systems. Two principal frameworks dominate current theoretical understanding: core accretion and gravitational (disc) instability, each operating under different physical conditions and timescales. In the core accretion model, micron-sized dust grains within a protoplanetary disc clump together into planetesimals, which subsequently grow through runaway and oligarchic accretion into planetary embryos capable of gravitationally capturing gaseous envelopes (Pollack et al. 1996; Kokubo & Ida 1998). This mechanism naturally explains the observed correlation between stellar metallicity and the occurrence rate of giant planets (Gonzalez 1997; Santos et al. 2001; Fischer & Valenti 2005; Johnson et al. 2010), as higher metallicity enhances the solid surface density required for rapid core growth. However, the relatively slow timescale of core accretion poses challenges for forming massive planets in the outer regions of discs before gas dispersal (Dodson-Robinson et al. 2008).

In contrast, the gravitational instability model proposes that massive, cold discs can become gravitationally unstable and fragment directly

into self-gravitating clumps that may contract to form giant planets or brown dwarfs (Boss 1997; Durisen et al. 2007). This pathway is more efficient in the outer disc, where cooling times are shorter and local surface densities can be high enough for fragmentation (Gammie 2001; Rafikov 2005).

Hybrid mechanisms, such as core-assisted gas capture (Nayakshin 2017) and pebble accretion (Ormel & Klahr 2010; Lambrechts & Johansen 2012), have recently gained prominence for bridging the gap between the classical paradigms offering routes for rapid core growth that reconcile observational constraints on planet masses and formation timescales.

These developments suggest that multiple formation channels may operate concurrently within the same disc, depending on local conditions and evolutionary stage. Consequently, the diversity of exoplanetary systems likely reflects the interplay of these mechanisms, influenced by disc physics, migration processes, and the broader stellar environment.

2 Data and methodology

In this section, I present the observational strategy, data acquisition, and methodology employed throughout my research. High-resolution spectroscopic observations were carried out to determine the atmospheric parameters and chemical compositions of a large, homogeneous sample of F-, G-, and K-type stars hosting confirmed planetary companions. These observations form the foundation for a detailed chemical abundance analysis aimed at probing potential links between stellar composition and planet formation.

2.1 Sample selection, observations and data reduction

The stellar targets analysed in this thesis were selected from the NASA Exoplanet Archive, focusing on bright (V$\leq$8.5 mag) exoplanet-hosting stars. These stars are located in the northern hemisphere, some of which cover the TESS continuous viewing zone (CVZ). The main sample comprises 160 PHS, which includes 25 stars discussed in Paper I, 149 stars in Paper II, and 160 stars in total in Paper III, reflecting an updated and extended dataset with additional confirmed planets. The selection includes both main-sequence stars and evolved stars to probe chemical signatures across different stages of stellar evolution.

High-resolution spectroscopic observations were conducted using the Vilnius University Echelle Spectrograph (VUES) (Jurgenson et al. 2016), mounted on the 1.65 meter Ritchey-Chrétien telescope located at Molėtai Astronomical Observatory (MAO) in Lithuania. The spectrograph covers the visible wavelength range from 4060 to 9100 Å and is operated in $R \sim 36\,000$, $\sim 51\,000$, and $\sim 68\,000$ resolution modes. For our work, we used two resolution modes: $R \sim 36\,000$ & $68\,000$ depending on the brightness of targets. Exposure times varied from 900 to 7200 seconds to achieve S/N typically in the range of 75 to 200. All the observations were carried out from 2021 through 2024.

In general, the extraction of information from high-resolution spectra involves several technical steps. First, the raw data must be processed through a reduction pipeline, which performs bias subtraction, flat-fielding, cosmic ray removal, wavelength calibration (often using thorium-argon), and order merging. After reduction, continuum normal-

isation is applied to remove the broad spectral shape imposed by the instrument response and stellar flux distribution. This step is critical for accurate line profile analysis, particularly when measuring equivalent widths or performing spectral synthesis. Each absorption line encodes information about the physical state of the stellar photosphere and the abundance of the corresponding element. The depth, shape, and asymmetry of lines are influenced by temperature, pressure, microturbulence, rotation, and magnetic activity. By comparing observed line strengths with predictions from model atmospheres, one can derive the main atmospheric parameters of a star. These parameters form the basis of stellar characterisation, upon which detailed abundance analyses are built.

Our spectral data reduction was carried out using the VUES automated pipeline described in the work of Jurgenson et al. (2016), which performs standard procedures such as bias subtraction, flat-field correction, wavelength calibration using a ThAr lamp, cosmic ray removal, and extraction and merging of echelle orders. The final spectra were one-dimensional, wavelength-calibrated, and continuum-normalised, suitable for detailed spectroscopic analysis.

To ensure high-quality abundance measurements, stars with high rotational velocities ($v\sin i \geq 20$ km s^{-1}), or those exhibiting double- or triple-lined spectroscopic binary signatures, were excluded from the final sample due to line broadening or blending that compromises abundance determinations. After applying these quality filters, a final well-characterised sample of 160 confirmed PHS was established. This final sample consists of 86 main-sequence stars, hereafter referred to as dwarf stars, along with 74 stars that are at their evolved stages, hereafter referred to as giant stars, hosting a combined total of 222 exoplanets, spanning a broad range of planetary masses and system architectures.

2.2 Comparison sample

To compare the chemical composition of PHS with that of stars without detected planetary companions, carefully selected comparison samples were used throughout this work. For the C, N, O, and α-element abundance analysis, a comparison sample of 740 bright field stars was adopted from our previous studies (Mikolaitis et al. 2019; Stonkutė et al. 2020; Tautvaišienė et al. 2022). These stars were observed and analysed homo-

geneously using the same instrumentation, stellar atmosphere models, and analysis pipeline as the planet-host sample. For analysing *n*-capture elements, we compiled a comparison sample comprising 491 stars, including 222 dwarfs and 269 giants with chemical abundances previously determined in Tautvaišienė et al. (2021). The chemical abundances in this group were also determined using homogeneous methodology, enabling robust investigation of abundance trends with metallicity, elemental condensation temperature slopes (Δ[El/H]-$T_{\rm cond}$), and potential abundance differences, likely associated with the presence of planets.

2.3 Stellar atmospheric parameters

The atmospheric parameters of a star define the thermodynamic structure of its atmosphere and directly influence the formation and strength of spectral lines. Accurately determining the fundamental stellar atmospheric parameters (effective temperature, $T_{\rm eff}$ (K); surface gravity, $\log g$ (dex); microturbulence velocity, $v_{\rm t}$ (km s^{-1}); and metallicity, [Fe/H] (dex)) is crucial, as these parameters form the basis for chemical abundance determinations.

We have uniformly determined the main atmospheric parameters for our stellar sample using a well-established classical equivalent width (EW) approach based on the analysis of atomic neutral (Fe I) and ionised (Fe II) iron absorption lines. This method involves measuring the strength of Fe I and Fe II lines in a stellar spectrum, known as the equivalent width, by fitting the line profiles with a model (e.g., Gaussian, Lorentzian, or a more complex fitting function) and calculating the area under the curve.

EWs of selected Fe I and Fe II lines were measured using the DAOSPEC software (Stetson & Pancino 2008), in the same way as the Vilnius node used in the *Gaia*-ESO Survey (Smiljanic et al. 2014; Mikolaitis et al. 2018). It automatically fits Gaussian profiles to absorption lines in high-resolution spectra and provides reliable EW measurements suitable for abundance analysis. The initial iron abundance analysis was carried out using the 2017 version of the MOOG code (Sneden 1973), a widely used LTE spectral analysis program. The model atmospheres employed were interpolated from the MARCS grid of one-dimensional, plane-parallel, hydrostatic stellar atmospheres (Gustafsson et al. 2008),

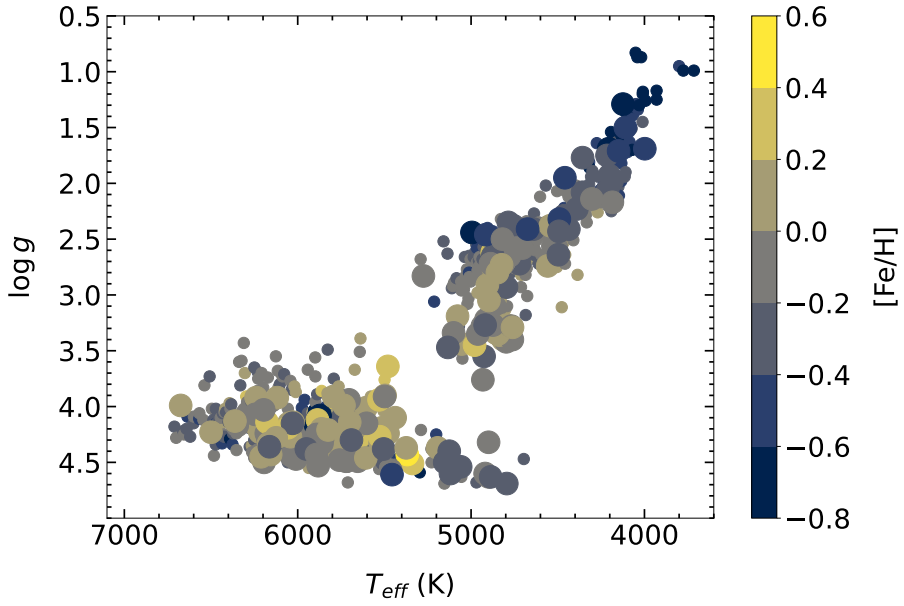

Figure 1: Effective temperature ($T_{\rm eff}$) versus surface gravity (log g) diagram for analysed planet host stars, colour-coded by metallicity [Fe/H]. Comparison stars from Tautvaišienė et al. (2021) are marked with smaller symbols.

which assume LTE and are suitable for a broad range of stellar parameters relevant to FGK-type stars.

The effective temperature, $T_{\rm eff}$, was determined by applying the excitation equilibrium condition to Fe I lines. For a given model atmosphere, we computed the iron abundance from each Fe I line and examined whether there was a systematic trend between the derived abundance and the excitation potential of the line. If the temperature was underestimated, lines with higher excitation potentials yielded higher abundances, and vice versa. By iteratively adjusting the temperature in the model atmosphere, we aimed to minimise this correlation. The final effective temperature was adopted when the slope of abundance versus excitation potential approached zero, indicating that the excitation balance condition was satisfied.

The surface gravity, log g was determined by ionisation equilibrium between neutral and ionised iron lines ensuring that the derived iron abundances from Fe I and Fe II lines were the same. Since these two ionisation stages respond differently to changes in electron pres-

sure, achieving agreement between the mean abundances derived from each set of lines ensures a physically consistent value of log g. The adopted surface gravity corresponds to the point where this difference was minimised, indicating a balance between the two ionisation states and satisfying the ionisation equilibrium condition.

The microturbulence velocity, v_t, which accounts for small-scale turbulent motions in the stellar atmosphere, is derived by requiring that the iron abundance derived from Fe I lines does not depend on the reduced equivalent width of the selected lines. The reduced equivalent width is defined as $\log(\mathrm{EW}/\lambda)$, where EW is the equivalent width of the spectral line and λ its wavelength. This quantity provides a normalized measure of line strength, allowing lines at different wavelengths to be compared consistently. Once these atmospheric parameters were optimised, the stellar metallicity [Fe/H] was calculated as the mean abundance from Fe I lines. The final set of parameters was determined through an iterative process, refining each parameter until the excitation equilibrium, ionisation balance, and line strength independence were simultaneously satisfied. This methodology was applied uniformly to all PHS analysed in our study.

The effective temperature, T_{eff}, of the overall sample exhibits a broad range from 4000 to 6680 K. Surface gravity, log g, which highlights the intrinsic differences between dwarf and giant stars, log g, ranges from 1.3 to 3.5 dex for giant stars, with a mean value of 2.8 ± 0.6 dex, while for dwarf stars, log g values ranges from 3.6 to 4.7 dex, with a mean value of 4.2 ± 0.2 dex. Metallicity [Fe/H], a key parameter indicative of the giant planet occurrence rate, ranges from -0.76 to 0.45 dex, with a mean of -0.09 ± 0.24 dex. The atmospheric parameters for the full sample of 160 stars are provided and made publicly available in machine-readable form at the CDS via https://cdsarc.cds.unistra.fr/viz-bin/cat/J/A+A/701/A153.

Figure 1 presents the investigated stars with planets in an effective temperature versus surface gravity diagram, with the comparison stars from Tautvaišienė et al. (2021) represented by smaller symbols. The analysed sample is approximately evenly distributed between evolved and main-sequence stars.

2.4 Elemental abundance analysis

With the atmospheric parameters determined, the next step in the analysis involved determining the chemical abundances of individual elements in the stellar atmospheres. The aim is to explore the abundance patterns of both light and heavy elements, particularly those with implications for Galactic chemical evolution and planet formation. The analysis focused on a selection of light elements: C, N, α-elements: O, Mg, and Si; and a set of *n*-capture elements produced through different neutron-capture processes (Sr, Y, Zr, Ba, La, Ce, Pr, Nd, and Eu).

The analysis of high-resolution spectra is typically carried out using either equivalent width (EW) measurements or spectral synthesis. Equivalent width methods involve measuring the area of a line profile and comparing it to theoretical predictions based on model atmospheres. This approach is efficient and widely used for large datasets; however, it becomes less accurate in regions with blended lines or low signal-to-noise (S/N) ratios. In contrast, spectral synthesis compares observed spectra with synthetic spectra generated by radiative transfer codes, allowing for detailed line profile fitting and the inclusion of blending, NLTE effects, and hyperfine structure.

Commonly used tools include MOOG (Sneden 1973), SME (Valenti & Piskunov 1996), and iSpec (Blanco-Cuaresma et al. 2014) among others, all of which interface with libraries of model atmospheres such as ATLAS9 (Kurucz 1993), MARCS (Gustafsson et al. 2008), and PHOENIX (Husser et al. 2013). A critical aspect of high-resolution analysis is the selection of clean and reliable spectral lines. Line lists must be carefully curated, avoiding regions with strong blends or poorly known atomic data. Databases such as the Vienna Atomic Line Database (VALD; Ryabchikova et al. 2015) and the NIST Atomic Spectra Database (Kramida et al. 2023) provide essential line parameters, including wavelengths, excitation potentials, oscillator strengths, and damping constants. For precise abundance studies, especially for *n*-capture elements or elements with significant hyperfine structure, updated laboratory measurements are often necessary.

The elemental abundances in our work were derived using the spectral synthesis method with a differential approach relative to the Sun. This method employs a line-by-line comparison of the high-resolution

observed spectra to the modelled spectra. We used the TURBOSPECTRUM code (Alvarez & Plez 1998) to generate synthetic stellar spectra using the main atmospheric parameters of our host stars. For model atmospheres, we adopted a grid of plane-parallel, one-dimensional, hydrostatic model atmospheres under the assumption of local thermodynamic equilibrium (LTE), obtained from the MARCS stellar model atmosphere library (Gustafsson et al. 2008). All abundance determinations were performed differentially with respect to the Sun to reduce systematic uncertainties arising from atomic data and modeling assumptions. The solar abundances adopted for reference were taken from Grevesse et al. (2007), ensuring consistency with our earlier abundance studies (e.g. Stonkutė et al. 2020).

For each element, we selected good-quality spectral lines based on their reliability, minimal blending, and well-characterised atomic data. Spectrum synthesis was performed around each selected line, comparing synthetic spectra to the observed profiles. The best-fit abundance was determined by minimising the difference between observed and modeled spectra. In cases where lines were weak or blended, additional care was taken in the placement of the local continuum and fitting of nearby features. Hyperfine structure (HFS) and isotopic splitting (IS) were included where relevant, particularly for *n*-capture elements such as Ba, La, Pr, and Eu. For each element, abundances were determined from multiple lines whenever possible, and the final abundance was computed as the average of individual measurements. For elements with only one usable line (e.g. O, Eu), abundance uncertainties were estimated from the continuum variation due to S/N.

2.4.1 CNO and Mg, Si abundances

The abundances of carbon, nitrogen, and oxygen were determined using molecular and atomic lines. Carbon abundances were derived from the C_2 Swan bands, specifically the (1, 0) band head at 5135 Å and the (0, 1) band head at 5635 Å (Brooke et al. 2013; Ram et al. 2014). Nitrogen abundances were obtained by synthesising $^{12}C^{14}N$ molecular feature in two spectral regions: 6470-6485 Å and 7980-8005 Å (Sneden et al. 2014). Oxygen was measured using the forbidden [O I] line at 6300 Å, which is relatively unaffected by non-LTE or 3D effects and is a well-

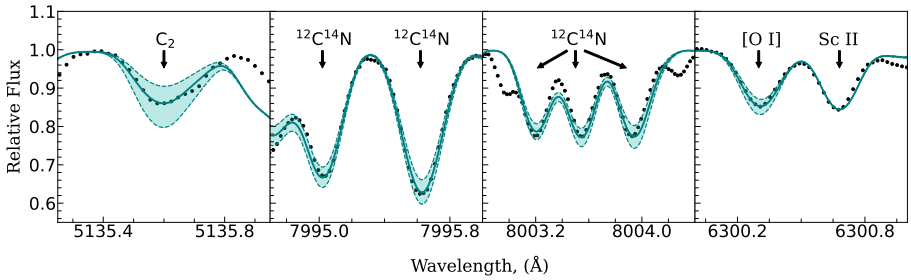

Figure 2: Example of spectral synthesis for representative molecular and atomic features used in the abundance analysis. Observed spectra are shown as black dots, while the solid green line represents the best-fitting synthetic spectrum, with dashed lines indicating variations of ± 0.10 dex from the optimal abundance.

established abundance indicator in FGK-type stars (Amarsi et al. 2021). The oscillator strength values for ^{58}Ni and ^{60}Ni, which blend the [O I] line, were taken from Johansson et al. (2003).

Figure 2 presents a representative example of the spectral synthesis employed to derive elemental abundances, illustrating the fitting of prominent C_2, $^{12}C^{14}N$, and [O I] spectral features. The figure demonstrates the quality of the fit between the observed spectrum and the synthetic profiles computed for different abundance values.

An important consideration in the determination of C, N, and O abundances is their mutual coupling through molecular equilibrium in the stellar atmosphere. In cool stars, a significant fraction of carbon and oxygen atoms are bound in carbon monoxide (CO) molecules, which are highly stable and form preferentially over other molecular species. As a result, the availability of free carbon atoms for forming C_2 molecules or free oxygen atoms for forming OH or [O I] lines is directly affected by the abundance of the other element. Therefore, the carbon and oxygen abundances cannot be treated independently but must be determined iteratively.

The process begins by determining an initial value for the oxygen abundance and determining the carbon abundance from C_2 molecular features. The oxygen abundance is then derived from the [O I] line, using the newly estimated carbon value as input. Since changes in one element affect the molecular formation of the other, this procedure is re-

peated. Iterations continue until the changes in both O and C abundances between successive steps become negligible, indicating convergence. Once consistent values for carbon and oxygen are established, nitrogen abundances are derived using CN molecular lines.

The CN molecule forms from available carbon and nitrogen atoms, and its line strength depends strongly on the C abundance already fixed through CO formation. Therefore, accurate nitrogen determination requires that both C and O abundances be fixed beforehand. The CN synthesis then proceeds with these inputs, adjusting only the nitrogen abundance to match the observed spectral features. This iterative, equilibrium-aware procedure ensures that the derived C, N, and O abundances are physically self-consistent and reliable, particularly in cool stars where molecular effects are strongest. The method has been applied uniformly across the sample.

The α-elements, magnesium and silicon, were analysed using multiple atomic lines. For Mg I abundance determination, atomic lines at 5528, 5711, 6318, and 6319 Å were employed, with the choice of lines depending on spectral quality and S/N. Silicon abundances were derived from up to twelve Si I lines distributed across the spectral range. Line selection prioritised minimal blending and strong, well-defined features. For both Mg and Si, the synthetic spectra were fitted to individual lines, and final abundances were averaged from multiple measurements per star. A comprehensive summary of the derived C, N, and α-element abundances, including uncertainties for 149 stars analysed in Paper I and Paper II, is provided in Table A1.

2.4.2 Abundances of neutron-capture elements

The chemical abundances of *n*-capture elements in our stellar sample were determined by analysing the stellar spectra using the same differential model atmosphere technique as for light elements. We used version 5 of the *Gaia*-ESO survey (GES) line list (Heiter et al. 2021). Spectral lines for each element were selected based on their strength and minimal contamination from neighbouring features.

Once the line list was finalised, we calibrated the adopted line list using a high-resolution solar spectrum from Kurucz (2005) to ensure the reliability of the spectral line data used in the abundance analysis.

We verified that this calibration reproduces known solar abundances by Grevesse et al. (2007) within the uncertainties. Moreover, heavy elements often comprise several isotopes, and their spectral lines can be affected by hyperfine splitting. Thus, hyperfine structure and isotopic splitting were incorporated where applicable to account for broadening and asymmetry in the line profiles. The corresponding spectral lines used for abundance determinations of each investigated chemical element are described in detail below.

STRONTIUM. We selected two Sr I spectral lines, one at 4607 Å and the other at 7070 Å.

YTTRIUM. The abundances of yttrium were derived from up to seven Y II lines at wavelengths 4883, 4900, 4982, 5087, 5200, 5289, and 5402 Å.

ZIRCONIUM. The abundances were measured using both neutral (Zr I) and ionised (Zr II) lines. The selected Zr I lines were at 6127 and 6134 Å, and the Zr II lines were at 5350.1 and 5350.3 Å.

BARIUM. The abundances were determined using the Ba II lines at 5853, 6141, and 6496 Å. For all Ba II lines, the $\log gf$, and the HFS and IS values were taken from Davidson et al. (1992). The strong barium lines include a background line list with Ba II data from Miles & Wiese (1969).

LANTHANUM. The abundances were derived from up to five La II spectral lines at wavelengths 4748, 4804, 5123, 5303, and 6390 Å. The HFS and IS values for the La II 5123, 5303, and 6390 Å lines were taken from Lawler et al. (2001a).

CERIUM. Up to four Ce II lines at 5274, 5472, 5512, and 6043 Å were used to determine Ce abundances.

PRASEODYMIUM. The abundances were determined using two Pr II lines at 5259 and 5322 Å. The HFS and IS values for all Pr II lines were taken from Sneden et al. (2009).

NEODYMIUM. The abundances were derived from five Nd II lines at 5092, 5255, 5276, 5357, and 5740 Å. The HFS and IS values were taken for the Nd II 5092 and 5740 Å lines from Den Hartog et al. (2003) and for the 5276 Å line from Meggers et al. (1975).

EUROPIUM. The abundances were derived using the Eu II line at 6645 Å. The HFS and IS values for the Eu II line were obtained from

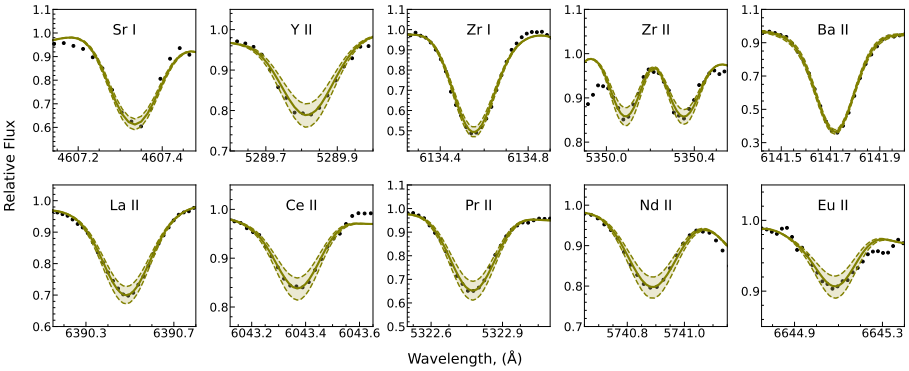

Figure 3: Representative examples of synthetic spectral fits for selected neutron-capture element lines in planet-host stars. The observed spectra (black dots) are compared with best-fitting synthetic profiles (yellow solid lines), with dashed lines indicating variations of ± 0.10 dex from the optimal abundance as in Fig. 2.

Lawler et al. (2001b).

For each spectral line, synthetic spectra were generated using carefully selected atomic data and nearby blends. All abundances were determined by iteratively adjusting the element's input abundance in the synthetic spectrum until the best fit to the observed profile was achieved. Continuum normalisation was performed locally around each line to avoid distortions caused by broader features. In stars where multiple lines of a given element were available, the final abundance was taken as the mean of the individual line-based values, while for elements with only one measurable line, the abundance derived from that line is the final abundance. Table A2 provides a complete set of the measured *n*-capture abundances, incorporating the individual line analyses and their corresponding uncertainties. Figure 3 illustrates examples of our spectral synthesis fits for *n*-capture elements in selected planet-hosting stars.

2.4.3 (Non)-local thermodynamic equilibrium effects

The abundance analysis in this thesis is primarily based on one-dimensional (1D) model atmospheres computed under the assumption of local thermodynamic equilibrium. However, departures from LTE can become significant when radiative processes dominate over collisional processes in stellar atmospheres, leading to systematic biases in derived abun-

dances. These (Non)-local thermodynamic equilibrium effects may affect level populations and line strengths for certain species, and must therefore be assessed to ensure that any abundance differences we report are robust.

In the context of PHS, accounting for NLTE effects is especially relevant because subtle abundance differences between stars with and without planets are typically of the order of a few hundredths of a dex. Systematic errors introduced by LTE assumptions can therefore mimic or mask genuine chemical signatures related to planet formation. In this work, NLTE corrections were applied for several elements using the TSFitPy wrapper (Gerber et al. 2023). For other elements considered in this work, NLTE effects were not explicitly applied but were instead assessed based on results reported in the literature. The discussion below therefore, combines NLTE corrections obtained in the present analysis for the elements where such corrections were available with a brief overview of previously published NLTE studies for the remaining species analysed in this work.

While many previous works have focused on NLTE corrections for metal-poor halo and thick disc stars, where these effects are most pronounced, our sample consists of PHS with an average metallicity of <[Fe/H]>= -0.09. The most metal-poor star in our dataset has a metallicity of [Fe/H]= -0.76.

The literature indicates that NLTE effects for molecular C_2 and CN bands commonly used to derive carbon and nitrogen are negligible in solar-type stars: molecular equilibria and the molecular line formation regions tend to be close to LTE, and abundance results from molecular lines agree well with those from atomic C and N diagnostics in solar-type atmospheres (e.g., Ayres & Wiedemann 1989; Ryabchikova et al. 2022). For oxygen, the forbidden [O I] 6300 Å line is weak, forms deep in the photosphere, and is practically immune to NLTE effects. Therefore, it remains one of the most reliable oxygen diagnostics in solar-type stars (e.g., Amarsi et al. 2021).

Recent NLTE grid calculations for Mg I show that line-by-line corrections are typically small (a few hundredths of a dex) for Sun-like parameters. In this work, magnesium abundances were checked for NLTE corrections using all lines through the TSFitPy framework. The

resulting corrections are generally minor, ranging from about -0.03 to 0.00 dex for our line list and stellar sample, with the 5711 Å line showing slightly larger sensitivity. Given the strength and sensitivity of the 5711 Å feature, it was generally excluded from the final computation of the average magnesium abundance.

The strontium line at 4607 Å has been extensively studied in Bergemann et al. (2012) for late-type stars over a broad metallicity range, from very metal-poor to near-solar compositions. Their study showed that NLTE effects are significant in metal-poor stars ([Fe/H] $\lesssim -1.0$), primarily due to overionisation processes. At moderately sub-solar metallicities (approximately $-0.7 \lesssim$ [Fe/H] < 0.0), the predicted corrections become considerably smaller. NLTE abundance corrections for Sr I lines were applied in this work. The Sr I 4607 Å line requires positive NLTE corrections that increase toward lower metallicity. The corrections span from +0.02 to +0.12 dex, with a typical value around +0.07 dex for dwarf stars. The effect is more pronounced in giant stars, where the required corrections increase substantially, covering a range of +0.06 to +0.30 dex with a median of +0.16 dex. In contrast, the Sr I 7070 Å line is insensitive to NLTE effects, with corrections effectively centered around zero (median correction $\approx$ 0.00 dex).

Alexeeva et al. (2023) conducted the first systematic investigation of NLTE effects on Y II lines, including those adopted in our analysis, using atmospheric models representing FGK-type stars across a wide metallicity range. Their results indicate that for stars close to solar metallicity, NLTE corrections for seven Y II lines used in our analysis reach a maximum of $+0.08$ dex. In metal-poor stars, NLTE corrections are stronger compared to solar metallicity stars, but do not exceed $+0.16$ dex for the lines adopted in our analysis. Given that our sample is, on average, more metal-rich, we expect only moderate NLTE corrections for Y II. According to the corrections applied in this work, the analysed Y II lines can be divided into two groups. First group (comprising 4883, 4900, 5087, and 5200 Å lines) shows relatively stronger departures from LTE, particularly in evolved stars (–0.03 to +0.14 dex). The remaining yttrium lines show only marginal NLTE deviations (–0.00 to +0.03 dex in dwarfs and –0.00 to +0.04 dex in giants). The mean NLTE corrections in both groups of lines remain close to zero, typically within +0.04 dex for both

dwarf and giant stars.

Barium is sensitive to NLTE effects because of its Ba II lines exhibiting large equivalent widths, making them difficult to model accurately under the LTE assumption. NLTE effects on Ba II 5853 Å transition are expected to be minimal, with LTE-derived abundances closely matching NLTE values across various stellar parameters. Even for the red Ba II lines at 6141 and 6496 Å, the LTE and NLTE abundances agree within ≈ 0.10 dex for sub-solar metallicities (Korotin et al. 2015; Eitner et al. 2019). Our analysis also showed relatively smaller corrections for 5853 Å transition (-0.12 to -0.02 dex for dwarfs and -0.17 to -0.02 dex for giants). In contrast, the red Ba II lines at 6141 Å and 6496 Å require more substantial negative corrections (-0.25 to -0.03 dex for dwarfs and -0.26 to 0.00 dex for giants). On average, NLTE corrections amount to approximately -0.13 dex in dwarfs and -0.08 dex in giants.

Shaltout et al. (2020) examined departures from LTE in praseodymium abundances for the solar atmosphere based on an analysis of 14 Pr II transitions, among them the 5259 and 5322 Å lines used in the present work. They concluded that NLTE effects introduce only a very small positive abundance offset, on the order of +0.01 dex. This suggests that, for solar-type stellar parameters, Pr II lines are essentially insensitive to NLTE effects. The NLTE ionisation balance between Nd II and Nd III was explored by Mashonkina et al. (2005) with an emphasis on cool A-type and chemically peculiar Ap stars. Their analysis revealed substantial departures from LTE in these comparatively hot atmospheres, especially within the effective temperature range of 7 500-9 500 K. The extent to which these conclusions can be extrapolated to cooler FGK stars, however, is not well established.

Finally, for europium, previous NLTE studies have reported only minor departures from LTE, particularly for the commonly used Eu II diagnostic line at 6645 Å. The available literature indicates that NLTE effects do not significantly alter europium abundance measurements, especially in sun-like stellar atmospheres (Mashonkina & Gehren 2000; Storm et al. 2024; Guo et al. 2025). In our analysis, europium abundances were derived from this single Eu II line, which exhibits modest sensitivity to NLTE effects, with dwarfs showing corrections ranging from –0.08 to +0.03 dex (mean –0.05 dex) and giants exhibiting values between

–0.11 and 0.00 dex, averaging –0.05 dex. Overall, these small corrections confirm that NLTE effects play a limited role in europium abundance measurements.

2.4.4 Uncertainty analysis

We have carefully accounted for uncertainties at every stage of the analysis, starting from the measurement of stellar absorption lines and extending through the determination of atmospheric parameters and final abundance derivations. These uncertainties can be systematic and random. Systematic uncertainties, such as those arising from uncertainties in atomic data, were largely minimised through the use of differential analysis relative to the Sun. Random uncertainties, on the other hand, that primarily arise from factors such as local continuum placement and the fitting of individual spectral lines were carefully addressed during the analysis.

Uncertainties in the determination of stellar atmospheric parameters were introduced through multiple channels: the measurement of equivalent widths (influenced by continuum placement, line-fitting, and S/N), and the statistical uncertainty in the linear regression fits used to determine excitation and ionisation equilibrium. To mitigate these effects, we relied on an extensive and carefully selected list of Fe I and Fe II lines (86 and 7, respectively), which were selected to avoid any contamination by blends, telluric lines, or to avoid regions with difficult continuum determination. When evaluating the uncertainties for the determined atmospheric parameters, we used the standard deviation of linear regression fits and abundances. Those deviations were propagated to find the boundary conditions for effective temperature, surface gravity, and microturbulent velocity.

On average, the uncertainty in effective temperature is approximately 50 K, with a typical variation of $\pm$15 K depending on the spectral S/N and the slope of iron abundances versus the excitation potential plot. Uncertainties in surface gravity values are about 0.20 dex, with a variation of $\pm$0.05 dex, based on the sensitivity of ionisation equilibrium to line selection and measurement noise. Metallicity measurements have an associated uncertainty of approximately 0.09 dex, with a small internal variation of $\pm$0.02 dex. Microturbulent velocity, derived from

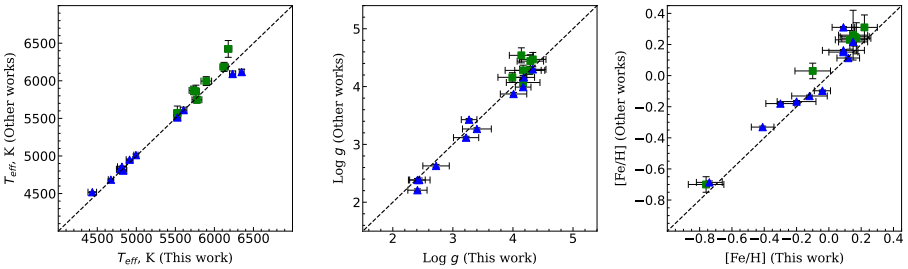

Figure 4: Comparison of spectroscopic stellar parameters derived in this work with those reported by Bensby et al. (2014, green squares) and APOGEE DR17 (Abdurro'uf et al. 2022, blue triangles).

trends between iron abundance and reduced equivalent width, exhibits an uncertainty close to 0.25 km/s with a typical range of $\pm$0.08 km/s. A detailed summary of these uncertainties for the full sample of 160 stars is provided and made publicly available in machine-readable form at the CDS via https://cdsarc.cds.unistra.fr/viz-bin/cat/J/A+A/701/A153.

Figure 4 shows a comparison of the spectroscopic stellar parameters derived in this work with the results of other works. We identified seven stars in common with Bensby et al. (2014) work and eleven stars common with the APOGEE DR17 (Abdurro'uf et al. 2022). The comparison shows that the derived values are consistent with those reported in the literature within the expected uncertainties.

Random uncertainties in elemental abundances originated primarily from line fitting, local continuum placement. For elements with multiple spectral lines, we calculated the scatter among individual line measurements and adopted it as the uncertainty for a given element. This methodology was uniformly applied across all elements.

Importantly, uncertainties in atmospheric parameters also propagate into the final abundance results. To evaluate the impact of uncertainties in abundances that arise from stellar parameters, we evaluated the sensitivity of each element's abundance that is investigated in this work to variations in the individual parameters. For this, we adopted the typical parameter uncertainties listed above and recalculated elemental abundances by varying one parameter at a time while keeping the others fixed. These tests were performed separately for dwarfs and giants, as the impact can differ depending on the stellar surface gravity. The sensitivity

Table 1: Effect of uncertainties in atmospheric parameters on the derived CNO and Mg, Si chemical abundances for the target stars.

Elements	$\Delta T_{\rm eff}$ $\pm$ 50 K	$\Delta \log g$ $\pm$ 0.20 dex	Δ[Fe/H] $\pm$ 0.09 dex	$\Delta v_{\rm t}$ $\pm$ 0.25 km/s
Dwarfs ($\log g > 3.5$)				
C (C_2)	$\pm$ 0.03	$\mp$ 0.01	$\pm$ 0.02	$\pm$ 0.00
N (CN)	$\pm$ 0.08	$\mp$ 0.01	$\pm$ 0.02	$\pm$ 0.00
O [O I]	$\pm$ 0.02	$\pm$ 0.10	$\mp$ 0.09	$\pm$ 0.00
Mg	$\pm$ 0.03	$\mp$ 0.02	$\mp$ 0.01	$\mp$ 0.02
Si	$\pm$ 0.01	$\pm$ 0.02	$\pm$ 0.00	$\pm$ 0.02
Giants ($\log g \leq 3.5$)				
C (C_2)	$\pm$ 0.00	$\pm$ 0.03	$\pm$ 0.02	$\pm$ 0.00
N (CN)	$\pm$ 0.00	$\pm$ 0.05	$\pm$ 0.02	$\pm$ 0.00
O [O I]	$\pm$ 0.00	$\pm$ 0.09	$\pm$ 0.01	$\mp$ 0.00
Mg	$\pm$ 0.02	$\pm$ 0.01	$\pm$ 0.00	$\mp$ 0.02
Si	$\mp$ 0.00	$\pm$ 0.04	$\pm$ 0.00	$\mp$ 0.04

Table 2: Effect of uncertainties in atmospheric parameters on the derived *n*-capture element abundances for the target stars.

Elements	$\Delta T_{\rm eff}$ $\pm$ 50 K	$\Delta \log g$ $\pm$ 0.20 dex	Δ[Fe/H] $\pm$ 0.09 dex	$\Delta v_{\rm t}$ $\pm$ 0.25 km s^{-1}
Dwarfs (log g > 3.5)				
Sr I	$\pm$ 0.06	$\mp$ 0.01	$\pm$ 0.01	$\mp$ 0.08
Y II	$\pm$ 0.01	$\pm$ 0.07	$\pm$ 0.02	$\mp$ 0.12
Zr I	$\pm$ 0.06	$\pm$ 0.01	$\mp$ 0.01	$\pm$ 0.01
Zr II	$\pm$ 0.01	$\pm$ 0.08	$\pm$ 0.02	$\mp$ 0.01
Ba II	$\pm$ 0.02	$\pm$ 0.02	$\pm$ 0.01	$\mp$ 0.14
La II	$\pm$ 0.02	$\pm$ 0.08	$\mp$ 0.05	$\mp$ 0.01
Ce II	$\pm$ 0.02	$\pm$ 0.08	$\mp$ 0.03	$\mp$ 0.01
Pr II	$\pm$ 0.01	$\pm$ 0.09	$\pm$ 0.02	$\pm$ 0.01
Nd II	$\pm$ 0.01	$\pm$ 0.09	$\pm$ 0.03	$\pm$ 0.01
Eu II	$\pm$ 0.01	$\pm$ 0.09	$\pm$ 0.02	$\pm$ 0.01
Giants (log $g \leq$ 3.5)				
Sr I	$\pm$ 0.05	$\mp$ 0.01	$\mp$ 0.01	$\mp$ 0.01
Y II	$\pm$ 0.01	$\pm$ 0.08	$\pm$ 0.02	$\mp$ 0.18
Zr I	$\pm$ 0.09	$\pm$ 0.01	$\mp$ 0.01	$\mp$ 0.01
Zr II	$\mp$ 0.01	$\pm$ 0.09	$\pm$ 0.03	$\mp$ 0.02
Ba II	$\pm$ 0.04	$\pm$ 0.04	$\mp$ 0.01	$\mp$ 0.20
La II	$\pm$ 0.01	$\pm$ 0.08	$\pm$ 0.03	$\mp$ 0.02
Ce II	$\pm$ 0.01	$\pm$ 0.09	$\pm$ 0.01	$\mp$ 0.04
Pr II	$\pm$ 0.01	$\pm$ 0.08	$\pm$ 0.04	$\mp$ 0.01
Nd II	$\pm$ 0.01	$\pm$ 0.08	$\pm$ 0.03	$\mp$ 0.03
Eu II	$\mp$ 0.01	$\pm$ 0.09	$\pm$ 0.03	$\pm$ 0.01

of abundance determinations to variations in atmospheric parameters is presented in Tables 1 and 2.

The sensitivity tests demonstrated that, in general, the derived chemical abundances are only mildly affected by typical uncertainties in the atmospheric parameters. This holds for both dwarf and giant stars. Among the light elements, only oxygen showed the most pronounced dependence on surface gravity. In the case of heavy elements, barium and yttrium were found to be especially sensitive to variations in microturbulence velocity. Ba II showed shifts up to ∓ 0.14 dex in dwarfs and ∓ 0.20 dex in giants and Y II up to ∓ 0.12 dex in dwarfs and ∓ 0.18 dex in giants, when $v_{\rm t}$ was changed by ± 0.25 km/s. The abundances of the remaining elements show only minor sensitivity to changes in $T_{\rm eff}$, $\log g$, [Fe/H], and $v_{\rm t}$.

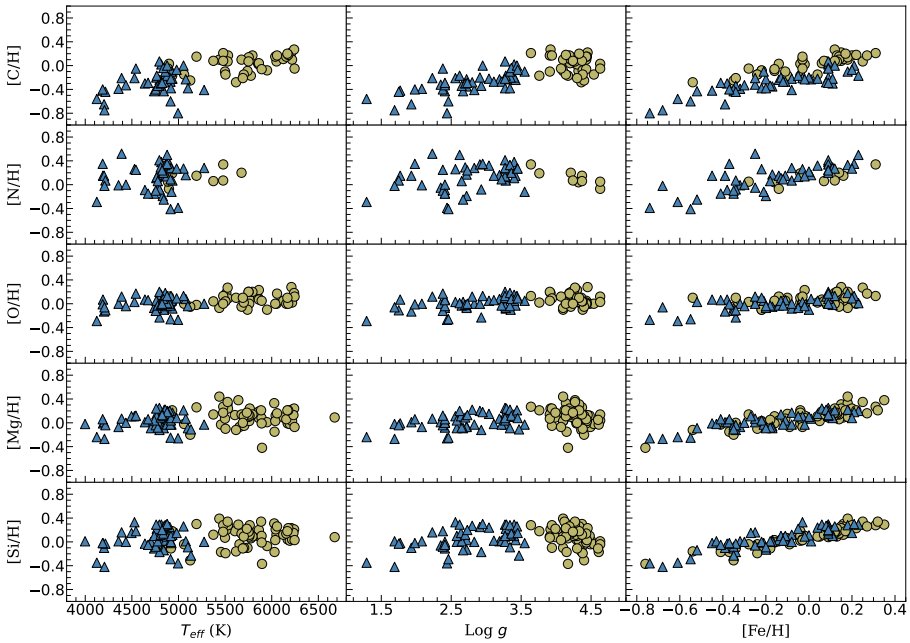

Figure 5: [X/H] abundance ratios for carbon, nitrogen, oxygen, magnesium, and silicon as functions of atmospheric parameters for the analysed planet-host stars. Dwarfs and giants are represented by circles and triangles, respectively.

Figures 5 and 6 show the abundance trends of all species studied in this work as functions of effective temperature ($T_{\rm eff}$), surface gravity ($\log g$), and metallicity ([Fe/H]). Dwarf and giant stars are represented by circles and triangles, respectively. In Fig. 6, the abundances of Sr, Y,

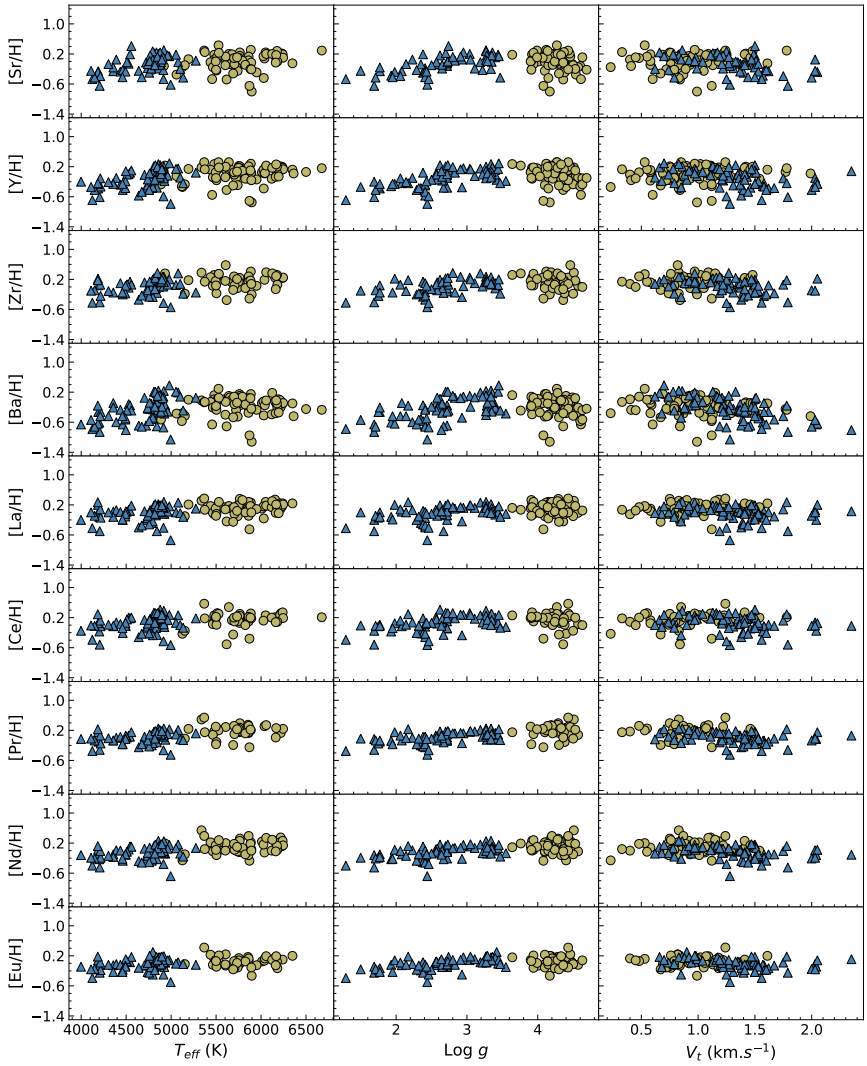

Figure 6: [X/H] abundance ratios for n-capture elements as functions of atmospheric parameters for the analysed planet-host stars. Symbols have the same meaning as in Fig. 5

Ba, and Eu include non-LTE corrections. The primary motivation was to evaluate whether there are systematic biases or trends in elemental abundances as a function of atmospheric parameters, which could potentially affect the interpretation of chemical patterns in PHS.

As expected, no significant systematic trends with $T_{\rm eff}$ or $\log g$ are observed within the parameter space covered, except for the expected stellar evolution effects, visible in the subplots of carbon and nitrogen,

particularly with decreasing $\log g$, which is consistent with post-main-sequence mixing processes in evolved stars.

2.5 Stellar kinematics and ages

The kinematic behaviour of stars in the Galaxy, together with their orbital properties and ages, plays an important role in shaping the spatial distribution and architectures of planetary systems across the Galaxy (Adibekyan et al. 2021). A detailed analysis of stellar kinematics and orbital parameters enables the reconstruction of stellar dynamical histories and allows us to probabilistically associate stars with distinct Galactic components, such as the thin and thick discs. In this study, we analyse the kinematic properties, orbital parameters, as well as ages of PHS in order to characterise their dynamical histories, age distribution, and Galactic disc membership.

We determined the Galactic space velocities (U, V, W), mean galactocentric distance, $R_{\rm mean}$, maximum vertical distance from the Galactic plane, $|z_{\rm max}|$, and orbital eccentricities, e, for each star. These quantities were calculated using the Python-based package for galactic-dynamics calculations, *galpy* [2] (Bovy 2015). The input data for the orbital calculations were sourced from the literature. Stellar distances were taken from Bailer-Jones et al. (2021) while other stellar parameters, such as proper motions and stellar coordinates, were taken from the *Gaia* data release 3 (EDR3) catalogue (Gaia Collaboration et al. 2016, 2021; Lindegren et al. 2021; Seabroke et al. 2021). These parameters were combined with precise radial velocities derived from our own spectroscopic analysis. For the star HD 62509 (V = 1.14 mag), which is not included in the *Gaia* EDR3 catalogue, the necessary astrometric data were taken from the Hipparcos catalogue (van Leeuwen 2007).

Using these inputs, we transformed the stellar positions and velocities from equatorial to Galactocentric coordinates, correcting for the solar motion relative to the local standard of rest (LSR). We adopted standard values for the Sun's position and motion from Bovy et al. (2012) ($R_{\rm gc\odot} =$ 8 kpc and $V_\odot = 220$ km s^{-1}), the vertical distance from the Galactic plane $z_\odot = 0.02$ kpc from Joshi (2007), and the LSR velocities from

[2] http://github.com/jobovy/galpy

Schönrich et al. (2010) (*U, V, W* = 11.1, 12.24, 7.25 $\mathrm{km\,s^{-1}}$). We then computed the Galactic orbits of the stars using *galpy*, adopting the *MilkyWayPotential2014* model. Each star's orbit was numerically integrated over a 5 Gyr timescale to trace its motion forward in time to capture its full range of dynamical behaviour. From these integrated orbits, we extracted the space velocities and orbital parameters of the stars.

To account for uncertainties in the derived kinematic parameters, we ran 1 000 Monte Carlo simulations for each star. In each simulation, the input astrometric and radial velocity values were randomly perturbed within their errors, assuming Gaussian distributions. The standard deviation in the resulting orbital parameters from these simulations was adopted as the uncertainty in each corresponding measurement. The kinematic parameters, along with their corresponding error values, for the sample of 25 PHS analysed in Paper I are available in machine-readable form at the CDS via https://cdsarc.cds.unistra.fr/viz-bin/cat/J/ApJS/259/45. Similarly, the parameters for the additional 124 stars included in Paper II are also accessible in machine-readable form at the CDS via https://cdsarc.cds.unistra.fr/viz-bin/cat/J/A+A/691/A160.

Once we have determined the galactic space velocities *U, V, W* for our stellar sample, we classified the stars into Galactic thin and thick disc populations based on the probabilistic approach described by Bensby et al. (2003, 2014). This method evaluates the probability of a star belonging to the thick disc relative to the thin disc based on its space velocity components, corrected for the solar motion. Using the previously calculated space velocity components, we computed the thick-to-thin disc probability ratio (TD/D) for each star. The probabilities were calculated assuming Gaussian velocity distributions, *f(U, V, W)*, for each Galactic component defined by their characteristic velocity dispersions and asymmetric drifts:

$$f(U,\,V,\,W) = k \cdot \exp\left(-\frac{U_{\mathrm{LSR}}^2}{2\sigma_U^2} - \frac{(V_{\mathrm{LSR}} - V_{\mathrm{asym}})^2}{2\sigma_V^2} - \frac{W_{\mathrm{LSR}}^2}{2\sigma_W^2} \right) \quad (4)$$

where,

$$k = \frac{1}{(2\pi)^{3/2}\,\sigma_U\,\sigma_V\,\sigma_W} \tag{5}$$

Here, k is the normalisation constant. σ_U, σ_V, σ_W are the characteristic velocity dispersions, and $V_{\rm asym}$ is the asymmetric drift. The specific values adopted for these parameters in the thin and thick disc populations, which define the Gaussian velocity distribution functions used in the probability calculations, are listed in Table 3.

Table 3: Adopted Gaussian velocity distribution parameters for the thin and thick disc populations used in the probability calculations, following the method of Bensby et al. (2003).

Population	σ_U (km s^{-1})	σ_V (km s^{-1})	σ_W (km s^{-1})	$V_{\rm asym}$ (km s^{-1})
Thin disc (D)	35	20	16	−15
Thick disc (TD)	67	38	35	−46

Once the Gaussian velocity distribution functions for the thin and thick disc populations were defined, we computed the likelihoods $P_{\rm thin}$ and $P_{\rm thick}$ for each star using its LSR-corrected Galactic velocities *(U, V, W)*. Each probability was calculated by multiplying the corresponding distribution function *f(U, V, W)* with the local stellar density normalisation factor X, adopted as 0.94 for the thin disc and 0.06 for the thick disc (Bensby et al. 2003). The thick-to-thin disc probability ratio for each star was then obtained using:

$$\mathrm{TD/D} = \frac{P_{\rm thick}}{P_{\rm thin}} = \frac{X_{\rm thick}\cdot f_{\rm thick}(U,V,W)}{X_{\rm thin}\cdot f_{\rm thin}(U,V,W)}. \tag{6}$$

This TD/D ratio quantifies the relative likelihood that a star belongs to the thick disc compared to the thin disc. Based on the resulting TD/D values, we assigned each star to a Galactic component using the methodology of Bensby et al. (2003). Stars with TD/D ≤ 0.2 were classified as thin disc members, those with TD/D ≥ 5 were considered thick disc stars, and stars with intermediate values ($0.2 \leq$ TD/D ≤ 5) were assigned to the in-between sample.

To visually assess the kinematic classification of our stars, we con-

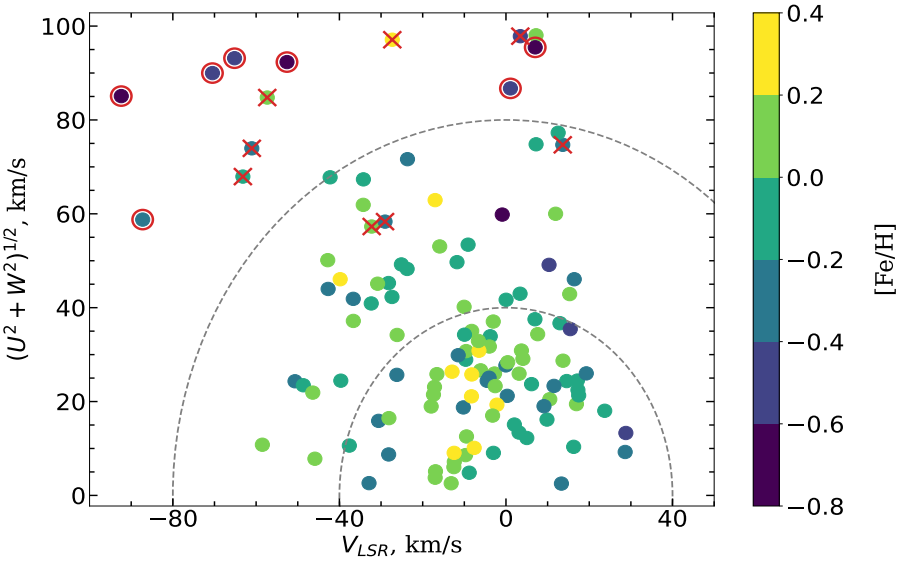

Figure 7: Toomre diagram for the analysed stars, with symbols colour-coded by metallicity [Fe/H]. The diagram displays the combined transverse velocity, $(U^2+W^2)^{1/2}$, plotted against the rotational velocity relative to the Local Standard of Rest, $V_{\rm LSR}$. Dashed curves represent contours of constant total space velocity ($v_{\rm tot} = (U^2_{\rm LSR} + V^2_{\rm LSR} + W^2_{\rm LSR})^{1/2)}$) at 40 and 80 km s^{-1}. Stars outlined in red correspond to thick-disc members, while crosses mark intermediate thin/thick-disc stars.

structed a Toomre diagram (see Fig. 7) that allows us to explore the kinematic properties of stars in a 2D space defined by their Galactic space velocities. Specifically, we plot the combined transverse velocity in the U and W directions, $\sqrt{U^2+W^2}$, against the rotational velocity component relative to the local standard of rest, $V_{\rm LSR}$. This representation helps distinguish stars belonging to different Galactic components based on their kinematic energy and lag in rotation.

Thin disc stars typically cluster near the origin, with low transverse velocities and small asymmetric drift, while thick disc stars occupy regions with higher total velocities and more negative $V_{\rm LSR}$. We overplot contours of constant total space velocity, $v_{\rm tot} = (U^2_{\rm LSR} + V^2_{\rm LSR} + W^2_{\rm LSR})^{1/2}$, to aid interpretation. In our sample, the majority of planet-hosting stars lie within the $v_{\rm tot} < 50$ km s^{-1} region, consistent with thin disc kinematics, whereas the kinematically selected thick disc stars (shown as red circles) have total space velocities exceeding 80 km s^{-1}.

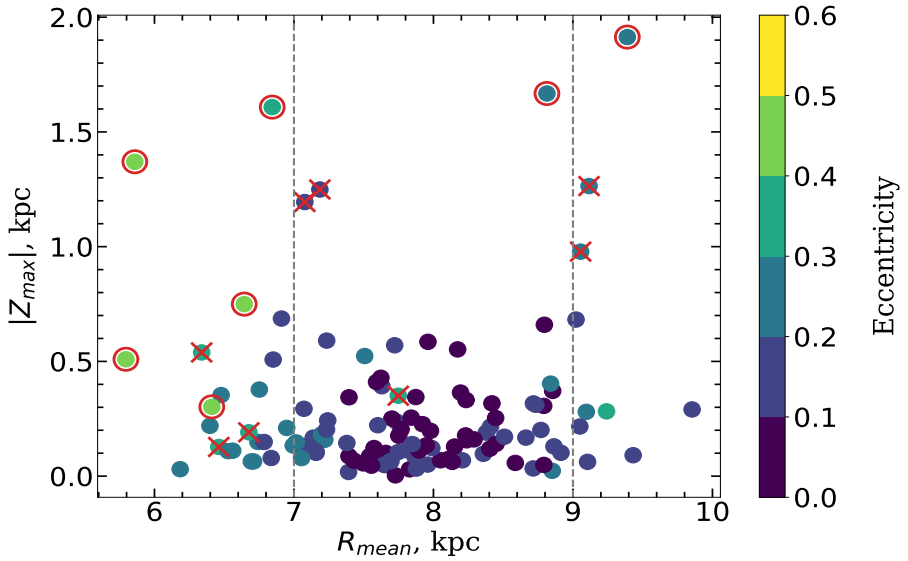

Figure 8: Mean Galactocentric distance ($R_{\rm mean}$) versus maximum Galactic height $|z_{\rm max}|$ for the observed stars, colour-coded by their orbital eccentricity. The vertical dashed lines mark the Solar neighbourhood ($7< R_{\rm mean} <9$ kpc).

Figure 8 represents the distribution of stars in the $|z_{\rm max}|$ versus $R_{\rm mean}$ plane, colour-coded by eccentricity. The two vertical dashed lines on the plot serve as boundaries demonstrating the region of the solar neighbourhood with $7< R_{\rm mean} < 9$ kpc. Stars with outer red circles here represent thick-disc members, while crosses indicate intermediate (thin to thick-disc) stars.

For stellar age determinations, we used the unified tool to estimate ages, masses and distances (UniDAM; Mints & Hekker 2017, 2018), which employs a Bayesian approach to match observed stellar parameters to theoretical isochrones. UniDAM uses PARSEC isochrones (Bressan et al. 2012) along with spectroscopic and photometric inputs to derive stellar ages and associated uncertainties. As input, we used spectroscopically determined stellar atmospheric parameters derived in this work, along with infrared photometry. The photometric data included J, H, and K magnitudes from the Two Micron All Sky Survey (2MASS; Skrutskie et al. 2006) and $W1$ and $W2$ magnitudes from the AllWISE catalogue (Cutri et al. 2021).

UniDAM compares the input parameters to the grid of PARSEC

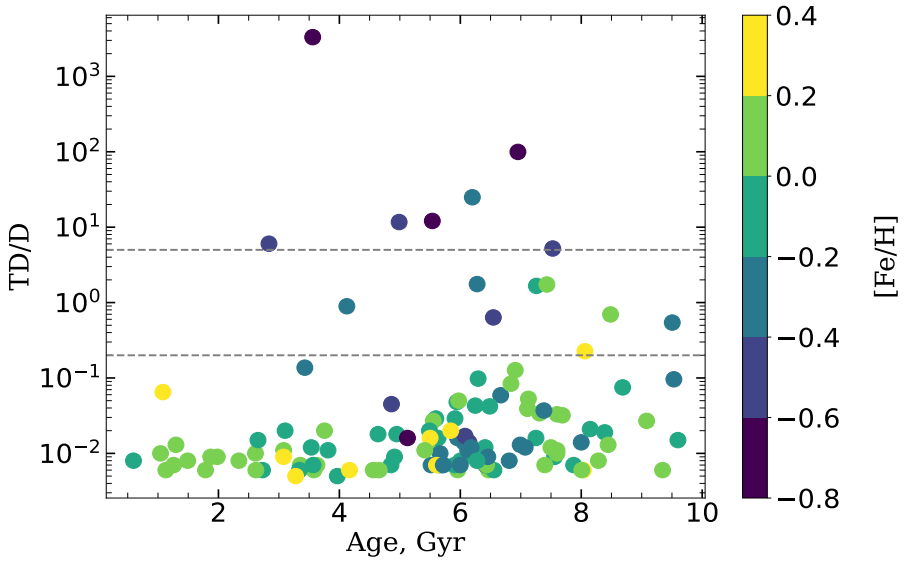

Figure 9: Stellar age versus kinematic thick-to-thin disc probability ratio (TD/D), with symbols colour-coded by metallicity [Fe/H]. The vertical dashed lines separate the boundaries between thin-disc, thick-disc, and intermediate populations.

isochrones and computes posterior probability distributions for the stellar parameters using a Bayesian framework. The output includes the most probable age, as well as confidence intervals that reflect the uncertainty in the derived age. We note that UniDAM assumes a scaled-solar abundance pattern, which may introduce biases in age estimates for stars with non-solar abundance ratios, particularly for α-enhanced thick disc stars.

Ages were successfully determined for the majority of stars in our sample, with typical uncertainties ranging from 10% to 30%, depending on evolutionary stage and data quality. The derived stellar ages are used in subsequent analyses to examine the temporal distribution of planet-hosting stars and to explore trends in chemical and kinematic properties across stellar lifetimes. It is known that the thin disc is generally younger and contains a higher proportion of young stars than the thick disc (Gilmore & Wyse 1985). To examine the relationship between stellar kinematics and their ages, we plot the kinematic thick-to-thin disc probability ratio (TD/D) against stellar ages in Fig. 9. Each point is colour-coded by the star's [Fe/H]. We see that the metal-rich

hosts show thin disc-like kinematics.

2.6 Planets in our sample

The discovery and characterisation of exoplanets rely on a suite of observational techniques, each of which is particularly sensitive to specific planetary properties and orbital configurations. The two most prolific methods to date: radial velocity (RV) and transit photometry, have collectively identified the majority of known exoplanets, while complementary approaches such as direct imaging, microlensing, and astrometry extend detection capabilities to otherwise inaccessible parameter spaces.

The radial velocity method measures the Doppler shifts in stellar spectral lines induced by the gravitational pull of an orbiting planet (Mayor & Queloz 1995; Butler et al. 1996). This technique is most sensitive to massive planets in close orbits around bright, slowly rotating stars, providing precise measurements of orbital periods, eccentricities, and minimum planet masses. Continued instrumental advances such as stabilised spectrographs like HARPS (Pepe et al. 2000), ESPRESSO (Pepe et al. 2014) allow detection thresholds approaching the Earth-mass regime.

Transit photometry, in contrast, detects the periodic dimming of starlight as a planet passes across its host star's disk (Charbonneau et al. 2000; Henry et al. 2000). This method provides planetary radii and, when combined with RV data, bulk densities that constrain internal compositions. Space-based missions such as Kepler and TESS have revolutionised the field by yielding statistically complete samples of thousands of transiting planets, enabling robust population studies of planetary size and orbital distributions (Borucki et al. 2010; Ricker et al. 2015).

Beyond these dominant techniques, direct imaging isolates thermal or reflected light from young, self-luminous giant planets at wide separations (Marois et al. 2008; Bowler 2016), offering crucial insights into atmospheric properties and formation environments. Gravitational microlensing, based on the temporary amplification of a background star's light by a foreground planetary system, is uniquely sensitive to low-mass planets at several astronomical units from their stars, even in distant Galactic fields (Bond et al. 2004; Gaudi 2012). Finally, as-

trometric methods such as those employed by *Gaia* detect the minute positional wobble of stars due to orbiting planets, providing direct mass measurements without inclination degeneracies (Perryman et al. 2014).

Each detection technique is subject to distinct biases: RV and transit surveys favour short-period planets, imaging targets young and massive systems, and microlensing detects planets at intermediate distances but rarely allows follow-up.

Our full stellar sample comprises 160 confirmed planet-hosting stars, collectively hosting 222 detected exoplanets. These systems span a broad range of planetary masses and architectures, from super-Earths to massive gas giants, providing a diverse testbed for investigating potential chemical and evolutionary signatures associated with planet formation. Among the 160 stars, 34 host multiple planets, with several systems containing up to five confirmed companions. Majority of planets in our sample detected via RV measurements.

Table 4: Table displaying planetary parameters for stars in our sample. The parameters are taken from NASA exoplanet archive.

Star ID	Planet ID	Planet Mass, M_p (M_E)	Orbital Period, P (days)	Semi Major Axis, a (au)	Ref.[(1)]
1949-2012-1	55 Cnc b	267.0	14.65171	0.11620	[1]
	55 Cnc c	54.4	44.38270	0.24320	[1]
	55 Cnc d	909.0	4820.00000	5.54000	[1]
	55 Cnc e	9.4	0.73654	0.01583	[1]
	55 Cnc f	46.9	260.98000	0.79200	[1]
...	...	...	...	...	...

References. [(1)] Planetary parameters references: [1] - Rosenthal et al. (2021).

The planetary parameters for the analysed star-planet systems, including planetary masses relative to Earth mass M_p/M_e, orbital period P, and semi-major axes a, were compiled primarily from the NASA Exoplanet Archive[3]. Of these systems, the parameters for 149 star-planet pairs analysed in Paper I and Paper II are summarised in Table 4, with the complete dataset provided in its entirety through CDS via https://cdsarc.cds.unistra.fr/viz-bin/cat/J/A+A/691/A160. Parameters for

[3] https://exoplanetarchive.ipac.caltech.edu/

Table 5: Planetary characteristics of eleven additional stars. The remaining sample was published in Paper II.

Host TYC ID	Planet	Planet Mass ($M_{\rm Jupiter}$)	Orbital Period (days)	Semi Major Axis (au)	Ref.
3131-1036-1	HD 175370 b	4.60	349.5	0.98	[1]
3500-1780-1	HD 153557 Ab	0.064	7.3	0.068	[2]
3500-1780-1	HD 153557 Ac	0.055	15.3	0.111	[2]
3568-2325-1	HD 184960 b	0.0384	3.4982	0.04853	[3]
4191-2696-1	HD 154391 b	9.10	5163.0	7.46	[4]
4405-1859-1	HD 118904 Ab	3.10	676.7	1.70	[5]
4425-567-1	HD 150010 Ab	2.40	562.0	1.40	[6]
4434-2189-1	HD 174205 b	4.20	582.0	1.70	[6]
4436-1423-1	HD 161178 b	0.57	279.3	0.84	[7]
4464-1666-1	HD 202432 b	1.90	418.8	1.20	[5]
4534-1837-1	HD 46588 b	0.25	223.0	–	[8]
4573-1915-1	HD 164428 b	5.70	599.6	1.60	[5]

References. [1] - Hrudková et al. (2017). [2] - Feng et al. (2022). [3] - Barnes et al. (2023). [4] - Xiao et al. (2024). [5] - Jeong et al. (2018). [6] - Jeong et al. (2022). [7] - Teng et al. (2022). [8] - Šubjak et al. (2023).

an additional 11 systems from Paper III are presented in Table 5. For detailed information on the uncertainties associated with the planetary parameter values, please refer to the NASA Exoplanet Archive.

Figure 10 shows the distribution of planetary mass as a function of orbital period for all confirmed planets in our sample, colour-coded by planet type. The planets span orbital periods from less than one day to several thousand days and cover a wide mass range, from super-Earths and Neptune-like planets to massive gas giants. For multi-planet systems, each confirmed companion is shown individually. Most super-Earth and Neptune-like planets in our sample are concentrated at short orbital periods, while massive gas giants are at much longer periods, typically beyond 100 days and often exceeding 1000 days. This distribution aligns with planet formation theory, wherein massive gas giants are expected to form beyond the ice line at several astronomical units and migrate inward only in select cases. The absence of low-mass planets at long

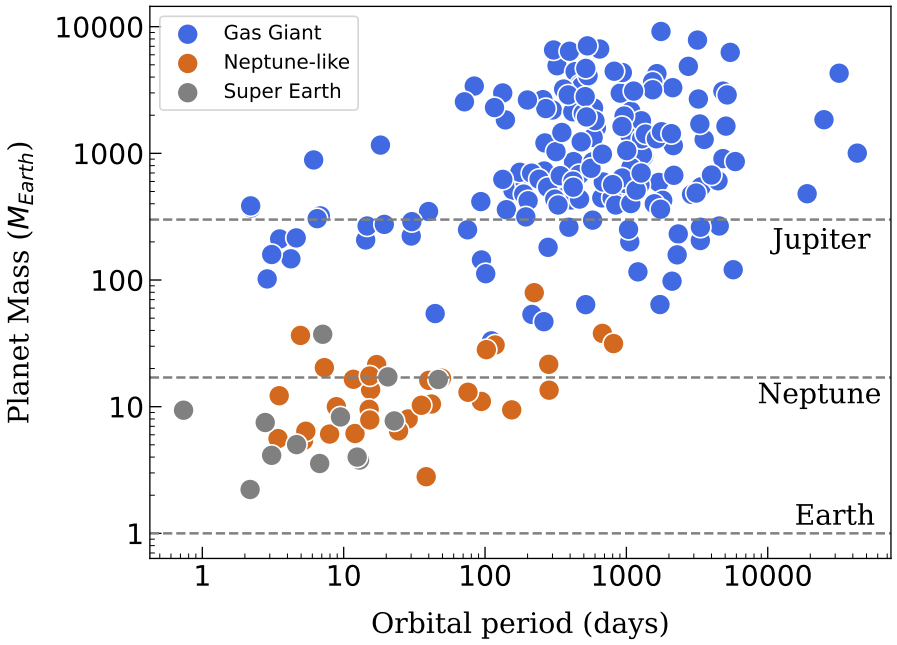

Figure 10: Planetary mass plotted against orbital period for all confirmed planets in the sample. Data points are colour-coded by planet type (super-Earths, Neptune-like, and gas giants). Reference lines corresponding to the masses of Earth, Neptune, and Jupiter are shown for comparison.

periods in our sample likely reflects a detection bias, especially in radial velocity and transit surveys, which are more sensitive to short-period planets. Conversely, the scarcity of high-mass planets at very short periods underscores the rarity of hot Jupiters in the overall population.

3 Implications of light elements in planet-host stars

In this section, I present the main results of our detailed abundance analysis of light elements: carbon, nitrogen, oxygen, magnesium, and silicon in 149 F-, G-, and K-type PHS. The aim is to investigate whether the chemical abundances of these elements exhibit signatures associated with planet formation, particularly through their potential correlations with stellar metallicity [Fe/H]. By comparing the PHS with a carefully selected control sample of stars without detected planets, we further examine whether distinct abundance patterns emerge that could serve as chemical markers of planetary systems. This discussion also explores how abundance trends vary between dwarfs and giants, across different Galactic components, and in relation to planet multiplicity, offering insights into both stellar evolution and the processes that shape planetary system architectures.

3.1 [(C; N; O)/Fe] abundance trends with [Fe/H]

Carbon, nitrogen, and oxygen are the dominant light elements in stellar atmospheres and are key tracers of both Galactic chemical evolution and the chemical environments of protoplanetary disks. By examining their abundance ratios relative to iron across the metallicity range, we aim to identify systematic differences between dwarfs and giants, assess evolutionary mixing effects, and compare PHS with field stars of similar properties. This approach allows us to test whether the presence of planets leaves measurable chemical signatures in the CNO abundances of host stars.

Figure 11 presents the abundance ratios [C/Fe], [N/Fe], and [O/Fe], along with the derived C/O[4] and N/O ratios, as functions of metallicity for our sample of planet hosts. The figure is divided into left and right panels for dwarfs and giants, respectively, to highlight evolutionary differences. PHS from the thin and thick discs are indicated using green and pink markers, respectively, with transitional ("in-between") stars marked by symbols filled with both colours. Results for PHS published in Paper I are shown as coloured diamonds, while the comparison sample

[4]C/O is defined as N_C/N_O, where N_C and N_O are the number densities of carbon and oxygen nuclei, respectively.

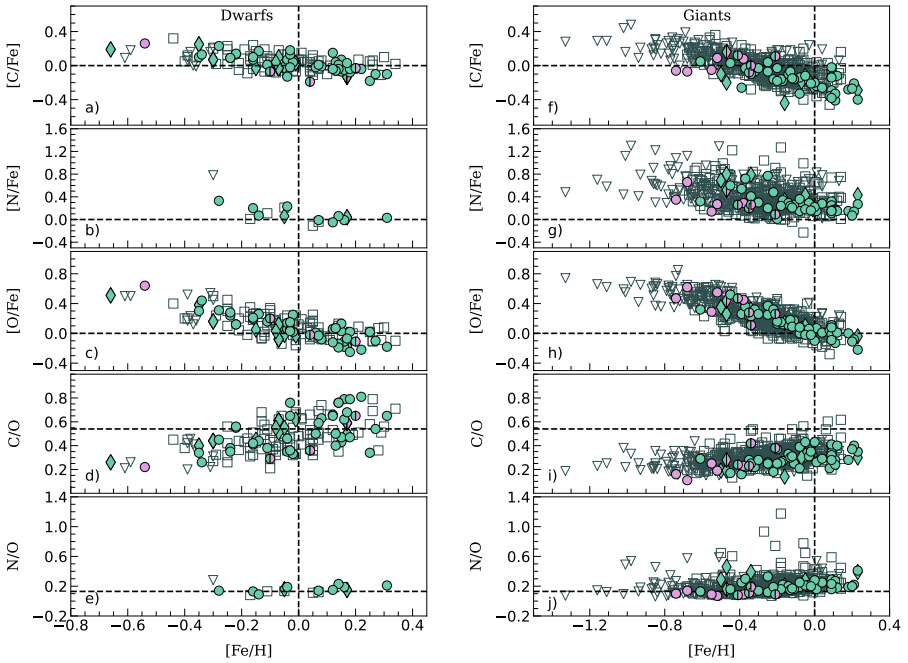

Figure 11: [X/Fe] abundance ratios for carbon, nitrogen, and oxygen, together with derived C/O and N/O ratios as functions of metallicity [Fe/H] for planet-host stars. The left and right panels show dwarfs and giants, respectively. Thin- and thick-disc stars are indicated in green and pink, and transitional stars are shown with mixed-colour symbols. Planet hosts from Paper I are represented by diamond symbols. Comparison sample without detected planets, taken from Stonkutė et al. (2020) and Paper I, is plotted in grey empty squares (thin disc) and triangles (thick disc).

of stars without detected planets is taken from Stonkutė et al. (2020) and Paper I, and plotted with grey squares (thin disc) and triangles (thick disc).

This figure enables a direct visual comparison between the chemical signatures of stars with and without planets, across evolutionary stages and Galactic populations. As mentioned in Sec. 2.5, the majority of our sample stars have thin-disc kinematics.

Among dwarf stars, both the [C/Fe] and [O/Fe] ratios show a clear decreasing trend with increasing [Fe/H], consistent with expectations from Galactic chemical evolution. Carbon and oxygen, produced primarily in short-lived massive stars and released into the interstellar medium (ISM) through core-collapse supernovae (SN II), were abundant in the

early Galaxy relative to iron, which is predominantly synthesised in Type Ia supernovae on longer timescales. As a result, [C/Fe] and [O/Fe] are enhanced at low metallicities and gradually decline with increasing [Fe/H] as iron production from Type Ia supernovae becomes dominant (Kobayashi et al. 2020). At low metallicities ([Fe/H] $\leq$ 0), both [C/Fe] and [O/Fe] are slightly supersolar, whereas at solar and super-solar metallicities, they decline to near or subsolar values.

At the metal-rich end, planet-hosting dwarfs exhibit slightly lower [C/Fe] values compared to non-hosts although the difference is modest and insufficient to serve as a clear chemical signature of planet presence. Importantly, no clear evidence of carbon or oxygen overabundance is observed among these stars; however, the limited statistics of this subsample prevents drawing firm conclusions about the presence or absence of a planet-formation-related enhancement.

The C and O abundances for the dwarf stars in our sample are in general agreement, within uncertainties, with earlier studies (Suárez-Andrés et al. 2017, 2018; Stonkutė et al. 2020; Unni et al. 2022). At the metal-rich end of the distribution, however, our carbon measurements exhibit a different behaviour compared to Suárez-Andrés et al. (2017). This discrepancy is likely related to differences in the choice of carbon lines or methodologies. Despite these differences, the overall consistency across studies supports the robustness of the abundance patterns and reinforces their relevance for tracing Galactic chemical evolution.

Nitrogen abundances exhibit more complex behaviour than carbon and oxygen due to the diversity of production channels and the challenges of observational determination.

In dwarfs, [N/Fe] remains close to the solar value across the metallicity range, with a slight increase at subsolar [Fe/H]. However, the small number of reliable nitrogen measurements, owing to weak CN features in warmer spectra, limits the robustness of this trend. Nevertheless, our findings are consistent with earlier work by Ecuvillon et al. (2004a), who reported similar [N/Fe] vs [Fe/H] behaviour for planet-hosting and comparison stars. While Suárez-Andrés et al. (2016) suggested that planet hosts appear nitrogen-rich compared to single stars, they attributed this difference to the overall metal-rich nature of host stars, since [N/Fe] increases linearly with [Fe/H]. Given these considerations, we empha-

sise the need for more extensive and homogeneous nitrogen abundance measurements to better understand the chemical behaviour of nitrogen in planet-hosting systems. Overall, our results do not indicate any nitrogen enhancement that can be attributed to the presence of planets, suggesting that, like carbon and oxygen, nitrogen abundances in stellar atmospheres are governed primarily by intrinsic stellar and Galactic processes.

In giants, [C/Fe] is systematically lower than in dwarfs by about 0.2 dex at a given [Fe/H]. This depletion is attributed to the first dredge-up mixing, which brings CN-processed material to the stellar surface and reduces the observable carbon abundance (e.g., Lagarde et al. 2019). In contrast, [N/Fe] in giants is enhanced by $+0.2$ dex, reflecting the internal conversion of carbon into nitrogen via CN cycling. The overall [C/Fe] and [N/Fe] trends with metallicity in giant stars are similar to those observed in the comparison sample. However, the scatter in [C/Fe] among giant stars with planets is somewhat smaller than in dwarfs, and the carbon abundances are on average lower at a given metallicity, than in the comparison sample.

Oxygen, being largely unaffected by mixing processes, shows consistent [O/Fe] distributions in both dwarfs and giants, with no systematic difference between planet hosts and non-hosts. Our oxygen abundances were derived using the forbidden [O I] 6300 Å line, which forms under LTE and is largely insensitive to NLTE effects (Amarsi et al. 2021).

To complement the discussion of elemental abundance trends, we have colour-coded our giant stars with their ages and masses, both determined in this work. Figure 12 presents the distributions of [C/Fe], [N/Fe], and [O/Fe] elemental abundances together with the derived C/O and N/O ratios as a function of overall metallicity, [Fe/H], for the sample of giant stars hosting planets. The left-hand panel shows the data colour-coded by stellar age, whereas the right-hand panel displays the same quantities colour-coded by stellar mass. The figure highlights how the stellar parameters contributing to the observed chemical patterns vary across the metallicity range.

The age-coloured panel reveals that metal-poor giants tend to be systematically older, whereas metal-rich giants are predominantly younger, consistent with the expected time evolution of Galactic chemical enrichment. The mass-coloured panel shows a complementary trend: stars with

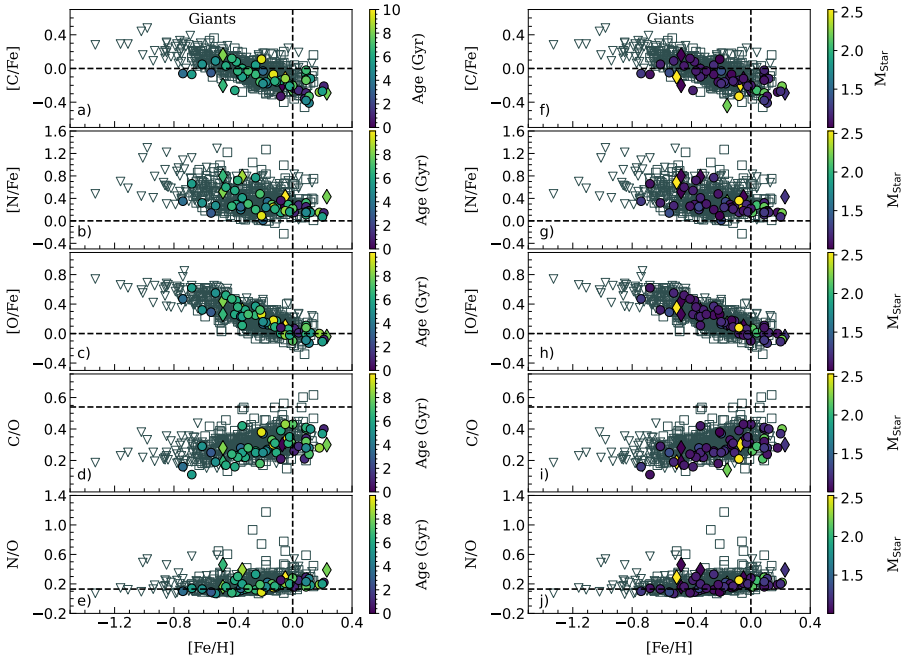

Figure 12: [X/Fe] abundance ratios for carbon, nitrogen, and oxygen, together with derived C/O and N/O ratios as functions of metallicity [Fe/H] for observed giant stars. The left-hand panel shows stars colour-coded by stellar age, and the right-hand panel by stellar mass. All symbol shapes have the same meaning as in Fig. 11.

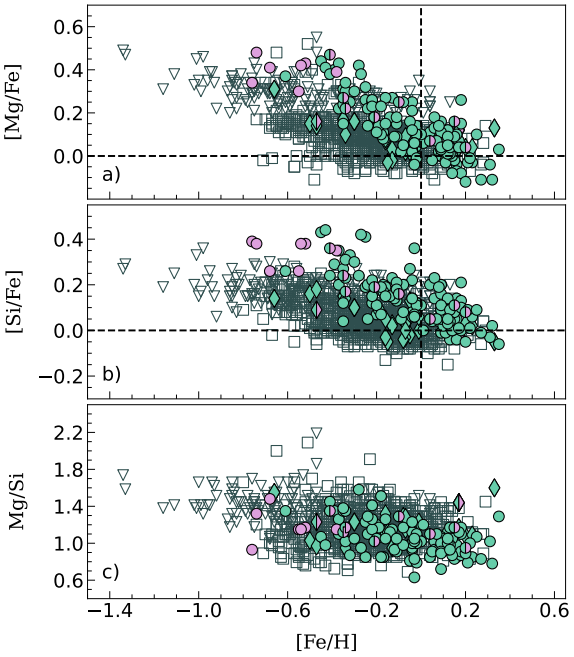

Figure 13: [X/Fe] abundance ratios for magnesium and silicon, together with derived Mg/Si ratio as functions of metallicity [Fe/H] for all observed stars. All symbols follow the same convention as in Fig. 11. The comparison data (empty grey squares for thin-disc and triangles for thick-disc) are from Mikolaitis et al. (2019) and Paper I.

higher metallicities generally exhibit higher stellar masses, reflecting the correlation between mass and evolutionary timescale in the sampled population.

3.2 [(Mg; Si)/Fe] abundance trends with [Fe/H]

To examine the behaviour of α-elements in our PHS, we analysed the [Mg/Fe], [Si/Fe], and Mg/Si ratios as functions of [Fe/H], as shown in Fig. 13. The same symbol scheme is used as in Fig. 11, and the results are compared with the comparison stars taken from Mikolaitis et al. (2019) and Paper I. This enables a direct comparison of chemical trends between planet-hosting and comparison stars.

Magnesium and silicon, both α-elements produced predominantly in Type II supernovae, follow the expected chemical evolution trend of [α/Fe]: higher values at low metallicities and a gradual decline at higher

metallicities. In our sample, both [Mg/Fe] and [Si/Fe] are enhanced in metal-poor stars and decrease steadily with increasing [Fe/H], reaching near-solar values at [Fe/H] $\gtrsim 0$. These patterns are consistent with those in the comparison stars and with previous studies of field stars (e.g. Adibekyan et al. 2012a; Bensby et al. 2014).

We also find an overabundance of both Mg and Si in PHS relative to comparison stars, particularly at lower metallicities. This overabundance is most prominent at [Fe/H] $\lesssim$ –0.1. This suggests that α-element abundances may facilitate planet formation in environments where iron content is relatively low. At solar and super-solar metallicities, PHS and non-PHS display largely overlapping α-element distributions.

Overall, our results support the idea that higher α-element abundances, particularly magnesium and silicon, can compensate for reduced iron content in the planet formation process. This suggests that while metallicity is an important factor in planet occurrence, other chemical pathways may also enhance the efficiency of planet formation. Our finding of modest Mg and Si overabundances in planet hosts at subsolar metallicities is consistent with earlier works (e.g., Haywood 2008; Adibekyan et al. 2012a), which have shown that α-rich stars are able to form planets even in iron-poor environments. In this sense, Mg and Si abundances may provide an alternative indicator of planet formation potential in regions of the Galaxy where iron enrichment is relatively low.

3.3 C/O, N/O, and Mg/Si ratios in planet-host stars

Elemental abundance ratios such as carbon-to-oxygen (C/O), nitrogen-to-oxygen (N/O), and magnesium-to-silicon (Mg/Si) are of particular interest in exploring the connection between stars and planets, as they directly bridge stellar chemistry to the mineralogy and volatile content of exoplanetary systems.

These ratios control the condensation sequence in protoplanetary disks and can strongly influence the interior and atmospheric compositions of planets. For instance, the C/O ratio sets the balance between carbides and oxides in planet-building material (Bond et al. 2010; Madhusudhan et al. 2012). A higher C/O ratio may increase the likelihood of forming carbon-rich compounds, including organic molecules, and could

influence the habitability and atmospheric characteristics of terrestrial planets. The N/O ratio constrains the volatile nitrogen budget available for icy planetesimals (Sahu et al. 2025).

The Mg/Si ratio determines the relative proportions of olivine and pyroxene in silicate mantles of terrestrial planets (Bond et al. 2010; Suárez-Andrés et al. 2018). Higher Mg/Si values favour the formation of magnesium-rich minerals, leading to denser, rocky planets, while lower Mg/Si values result in silicon-dominated compositions with potentially more volatile-rich or less dense structures.

3.3.1 Metallicity trends and comparison to non-hosts

The C/O and N/O abundance ratios as functions of metallicity are shown in Fig.11, alongside the trends of [C/Fe], [N/Fe], and [O/Fe]. The C/O ratio in dwarfs follows an increasing trend with some scatter across the whole metallicity range. No significant difference is observed between the C/O values of planet-hosting dwarfs and comparison stars in our sample. In giants, evolutionary mixing leads to systematically lower C/O ratios than in dwarfs, with a typical offset of 0.25 dex. Giant PHS exhibit, on average, lower C/O ratios than the comparison giants, and the scatter is smaller among hosts.

Importantly, all PHS in our sample show C/O < 0.8, consistent with previous studies (e.g., Delgado Mena et al. 2010; Suárez-Andrés et al. 2017), indicating that planet formation likely occurred in oxygen-rich environments. This suggests that silicate- and metal-dominated planets are more typical around these stars, as C/O > 0.8 is generally considered a prerequisite for forming carbon-rich planets.

The N/O ratio exhibits a relatively flat distribution in dwarfs, remaining close to the solar value across the metallicity range, with only a slight indication of an increase at higher [Fe/H]. The statistical significance of this trend, however, is limited by the small number of reliable nitrogen measurements. In contrast, giant stars display a clear increase in N/O with [Fe/H], systematically exceeding the values observed in dwarfs. This offset, typically on the order of 0.2-0.3 dex, reflects the effects of CN-cycle mixing. At a given metallicity, no significant difference is observed between planet-hosting and comparison giants, although the former show a more coherent distribution with noticeably reduced

scatter.

Figure 13 shows the Mg/Si abundance trend with [Fe/H], together with the corresponding [Mg/Fe] and [Si/Fe] relations. The Mg/Si ratio decreases with increasing metallicity, in agreement with expectations from Galactic chemical evolution (Adibekyan et al. 2012a; Delgado Mena et al. 2018). At a given [Fe/H], stars hosting planets tend to exhibit, on average, slightly lower Mg/Si ratios compared to the comparison sample.

3.3.2 Low mass vs high mass planet hosts: Statistical tests

To analyse whether the elemental ratios C/O, N/O, and Mg/Si differ between stars with planets and the comparison sample, we carried out two-sided Kolmogorov-Smirnov (K-S) and Anderson-Darling (A-D) tests. Within the planet-host sample, stars were further divided into two groups based on the masses of their companions: hosts of low-mass planets ($M_{\rm p} < 30 M_{\oplus}$) and hosts of high-mass planets ($M_{\rm p} > 30 M_{\oplus}$). This classification is motivated by the expectation that low- and high-mass planets may trace different formation pathways and, consequently, could leave distinct chemical imprints on their host stars.

Table 6: Kolmogorov-Smirnov (K-S) statistical test results for Mg/Si and C/O elemental ratio distributions for stars with and without planetary companions.

	$\text{K-S}^{\text{Low mass}}_{\text{Whole sample}}$		$\text{K-S}^{\text{Low mass}}_{\text{Thin disc}}$		$\text{K-S}^{\text{High mass}}_{\text{Whole sample}}$		$\text{K-S}^{\text{High mass}}_{\text{Thin disc}}$	
	Statistic	p-value	Statistic	p-value	Statistic	p-value	Statistic	p-value
C/O_D	0.28	0.39	0.21	0.81	0.23	0.07	0.21	0.17
C/O_G	–	–	–	–	0.22	0.01	0.22	0.02
N/O_G	–	–	–	–	0.11	0.49	0.20	0.06
$A(C+N+O)_G$	–	–	–	–	0.14	0.24	0.23	0.02
Mg/Si	0.19	0.55	0.23	0.38	0.30	$\leq$0.001	0.29	$\leq$0.001
With 1000 bootstrap iterations:								
C/O_D	0.38	0.20	0.34	0.34	0.25	0.13	0.24	0.20
C/O_G	–	–	–	–	0.24	0.03	0.25	0.04
N/O_G	–	–	–	–	0.16	0.21	0.22	0.09
$A(C+N+O)_G$	–	–	–	–	0.18	0.14	0.25	0.05
Mg/Si	0.27	0.30	0.29	0.27	0.31	$\leq$0.001	0.31	$\leq$0.001

Note: Here $_{\rm D}$ and $_{\rm G}$ stand for dwarf and giant stars respectively. Two-sided K-S statistics and corresponding p-values validated through 1000 bootstrap resampling iterations. The number of nitrogen abundance determinations in dwarf stars is small; hence, N/O and A(C+N+O) comparisons are not conclusive for this subsample.

Table 7: Anderson-Darling (A-D) statistical test results for Mg/Si and C/O elemental ratio distributions for stars with and without planetary companions.

	$\text{A-D}^{\text{Low mass}}_{\text{Whole sample}}$		$\text{A-D}^{\text{Low mass}}_{\text{Thin disc}}$		$\text{A-D}^{\text{High mass}}_{\text{Whole sample}}$		$\text{A-D}^{\text{High mass}}_{\text{Thin disc}}$	
	Statistic	p-value	Statistic	p-value	Statistic	p-value	Statistic	p-value
C/O_D	0.42	0.22	−0.45	≥0.25	1.71	0.06	1.07	0.12
C/O_G	–	–	–	–	4.19	0.01	3.72	0.01
N/O_G	–	–	–	–	−0.56	≥0.25	1.20	0.10
$A(C+N+O)_G$	–	–	–	–	1.15	0.11	4.41	0.01
Mg/Si	−0.42	≥0.25	0.32	≥0.25	29.82	≤0.001	24.87	≤0.001
With 1000 bootstrap iterations:								
C/O_D	1.64	0.14	0.70	0.18	3.00	0.09	2.45	0.10
C/O_G	–	–	–	–	5.72	0.02	5.31	0.03
N/O_G	–	–	–	–	0.76	0.17	2.35	0.09
$A(C+N+O)_G$	–	–	–	–	2.35	0.10	5.84	0.03
Mg/Si	0.87	0.17	1.95	0.13	31.17	≤0.001	26.15	≤0.001

Note: Here $_D$ and $_G$ stand for dwarf and giant stars respectively. Two-sided A-D statistics and p-values validated through 1000 bootstrap resampling iterations. The critical value for a 5% significance level is 1.961. Elemental C/O and N/O ratios in dwarf stars are inconclusive due to limited nitrogen measurements.

For multiplanet systems, stars were assigned to the high-mass group if all planets exceeded $30M_{\oplus}$ and to the low-mass group if all planets were below this threshold. Systems hosting both mass regimes were considered in both groups. Additionally, we examined subsamples restricted to thin-disc kinematics. The analysis was done separately for dwarfs and giants to account for evolutionary effects. The results of these statistical comparisons are summarised in Tables 6 and 7, which list the K-S and A-D test values along with the p-values, respectively.

Figure 14 shows the corresponding cumulative distributions for the C/O, N/O, and Mg/Si ratios. To ensure reliability, we performed 1 000 bootstrap resamplings, confirming the robustness of the results. In the K-S test, the p-value represents the likelihood that the two samples originate from the same parent population, with significance taken at the 5% level ($p \leq 0.05$). The A-D test, which places more weight on differences in the distribution tails, rejects the null hypothesis if the statistic exceeds the critical value (AD_{crit}) of 1.961, thereby highlighting potentially subtle deviations between planet hosts and the comparison stars.

Panel *a* of Fig. 14 compares the C/O distributions for dwarf stars,

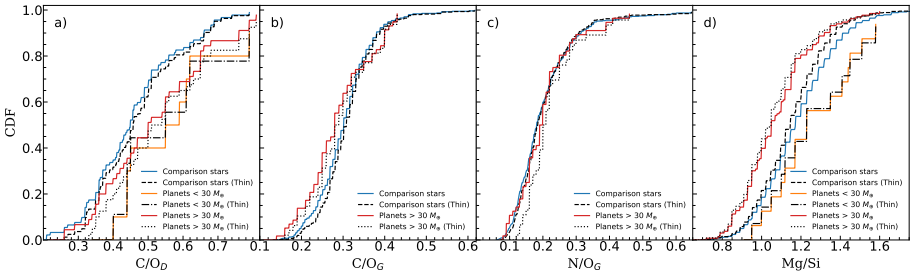

Figure 14: Cumulative distribution functions (CDFs) of elemental ratios C/O, N/O, and Mg/Si for stars with and without detected planets. Panel *a:* shows the cumulative C/O distributions for dwarfs. Solid orange and red lines represent hosts of low-mass ($M_\mathrm{p} < 30M_\oplus$) and high-mass ($M_\mathrm{p} > 30M_\oplus$) planets, respectively, while the solid blue line corresponds to comparison stars without planets. Black lines denote the corresponding thin-disc subsamples. Panels *b* and *c:* display the cumulative distributions of C/O and N/O ratios for giant stars, and panel *d:* shows the cumulative Mg/Si distributions for all stars with planetary companions compared to the control sample.

where the orange and red curves correspond to hosts of low-mass and high-mass planets, respectively, and the blue curve denotes the control sample of stars without detected planets. The corresponding thin-disc subsamples are indicated by black curves. Panels *b* and *c* display the cumulative distributions of C/O and N/O for giant stars, respectively. Panel *d* illustrates the Mg/Si distributions for the combined sample of PHS in comparison with the non-host sample.

C/O ratio in low-mass planet host. For dwarfs hosting low-mass planets, the cumulative distributions of the C/O ratio (C/O$_\mathrm{D}$) show no significant differences compared to the comparison sample (see panel *a* of Fig. 14). The K-S test yielded a statistic of 0.28 with a *p*-value of 0.39, indicating a 39% probability that both samples originate from the same distribution. Bootstrap resampling supports this result (*p*-value = 0.20). Likewise, the A-D test shows no statistically significant deviation, with a statistic of 0.42 and 1.64 after resampling. When restricting to thin-disc stars, results remain consistent (K-S statistic = 0.21, *p*-value = 0.81; A-D statistic = -0.45, *p*-value = $\geq$0.25), with bootstrap tests confirming the lack of significance.

These results suggest that the C/O ratios in dwarfs hosting low-mass planets are indistinguishable from the comparison sample. Due to the

small number of nitrogen determinations in dwarfs, the N/O ratio could not be statistically assessed in this subgroup.

C/O and N/O ratio in high-mass planet host. For dwarf stars hosting high-mass planets, both statistical tests and bootstrap resampling indicate that there is no significant deviation of the C/O_D ratio relative to the comparison sample. In contrast, giant stars exhibit a statistically significant difference in their C/O ratios (C/O_G): the K-S test yields a statistic of 0.22 (p-value = 0.01), and the A-D test likewise rejects the null hypothesis, suggesting a real distinction between giant hosts of massive planets and the comparison sample.

The N/O ratio (N/O_G) in giants hosting high-mass planets shows no significant overall difference, though a moderate level of significance emerges within the thin-disc subsample at the 5% significance level, with both the K-S and A-D tests supporting this result.

Mg/Si ratio in low- and high-mass planet hosts. The Mg/Si ratio presents the most striking contrast between low- and high-mass planet hosts. For stars with low-mass planets, the K-S (statistic = 0.19, p-value = 0.55) and A-D tests show no evidence of deviation from the comparison sample. In contrast, hosts of high-mass planets display significantly lower Mg/Si ratios. The difference is highly significant, with K-S statistics of 0.30 and p-values well below 0.001, fully supported by the A-D test. (AD values > AD_{crit}). These results hold across both the whole sample and the thin disc subsample, demonstrating that low Mg/Si ratios are a robust feature of high-mass planet hosts.

The statistical analysis reveals that low-mass planet hosts show no clear chemical distinction from stars without detected planets, whereas high-mass planet hosts, particularly giants, display significant abundance differences. The lower C/O ratios in giant hosts and systematically reduced Mg/Si ratios across all high-mass hosts highlight the role of stellar chemistry in shaping the formation and evolution of massive planets.

3.4 Evolutionary effects in giants: Combined C+N+O abundances

The abundances of carbon, nitrogen, and oxygen in evolved stars are affected by internal mixing processes, which alter their surface compositions relative to the natal values. These evolutionary effects complicate

the direct use of individual abundances as tracers of the chemical composition. In contrast, the total abundance A(C+N+O) is conserved during these processes and therefore provides a more reliable diagnostic of the original stellar chemistry. To account for possible evolutionary mixing effects, we examined the summed A(C+N+O) values in our sample of giant stars hosting planets.

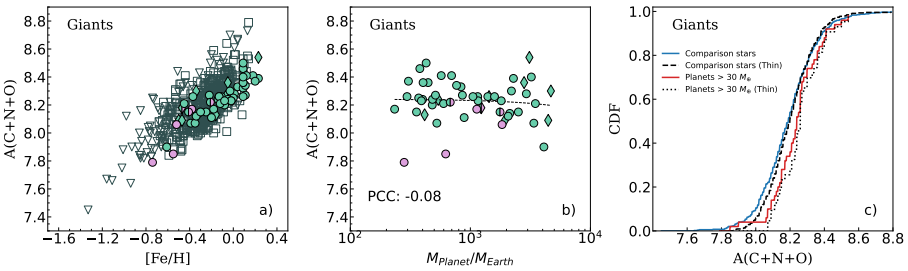

Figure 15: In panel *a:* Distribution of A(C+N+O) abundances with respect to [Fe/H]. Panel *b:* Same abundances versus planet mass for giant stars. Panel *c:* Cumulative A(C+N+O) distributions for giant stars. All symbols in panel (c) have the same meaning as in Fig 14.

Figure 15, panel *a*, presents the distribution of A(C+N+O) abundances in giant stars as a function of metallicity [Fe/H], with colour-coding consistent with the other figures. The results show a clear increase of A(C+N+O) with metallicity, following a well-defined trend and exhibiting minimal scatter. When compared against planetary mass (see Figure 15, panel *b*), no significant correlation is seen between the total C+N+O absolute abundance and planet mass in giant hosts. The Pearson correlation coefficient (PCC) of -0.08 confirms an essentially flat relationship between the two quantities.

The cumulative distributions of A(C+N+O) for giant stars are shown in Fig. 15, panel *c*. When considering the full sample, the K-S and A-D tests yield no statistically significant differences between giants with high-mass planets and the comparison stars (p-values = 0.24 and 0.11, respectively). However, when restricting the analysis to thin-disc giants, the separation becomes more pronounced. In this case, both tests suggest a significant difference at the 5% level, with p-values of 0.02 (K-S) and 0.01 (A-D), supported by 1 000 bootstrap resampling iterations (p = 0.05 and 0.03, respectively). These results indicate that, within

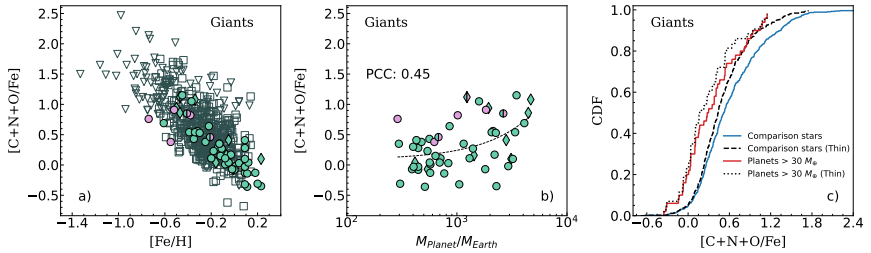

Figure 16: In panel *a:* Distribution of [(C+N+O)/Fe] abundances with respect to [Fe/H]. Panel *b:* Same abundances versus planet mass for giant stars. Panel *c:* Cumulative [(C+N+O)/Fe] distributions for giant stars. All symbols in panel (*c*) have the same meaning as in Fig 14.

the thin-disc population, the total C+N+O abundance of giants hosting massive planets may differ systematically from that of comparison stars. Due to the small number of reliable C, N, and O measurements in dwarf stars, a similar analysis could not be extended to dwarf stars. Additional homogeneous data will be needed to test whether comparable trends exist among main-sequence stars.

Fig. 16, similar to Fig. 15, presents the distribution of the combined carbon, nitrogen, and oxygen abundance relative to iron, [(C+N+O)/Fe], for the sample of giant stars hosting planets. All symbols in this figure have the same meaning as in Fig. 15. Panel *a* in Fig. 16 shows [(C+N+O)/Fe] as a function of [Fe/H], revealing a clear decreasing trend of [(C+N+O)/Fe] with increasing metallicity. This behaviour is consistent with expectations from Galactic chemical evolution, where metal-poor (typically thick-disc) stars exhibit higher relative C+N+O abundances compared to their metal-rich, thin-disc counterparts. Panel *b* displays the [(C+N+O)/Fe] abundance as a function of planetary mass. A positive correlation for both thin- and thick-disc stars is evident, with a PCC of 0.45, indicating that giant stars hosting more massive planets tend to have higher [(C+N+O)/Fe] ratios. Panel *c* shows the CDFs of [(C+N+O)/Fe] for giant stars hosting planets and for comparison stars. The CDFs indicate that planet hosts are, on average, slightly more enriched in C+N+O relative to iron than the comparison sample. The thin-disc subsample is also plotted separately to illustrate the influence of Galactic disc membership.

4 Heavy elements in planet-host stars: *n*-capture species

We investigated the abundance trends of nine neutron-capture elements (Sr, Y, Zr, Ba, La, Ce, Nd, Pr, and Eu) with metallicity in our sample of PHS. Elemental abundances relative to iron, [X/Fe], were determined for both *s*- and *r*-process dominated species and compared to a large control sample of non-host stars observed with the same instrumentation. The results are presented in Fig. 17, where [X/Fe] is plotted against [Fe/H] for all analysed *n*-capture species. Dwarfs and giants are distinguished by circles and triangles, respectively, with colour coding according to the [Y/Mg] ratio, which serves as a chemical clock to trace stellar ages. The comparison sample of stars taken from Tautvaišienė et al. (2021) is shown as plus signs, while stars without Mg abundance determinations are represented by empty symbols. The average abundance uncertainties are indicated in the first panel.

Non-LTE corrections were applied to Sr, Y, Ba, Eu, and Mg for both samples. Details of the NLTE calculations derived in this work and their impact on the abundances are presented in Sec. 2.4.3. These elements originate from diverse nucleosynthetic sites, including AGB stars, core-collapse supernovae, and neutron star mergers, and their relative abundances trace both stellar population membership and the timescales of Galactic chemical evolution. By comparing the behaviour of PHS with that of stars lacking detected planets, we aim to identify potential *n*-capture element abundance signatures that may be linked to the presence of planetary systems.

4.1 The first *s*-process peak. The light *s*-process elements Sr, Y, Zr

The light *s*-process elements strontium, yttrium, and zirconium represent the first peak of the slow neutron-capture process and are primarily synthesised in low- and intermediate-mass stars during the AGB phase. In the Solar System, their synthesis is largely dominated by the *s*-process, amounting to about 91% for Sr, 78% for Y, and 82% for Zr (Prantzos et al. 2020). Examining the behaviour of these elements as a function of metallicity provides valuable insight into how the interplay between neutron-capture nucleosynthesis and iron production from Type Ia supernovae shapes stellar chemical compositions.

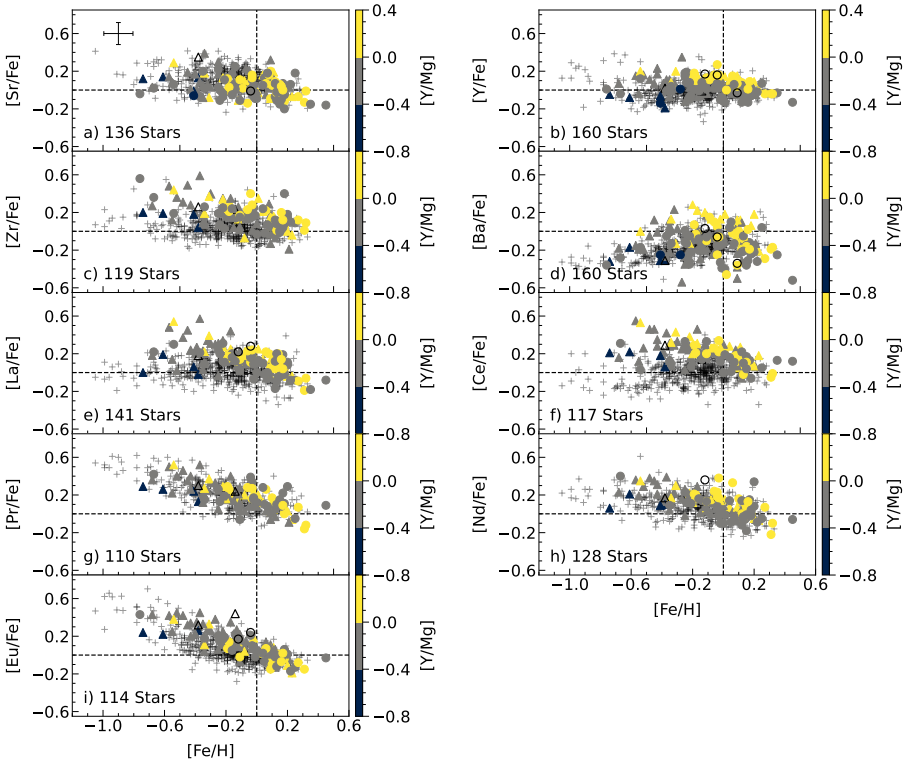

Figure 17: Abundances of neutron-capture elements [El/Fe] as functions of metallicity [Fe/H] for all investigated stars. Dwarf stars are represented by circles, while giant stars (with $\log g \leq 3.5$) are denoted by triangles. The stars are colour-coded according to their [Y/Mg] ratio. Average error bars are displayed in panel *a*. The comparison sample of disc stars is denoted by plus signs and taken from Tautvaišienė et al. (2021).

Fig. 17 (panels *a*-*c*) shows the [Sr/Fe], [Y/Fe], and [Zr/Fe] ratios for our sample of PHS. Strontium and yttrium follow an increasing trend in [Sr/Fe] and [Y/Fe] as the metallicity decreases. These ratios decline at lower metallicities in PHS, which subsequently flattens at intermediate metallicities, reflecting the balance between ongoing *s*-process enrichment and the rise of Fe production from type Ia supernovae. We also observed higher average Sr and Y abundances in younger, more metal-rich dwarf stars (indicated by their higher [Y/Mg] values). This pattern is consistent with the scenario in which successive stellar generations formed from interstellar material increasingly enriched by AGB ejecta.

Overall, our analysis does not reveal any systematic differences in the distributions of [Sr/Fe] and [Y/Fe] between PHS and their stellar analogues without detected planets, indicating that these elements in host stars do not deviate significantly from general Galactic trends. The shallower slopes and larger scatter observed in [Sr/Fe] may be linked to higher uncertainties in Sr abundance measurements or to a more intricate mix of nucleosynthetic channels, including potential contributions from the weak *r*-process and charged-particle reactions in massive stars.

Zirconium, like Sr and Y, is also a light *s*-process element, and shows a stronger positive trend in [Zr/Fe] with decreasing metallicity, particularly below [Fe/H] $\approx$ –0.3. This behaviour suggests that zirconium production in the early Galaxy kept pace with, or even outpaced, iron synthesis in some environments, possibly due to contributions from massive stars or early AGB populations. This behaviour is in good agreement with previous studies (e.g. Mishenina et al. 2016; Delgado Mena et al. 2018), which reported a similar increase in [Zr/Fe] at low metallicities.

Within our dataset, younger, metal-rich dwarfs also exhibit enhanced Zr abundances, though the global trend is dominated by the metallicity dependence. Furthermore, we find an overabundance of [Zr/Fe] in PHS compared to the control sample, particularly at low metallicities. The statistical significance of this difference was evaluated using bootstrap resampling (please refer to Sec. 4.4).

4.2 The second *s*-process peak

The second peak of the slow *n*-capture process encompasses elements that are predominantly synthesised in AGB stars through the main *s*-

process component. Among these, barium, lanthanum, and cerium are largely of *s*-process origin, while praseodymium and neodymium have significant contributions from both *s*- and *r*-processes (Prantzos et al. 2020). In the following, we discuss separately the behaviour of the heavy *s*-process elements (Ba, La, Ce) and the mixed-process elements (Pr, Nd) in our sample of PHS.

4.2.1 The heavy *s*-process elements Ba, La, Ce

Ba, La, and Ce belong to the second peak of the slow *n*-capture process and are mainly produced in low- to intermediate-mass AGB stars during the thermal pulsing phase. While a minor fraction of their production may still come from the *r*-process, the overall abundance patterns of these elements in stellar atmospheres are expected to be largely governed by their common *s*-process origin (Busso et al. 1999). According to (Prantzos et al. 2020), in the Solar System, their abundances are attributed primarily to the *s*-process, with estimated contributions of 89% for Ba, 80% for La, and 85% for Ce. Within our sample of PHS, these elements exhibit distinct abundance behaviours with metallicity, as shown in panels *d*, *e*, and *f* of Fig. 17.

Barium shows a modest increase at super-solar metallicities, followed by a flattening and decline at sub-solar metallicities ([Fe/H] $\lesssim -0.2$). This behaviour is consistent with the trends observed in the comparison sample and in previous works such as Delgado Mena et al. (2018). Importantly, PHS in our dataset do not display any peculiarities in the [Ba/Fe] vs [Fe/H] relation when compared to non-hosts, suggesting that barium abundances are shaped mainly by Galactic chemical evolution rather than by processes directly associated with planet occurrence.

In contrast, the [La/Fe] ratio increases toward lower metallicities, indicating enhanced La abundances in more metal-poor stars. On average, PHS are found to be overabundant in La at a given [Fe/H] relative to the comparison stars, particularly among giants. The result suggests that La may play a distinctive role in the chemical environments of PHS. However, due to possible influences from Galactic chemical evolution and the small absolute magnitude of the differences comparable to typical abundance uncertainties, these results should be interpreted cautiously and do not alone provide strong evidence for a planet formation signature.

Cerium follows a broadly similar pattern to lanthanum. The [Ce/Fe] ratio increases as metallicity decreases, and stars with planets tend to be overabundant in Ce compared to stars without detected planets at a given [Fe/H]. This may suggest a possible link between heavy *s*-process enrichment and conditions favourable for planet formation. Yet, as with La, the differences remain small relative to the uncertainties, underscoring the need for additional observations to establish this link with confidence.

4.2.2 The mixed-process elements Pr and Nd

Praseodymium and neodymium are *n*-capture elements with mixed nucleosynthetic origins, receiving contributions from both the slow and rapid processes. According to Prantzos et al. (2020), approximately 54% of Pr and 62% of Nd in the Solar System are attributed to the *s*-process, with the remaining originating from the *r*-process. Their dual origin makes these elements particularly valuable for tracing overlapping enrichment pathways in the Galaxy. Panels *g* and *h* of Fig. 17 illustrate their [X/Fe] ratios as functions of metallicity.

In our sample, both Pr and Nd show increasing trends with decreasing metallicity, consistent with expectations from Galactic chemical evolution, where early enrichment is driven by the *r*-process in massive stars, and later, the *s*-process gradually contributes through AGB stars. The [Nd/Fe] trend is more gradual and consistent across the full metallicity range, while [Pr/Fe] shows somewhat more scatter, particularly in giants.

No significant differences are observed in the overall [Pr/Fe] or [Nd/Fe] abundance trends across the investigated stellar sample when compared with the comparison stars. This indicates that the presence of planetary systems does not strongly affect the surface abundances of these mixed-process elements. Consequently, our results reinforce the conclusion that the abundances of Pr and Nd in PHS are primarily shaped by Galactic chemical evolution processes and are not systematically distinct from those of the broader comparison star population.

4.3 The *r*-process dominated element Eu

Europium is one of the clearest tracers of the rapid neutron-capture process, with about 95% of its Solar System abundance attributed to the *r*-process (Prantzos et al. 2020). Its production is closely linked to massive stars (Matteucci 2021) and explosive astrophysical events, and therefore its abundance trends provide an important diagnostic of the early enrichment history of the Galaxy. Panel *i* of Fig. 17 presents the [Eu/Fe] ratios for our sample as a function of metallicity.

The [Eu/Fe] ratio shows a clear increasing trend with decreasing metallicity in our sample of PHS. This behaviour is consistent with the nucleosynthetic origin of europium, as *r*-process enrichment from massive stars dominated the early Galaxy, while iron enrichment from type Ia supernovae reduced [Eu/Fe] at later times. Consequently, metal-poor PHS tend to show enhanced europium abundances relative to their metal-rich counterparts.

The similarity of europium abundance patterns in PHS and comparison stars indicates that the observed [Eu/Fe] vs [Fe/H] trend is primarily driven by Galactic chemical evolution rather than planet-related processes. However, the systematically higher [Eu/Fe] ratios in metal-poor hosts compared to metal-rich hosts highlight that Eu abundances, together with those of other *r*-process contributors such as Pr and Nd, may still carry indirect relevance for planet formation through their role in setting the overall chemical environment of the protoplanetary disc.

4.4 Statistical tests

We conducted a dedicated statistical analysis comparing our sample of PHSs with a comparison sample of stars without detected planets taken from previous work (Tautvaišienė et al. 2021) to examine whether the presence of planets is associated with systematic differences in *n*-capture element abundances. Since the internal structures and evolutionary states of dwarf and giant stars can influence observed abundances, the analysis was performed separately for these two stellar classes. For each PHS, an average of five comparison stars was drawn from the control sample that closely matched its atmospheric parameters. The typical range of stellar parameters chosen to sort the comparison stars is as follows:

effective temperature ($T_{\rm eff}$ $\pm$100 K), surface gravity (log g $\pm$0.2 dex), and metallicity ([Fe/H] $\pm$0.1 dex). This matching procedure ensured that any detected chemical difference could be attributed primarily to the presence of planetary companions rather than to intrinsic stellar parameter variations or evolutionary effects.

The abundance comparison was implemented using a bootstrap resampling approach to provide a robust estimate of mean abundance differences and their statistical significance. In each of the 10 000 bootstrap iterations, one control star was randomly drawn from the matched set corresponding to each planet host, and the mean difference in the abundance ratio, $\langle$[El/Fe]$\rangle$, between the PHSs and their selected counterparts was computed. Repeating this process thousands of times effectively simulated many possible realisations of the control sample, thereby accounting for random fluctuations and preventing the outcome from being dominated by any single outlier or particular subset of stars. The resulting bootstrap distributions provide confidence intervals for the mean offsets and yield two-tailed p-values assessing whether the observed differences could arise by chance. Through this resampling design, it was possible to disentangle genuine abundance contrasts from stochastic sampling noise and to evaluate the overall robustness of the trends.

The results of the bootstrap tests are summarised in Table 8. For dwarf stars, several n-capture elements showed systematically higher [El/Fe] ratios in planet hosts compared with their control counterparts. The largest mean differences were obtained for Zr, Ce, and La, with Δ = $+0.14$, $+0.13$, and $+0.12$ dex respectively, all with $p \leq 0.001$. Eu also displayed a moderate but highly significant enhancement of $+0.06$ dex ($p \leq 0.001$). Nd exhibited a smaller yet statistically significant enrichment (Δ = $+0.07$ dex, $p \leq 0.001$), while Y showed a mild positive offset of $+0.04$ dex. In contrast, the light s-process element Sr was slightly underabundant in planet-hosting dwarfs ($\Delta = -0.02$ dex, $p = 0.012$), and Barium abundance similarly showed a small negative difference ($\Delta = -0.02$ dex, $p = 0.008$). Pr displayed a marginal enrichment (Δ = $+0.03$ dex) with a p-value of 0.052, lying at the threshold of statistical significance. Overall, these outcomes reveal that most s- and r-process elements are either enhanced or comparable in abundance among planet-hosting dwarfs relative to similar field stars, with only Sr and Ba showing

Table 8: Bootstrap resampling test results for n-capture elemental ratio distributions for stars with and without planetary companions.

	Dwarfs		Giants	
	Difference (Δ)	p-value	Difference (Δ)	p-value
[Sr/Fe]	-0.02	0.012	-0.08	≤ 0.001
[Y/Fe]	0.04	≤ 0.001	0.09	≤ 0.001
[Zr/Fe]	0.14	≤ 0.001	0.14	≤ 0.001
[Ba/Fe]	-0.02	0.008	0.06	≤ 0.001
[La/Fe]	0.12	≤ 0.001	0.10	≤ 0.001
[Ce/Fe]	0.13	≤ 0.001	0.24	≤ 0.001
[Pr/Fe]	0.03	0.052	-0.02	0.015
[Nd/Fe]	0.07	≤ 0.001	0.01	0.171
[Eu/Fe]	0.06	≤ 0.001	0.08	≤ 0.001

Note: The test is conducted across 10 000 iterations.

mild depletions.

For the sample of giant stars, the bootstrap analysis likewise revealed significant chemical distinctions. The strongest positive offsets occurred again for Ce ($\Delta = +0.24$ dex, $p \leq 0.001$) and Zr ($\Delta = +0.14$ dex, $p \leq 0.001$), followed by La ($+0.10$ dex, $p \leq 0.001$) and Eu ($+0.08$ dex, $p \leq 0.001$). Y was also enhanced ($+0.09$ dex, $p \leq 0.001$), while Ba, which had shown a depletion among dwarfs, appeared slightly overabundant in the giants ($+0.06$ dex, $p \leq 0.001$). Sr remained deficient ($\Delta = -0.08$ dex, $p \leq 0.001$), and Pr exhibited a weak negative shift ($\Delta = -0.02$ dex, $p = 0.015$). The difference in Nd abundance for giants ($+0.01$ dex) was statistically insignificant ($p = 0.171$), indicating that the element follows the Galactic trend without a clear planet-related signal.

The consistency of low p-values across many of the tested species suggests that the observed differences are not random fluctuations but likely reflect subtle yet genuine chemical distinctions between stars with and without planetary systems.

To visualise these results, histograms of the bootstrap distributions

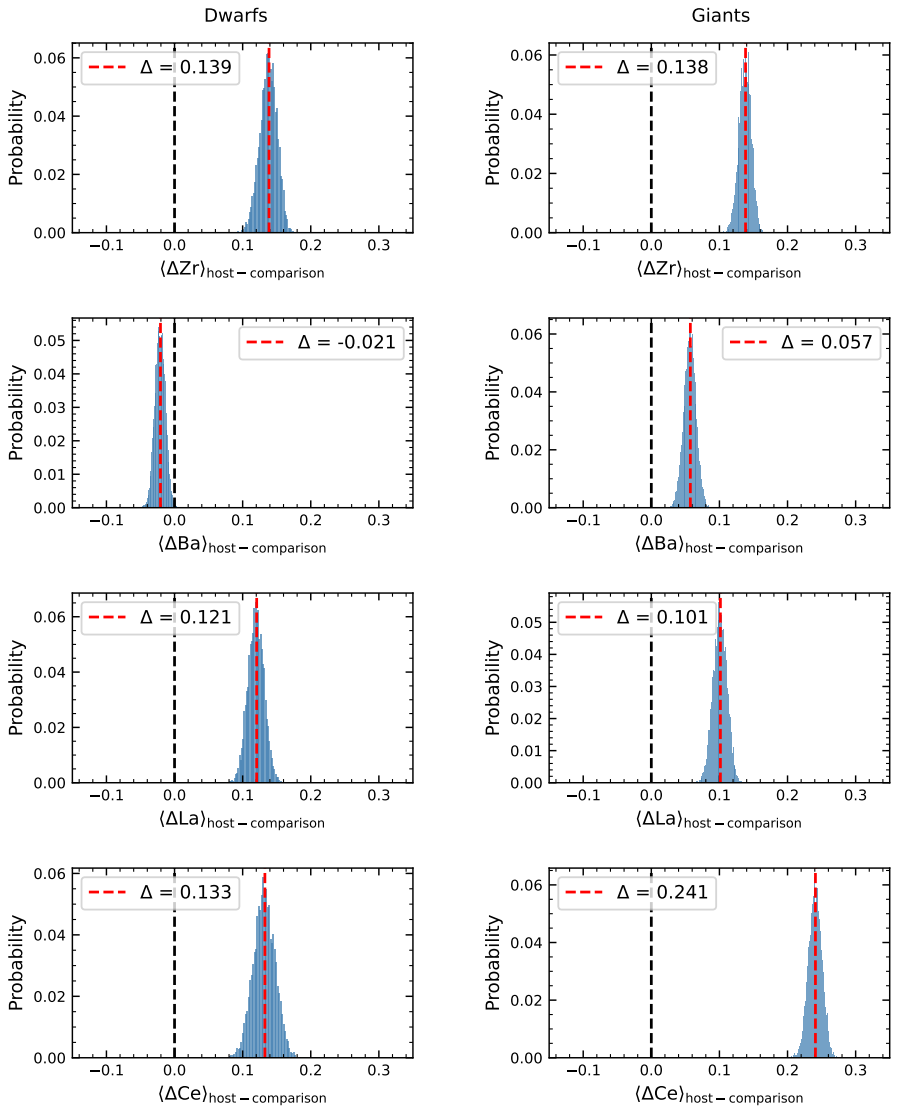

Figure 18: Bootstrap distributions of mean abundance differences ($\Delta = [\mathrm{X/Fe}]_{\mathrm{host}} - [\mathrm{X/Fe}]_{\mathrm{comparison}}$) for selected *n*-capture elements (Zr, Ba, La, and Ce) in dwarfs and giants. Each histogram represents the result of 10 000 resampled comparisons with a control sample matched in T_{eff}, $\log g$, and [Fe/H]. Vertical dashed lines mark $\Delta = 0$ (black) and the observed mean Δ (red). Histograms are normalized to show probability per bin.

were generated for representative elements (see Fig. 18). Each distribution corresponds to 10 000 resampled abundance differences ($\Delta = [\mathrm{El/Fe}]_{\mathrm{host}} - [\mathrm{El/Fe}]_{\mathrm{comparison}}$) and illustrates both the spread and the direction of the mean offset. For elements such as zirconium, lanthanum, and cerium, the distributions are clearly shifted toward positive Δ values, indicating systematic overabundance in PHS. In contrast, barium exhibits a negative shift among dwarfs but a positive one among giants, consistent with the numerical results of the resampling test. The widths of these distributions also provide insight into the element-to-element scatter within the sample, showing that the observed mean shifts are typically larger than the internal dispersion expected from measurement uncertainties alone.

5 [Y/Mg] as age indicator

Recent studies have highlighted a correlation between elemental abundances and stellar ages. In particular, the ratio of *s*-process elements to α-elements, such as [Y/Mg], exhibit a nearly linear dependence on stellar age (e.g. Nissen 2015; Feltzing et al. 2017; Slumstrup et al. 2017; Tautvaišienė et al. 2021; Shejeelammal et al. 2024). This [Y/Mg]-age correlation arises from the distinct nucleosynthetic timescales of the two elements: while Mg is primarily produced in Type II supernovae on short timescales, Y is synthesised during the AGB phase of low- and intermediate-mass stars, which occurs on much longer timescales. Consequently, the [Y/Mg] ratio decreases steadily with stellar age and can serve as a "chemical clock".

Figure 19 presents the NLTE [Y/Mg] versus age relation for our sample of PHS. Dwarfs and giants are shown as circles and triangles, respectively, colour-coded by metallicity, [Fe/H]. Stars identified as part of the thick disc are outlined in red. The symbol size scales with planetary mass, representing either the average mass in multiplanet systems or the individual planet mass in single-planet systems. Stellar ages and

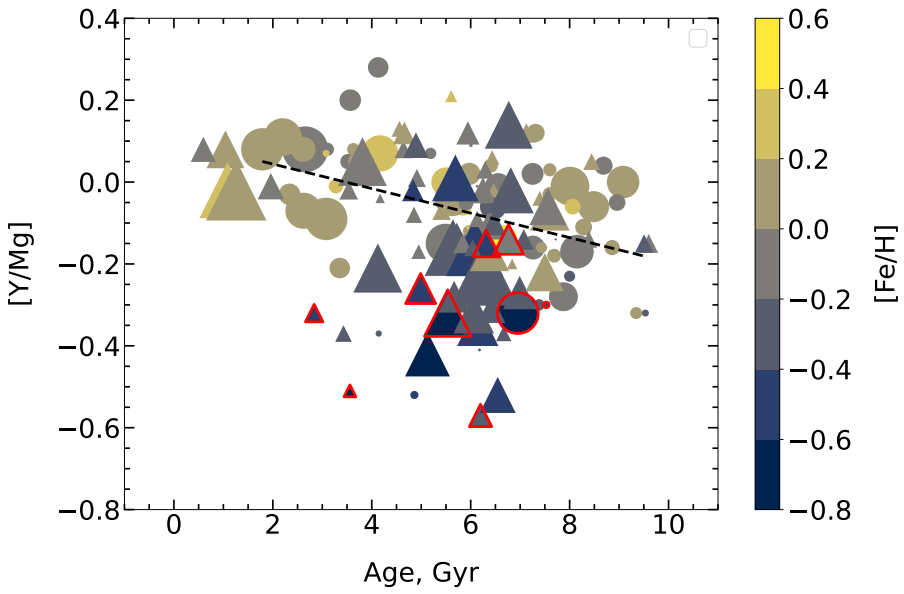

Figure 19: [Y/Mg] NLTE ratio as a function of stellar age in Gyr's. Stars are colour-coded by [Fe/H]. All symbols have the same meaning as in Fig. 17

magnesium abundances were taken from our earlier work (Paper II). A clear correlation is observed for thin-disc dwarf stars hosting planets, with a derived slope of -0.030 ± 0.008. This slope is consistent with results obtained for solar-neighbourhood thin-disc stars (Tautvaišienė et al. 2021), thereby confirming that the [Y/Mg] ratio functions as a reliable age indicator also for PHS. Metal-poor thick-disc stars in our sample exhibit enhanced magnesium abundances and correspondingly lower [Y/Mg] ratios. This feature suggests that magnesium enrichment may play a compensatory role for reduced iron content during planet formation in such systems (see e.g. Adibekyan et al. 2012a,b; Bashi & Zucker 2019).

6 Δ[El/H]-$T_{\rm cond}$ trends

The link between stellar elemental abundances and elemental condensation temperatures ($T_{\rm cond}$) has been widely studied as a potential tracer of planet formation. The condensation temperature of an element refers to the temperature at which 50% of that element transitions from the gas phase to the solid phase under equilibrium conditions in a cooling protoplanetary disk of solar composition (Lodders 2003). Elements with high condensation temperatures (typically $T_{\rm cond} \geq 1200$ K), referred to as refractory elements, condense early and are readily incorporated into solid material, whereas elements with low condensation temperatures ($T_{\rm cond} \leq 200$ K), known as volatiles, remain in the gas phase until much later stages.

Early evidence for a link between condensation temperature and stellar abundances came from the study of Meléndez et al. (2009), who compared the chemical composition of the Sun with that of solar twins and found that the Sun is relatively depleted in refractory elements compared to volatiles. This depletion has been interpreted as evidence that refractory material was sequestered into planetesimals and, ultimately, into planets during the formation of the Solar System, leaving the solar photosphere relatively deficient in these elements.

Subsequent studies have explored whether similar abundance-$T_{\rm cond}$ signatures are present in other PHS. González Hernández et al. (2013) examined a sample of 61 F- and G-type stars, including 29 planet hosts, and found that the majority of their stars exhibited flat or slightly negative abundance-$T_{\rm cond}$ slopes. In a follow-up analysis of solar analogues hosting super-Earth-like planets, they reported that only about half of the investigated stars showed the expected positive correlation between elemental abundance and $T_{\rm cond}$. These results suggest that volatile-to-refractory abundance ratios do not always directly trace the presence of rocky planets and that such signatures may be obscured by other astrophysical processes.

Another study by Liu et al. (2020) that focused on 16 PHS and 68 comparison stars identified a diverse range of abundance-$T_{\rm cond}$ trends. Some stars showed positive slopes, while others showed negative or negligible correlations. Other studies have pointed to more complex

scenarios. For instance, Mack et al. (2014) studied the wide binary system HD 20782/81, where both stars host giant planets, and reported positive correlations between abundances relative to the Sun and $T_{\rm cond}$ for refractory elements. This was interpreted as evidence for the accretion of rocky material during planet formation.

More recently, Yun et al. (2024) extended the analysis to 227 PHS, focusing on refractory elements such as Mg, Si, Ca, Al, Mn, and Ni. Their results indicated that although [El/Fe]-$T_{\rm cond}$ slopes generally exist in stars, their strength and direction depend a lot on the planetary system architecture. After correcting for Galactic chemical evolution, they showed that hosts of giant planets were typically more depleted in refractories compared to systems with only rocky planets. This suggests that the presence of a giant planet might be linked to different chemical fingerprints in the star. Even within rocky-planet systems, the degree of refractory depletion appeared to correlate with planetary properties, such as planet radius and multiplicity, pointing to a connection between abundance-$T_{\rm cond}$ patterns and planetary system structure.

To explore whether $T_{\rm cond}$ signatures are present in our planet-hosting sample, we computed abundance differences relative to carefully selected comparison stars taken from Tautvaišienė et al. 2021. For each target, the mean abundances of stars with similar stellar parameters were subtracted from the measured abundances of the host star, yielding Δ[El/H] values. The matching tolerances were set to $\pm$75 K in effective temperature, $\pm$0.25 dex in surface gravity, and $\pm$0.11 dex in metallicity. Additionally, we accounted for the thin- or thick-disc membership of each star to ensure that Galactic population effects were properly controlled. Depending on the availability of comparison stars, up to 23 matches could be identified for a given host, with an average of six that have elemental abundances. The large comparison sample helps mitigate potential Galactic and stellar chemical evolution effects and biases, utilising homogeneous results from our previous studies.

The abundance dataset includes both the *n*-capture elements and lighter elements (C, N, O, Mg, and Si) determined in Paper I and Paper II and earlier studies (Stonkutė et al. 2020). This approach provided a comprehensive coverage of both volatile and refractory elements. Condensation temperatures were taken from the 50% $T_{\rm cond}$ values tabulated

by Lodders (2003) for a Solar System gas at solar composition. In this scheme, C, N, and O are classified as volatile elements ($T_{\rm cond}$ < 180 K), while all *n*-capture elements, along with Mg and Si, are refractory ($T_{\rm cond}$ > 1300 K).

For each host star, we then calculated the slope of the abundance difference Δ[El/H] in the star with planets minus comparison stars as a function of condensation temperature. This was done by comparing the corrected abundances of the host with those of its parameter-matched control stars for individual elements. Stars lacking measurements of volatile elements were excluded from the slope analysis to avoid biases in the derived correlations.

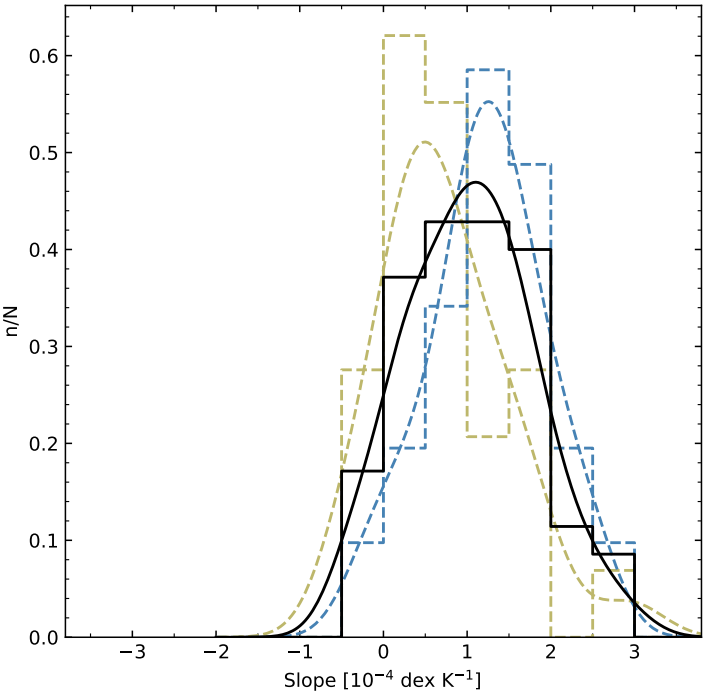

Figure 20: Distributions of the abundance-$T_{\rm cond}$ slopes for our stars with planets minus comparison star(s). The solid black line represents all planet hosts, while the yellow and blue dashed line represents dwarf and giant stars. The distribution is normalized to the total number of stars in each group.

The resulting distributions of Δ[El/H]-$T_{\rm cond}$ slopes were further examined separately for dwarfs and giants in order to investigate potential dependencies on stellar evolutionary stage. This allows us to test whether

PHS show systematic differences in refractory-to-volatile abundances compared to their stellar analogues.

Figure 20 presents the distributions of Δ[El/H]-$T_{\rm cond}$ slopes for our sample of PHS after correction with comparison stars. In this figure, the solid black line represents the entire sample, while dwarf and giant stars are shown separately by yellow and blue dashed lines, respectively. The slopes were derived using abundances of both volatile and refractory elements, ensuring that possible Galactic and stellar evolutionary effects were minimised through the comparison procedure.

The overall distribution exhibits a positive skew, with a median slope of $\mu_{1/2} = 1.03 \pm 0.76$ x 10^{-4} dex K^{-1}. This indicates that, on average, stars hosting planets are relatively enriched in refractory elements compared to their parameter-matched counterparts without detected planets. When restricted to dwarf stars only, the median slope is closer to zero, $\mu_{1/2} = 0.64 \pm 0.76$ x 10^{-4} dex K^{-1}, suggesting that the refractory enrichment signal is weaker in this subset. Giants, by contrast, contribute more strongly to the overall positive skewness of the distribution.

The diversity of Δ[El/H]-$T_{\rm cond}$ slopes seen in our dataset mirrors the range of behaviours reported in Paper I and earlier studies (e.g., Mishenina et al. 2016; Liu et al. 2020). While some stars show clear refractory enrichment relative to volatiles, others exhibit nearly flat or even negative slopes. This variation emphasises that abundance-$T_{\rm cond}$ correlations are not universal but may depend on a combination of stellar properties, evolutionary stage, and planetary system characteristics. To investigate whether condensation temperature slopes depend on stellar and/or planetary properties, we examined Δ[El/H]-$T_{\rm cond}$ slopes as functions of several stellar and planetary parameters. These relations are presented in Fig. 21, with each panel showing Δ[El/H]-$T_{\rm cond}$ slopes plotted against a different stellar and planetary parameter. The solid red line in each panel represents the weighted linear regression fit to the entire dataset, while dwarf and giant hosts are distinguished by dotted and dashed regression lines, respectively. The inverse of the variance (σ^2) of the slopes was used as weight in the linear regression. The stars are colour-coded according to the number of confirmed planets.

The abundance slopes in Fig. 21 show some weak correlations with both stellar and planetary parameters. Negative dependencies are found

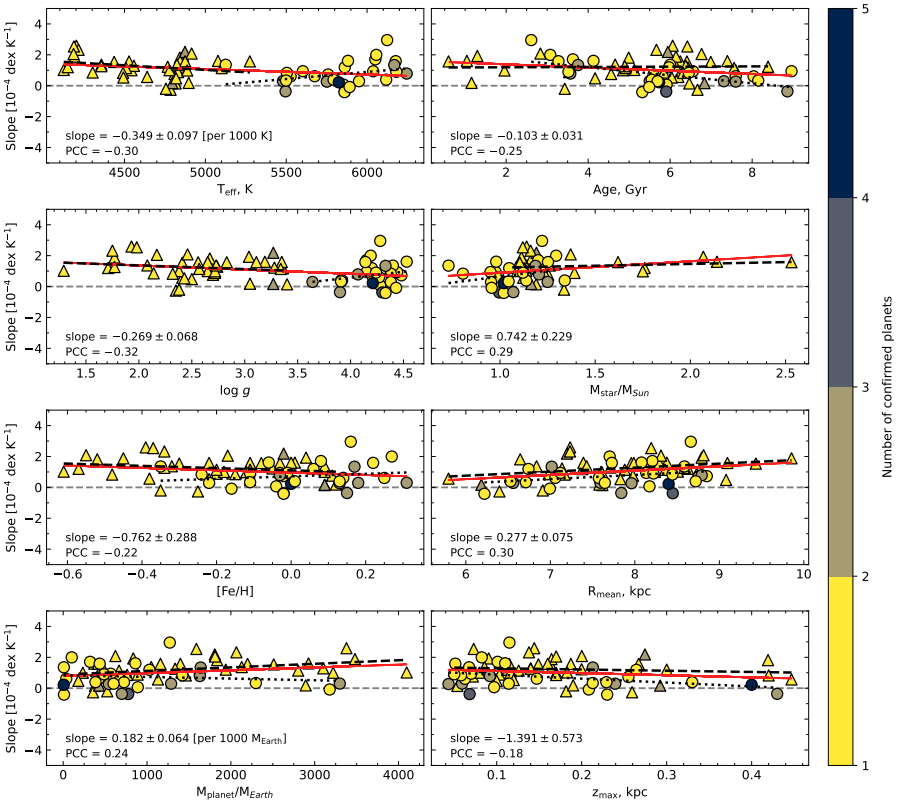

Figure 21: The elemental abundance–$T_{\rm cond}$ slopes as a function of stellar parameters and planetary mass. The stars are colour-coded according to their number of confirmed planets. The symbols are the same as in Fig. 17. The red line represents weighted linear regression fits to the data. The slopes and Pearson correlation coefficients are shown in the corners of the panels. See the text for more information.

with effective temperature, surface gravity, metallicity, stellar age, and maximum vertical distance from the Galactic plane, with PCC values ranging from -0.22 to -0.32.

In contrast, the stellar mass and the mean Galactocentric radius show weak positive correlations (PCC $\approx$ 0.29-0.30). Planetary mass also exhibits a slight positive correlation, with a slope of 0.182 ± 0.064 x 10^{-4} dex K^{-1} per 1000 $M_{\oplus}$ and PCC = 0.24. Although these correlations are not strong, they suggest that stars with higher masses, larger orbital radii, or more massive planets tend to display somewhat larger Δ[El/H]-$T_{\rm cond}$ slopes, whereas metal-poor, older, or dynamically hotter stars (with larger $|z_{\rm max}|$) are more likely to show flatter or negative slopes.

A trend with stellar age shows that younger dwarf stars (ages < 5 Gyr) generally exhibit positive slopes, while older dwarfs with multiple planets often show smaller or even negative slopes. This behaviour indicates that refractory enrichment relative to volatiles may be more pronounced in younger systems. In contrast, older systems, particularly those with multiplanet architectures, appear more chemically balanced or even refractory-deficient relative to volatiles.

The variety of Δ[El/H]-$T_{\rm cond}$ slopes observed in our PHS points to a complex interplay of factors that influence surface abundances. Several processes could be responsible for the positive slopes seen in many systems. For instance, the evolution of circumstellar discs can lead to diverse distributions of refractory material, while the accretion or ingestion of rocky bodies during or after planet formation may imprint detectable refractory enrichment. Similarly, the growth of terrestrial planets or the cores of giant planets could preferentially sequester refractory elements, thereby altering the chemical balance in the remaining stellar atmosphere. At the same time, the presence of stars with nearly flat or negative slopes cautions against interpreting Δ[El/H]-$T_{\rm cond}$ trends as a universal signature of planet formation. It is possible that in some systems, there is no physical connection at all between the presence of planets and condensation temperature behavior. An alternative explanation has recently been proposed by Soliman & Hopkins (2025), who argued that variations in dust-to-gas ratios during the birth of stars may naturally generate fluctuations in refractory element abundances.

According to this scenario, these abundance patterns would be imprinted at the time of formation and would persist throughout the lifetime of a star, even during phases when convection zones are deeper, producing both enhancements and depletions in refractory material independent of the planet formation.

7 Chemical signatures and planet properties

Planetary systems originate within protoplanetary discs whose chemical and physical properties are closely linked to those of their host stars. Since the stellar compositions reflect the primordial reservoirs from which planets form, variations in stellar element abundances can influence the efficiency of planetesimal formation, the accretion of solids and gas, and the ultimate architecture of the planetary system. Correlations between stellar abundances and planetary properties therefore, can provide a direct means to test theories of planet formation and to identify the key chemical factors that distinguish between rocky, icy, and gaseous planets.

Moreover, stellar abundances serve as critical proxies for the bulk compositions of exoplanets, which remain largely inaccessible to direct measurement. Establishing these abundance-planetary property relations not only constrains models of planetary interiors but also informs statistical studies of planet occurrence across different stellar populations. Such investigations are essential for building a predictive framework of planet formation and for guiding the search for potentially habitable worlds around stars with favourable chemical environments. In this section, I present the empirical links between stellar chemical patterns and planet properties that emerge from our homogeneous high-resolution VUES spectroscopy of PHS and the dedicated follow-ups of confirmed planet hosts.

7.1 Stellar chemistry versus planet mass relation

We investigated the correlations between the stellar abundances in our sample and the masses of their planetary companions. Planetary masses were obtained mainly from the NASA Exoplanet Archive[5], and companions exceeding $\sim$13 M_J, where M_J corresponds to the mass of Jupiter, were excluded to avoid brown dwarf contamination. This threshold approximately marks the onset of deuterium burning and is conventionally adopted to distinguish giant planets from substellar objects. Planetary masses together with other planetary parameters such as orbital periods

[5] https://exoplanetarchive.ipac.caltech.edu/

and semi-major axes are summarised in Table 4. Details on the associated parameter uncertainties can be found in the NASA Exoplanet Archive.

7.1.1 CNO and α-elements

The distributions of carbon, nitrogen, and oxygen abundances relative to iron ([C/Fe], [N/Fe], and [O/Fe]), together with the derived C/O and N/O ratios, were analysed as functions of planetary mass for a sample of 149 PHS. Figure 22 presents these trends, with dwarf and giant hosts shown separately and symbols colour-coded according to their Galactic disc membership: thin-disc stars in green, thick-disc stars in pink, and stars in between thin and thick disc in both colours. For systems hosting multiple planets, the most massive planet was adopted as the representative of the system. Tests including all planets were also performed, and no systematic differences in the observed trends were found (see Fig. 23).

To account for evolutionary effects, host stars were divided into dwarf and giant stars, and elemental abundances were correlated with planetary masses using linear regression fits. The strength and direction of these correlations were measured with PCC values, calculated separately for dwarfs, giants, and the combined sample. This approach allowed us to systematically probe whether stellar chemical compositions exhibit measurable dependencies on planetary mass, regardless of stellar type or system multiplicity.

Among dwarf hosts, [C/Fe], [N/Fe], and [O/Fe] display weak negative slopes with planetary mass, underscoring the absence of strong CNO dependence on planet mass in dwarf stars. These results are consistent with previous studies for dwarf stars (Stonkutė et al. 2020, Paper I). In contrast, giant hosts exhibit more pronounced behaviour. Carbon shows a weak positive correlation with planetary mass (PCC = 0.13), while nitrogen is clearly enhanced in stars hosting massive planets (PCC = 0.60). Oxygen also shows a moderate positive correlation with planetary mass (PCC = 0.30) in the direction of high-mass planet hosts. Together, these results suggest that in evolved stars, internal mixing and stellar evolution processes, in conjunction with the presence of massive companions, shape the observed CNO abundance trends.

In Fig. 22 (panels *d-e*), the elemental abundance ratios C/O and N/O

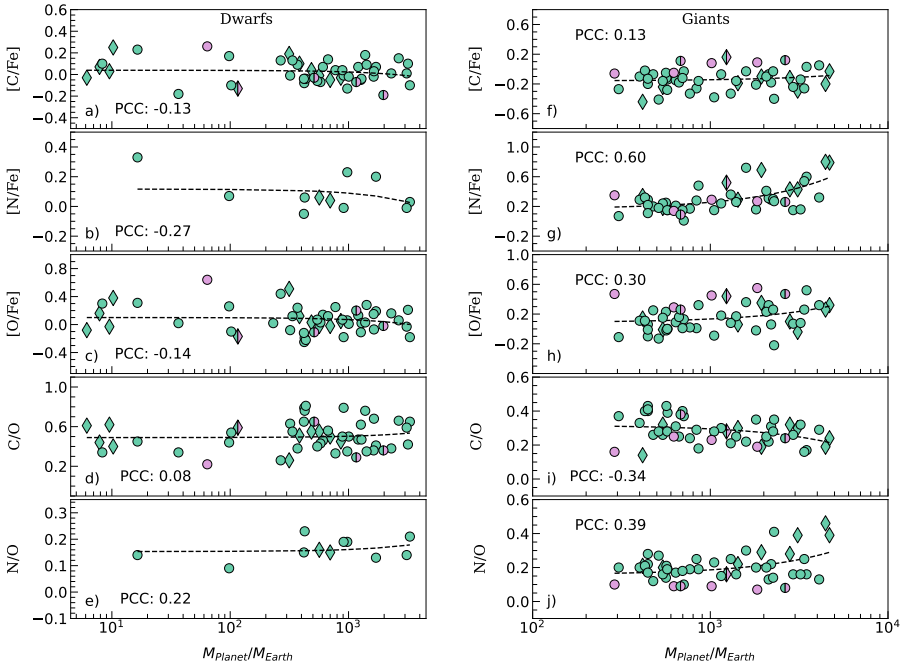

Figure 22: [C/Fe], [N/Fe], [O/Fe] abundances and C/O, N/O ratios plotted as functions of planet masses for investigated dwarfs (left panel) and giants (right panel). For multi-planet systems, only the most massive planet is considered. Green circles and diamonds represent thin disc stars, while pink circles represent thick disc stars. Linear regression fits were added as dashed lines.

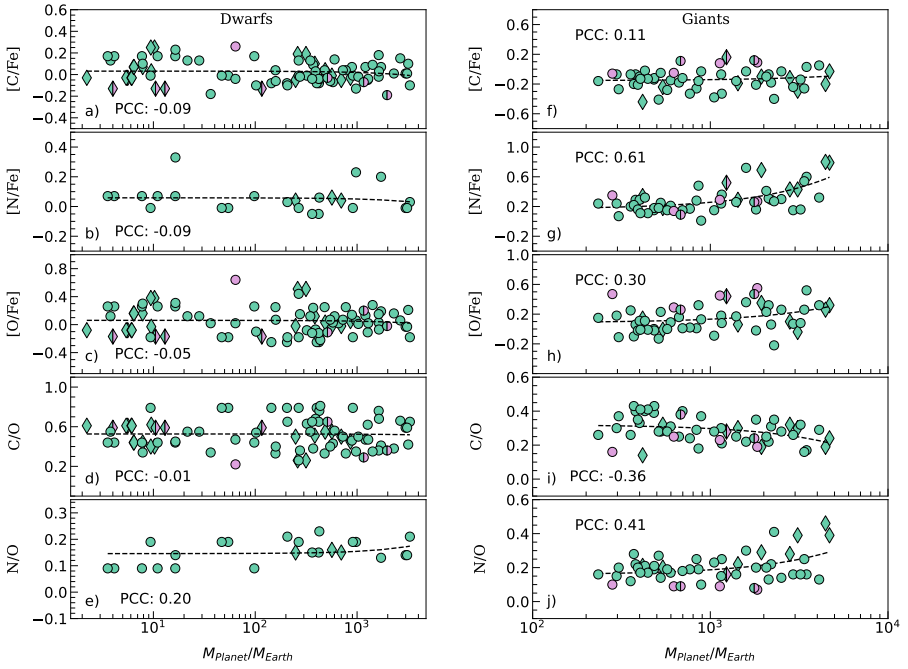

Figure 23: [C/Fe], [N/Fe], [O/Fe] abundances and C/O, N/O ratios as functions of planet masses for investigated dwarfs (left panel) and giants (right panel). All planets in multi-planet systems are considered in this figure. All symbols have the same meaning as in Fig. 22.

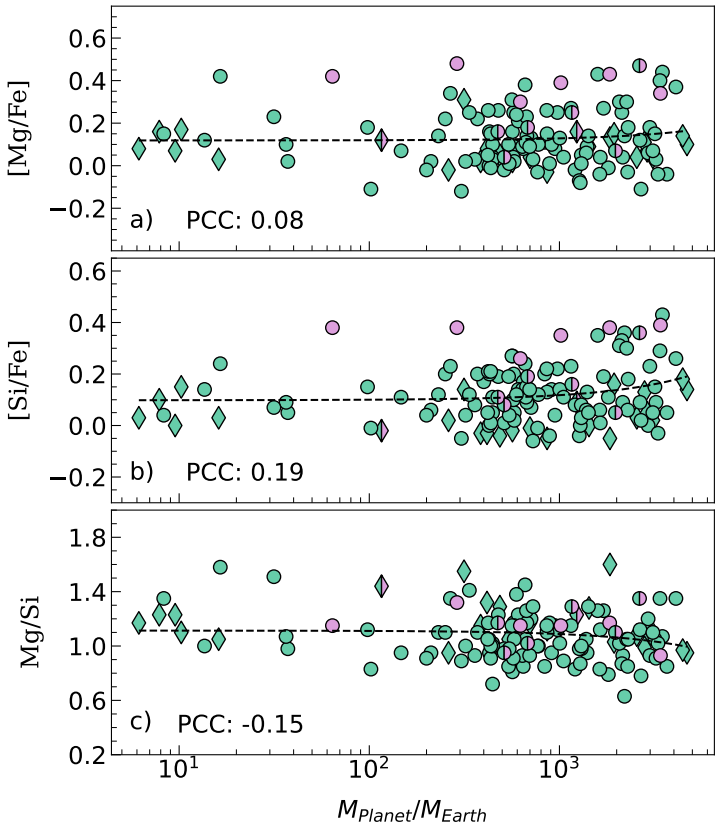

Figure 24: [Mg/Fe], [Si/Fe] abundances and their ratio Mg/Si plotted as functions of planet masses for all investigated stars. For multi-planet systems, only the most massive planet is considered. All symbols have the same meaning as in Fig. 23.

exhibit weak positive correlations with planetary mass among dwarf stars (PCC = 0.08 and 0.22, respectively) observed towards the stars hosting high-mass planets. The slope of the C/O ratio is effectively negligible, whereas the N/O ratio suggests a slight tendency toward higher values with increasing planetary mass. However, the number of low-mass planet hosts with reliable nitrogen measurements in our sample remains limited, and additional data will be required to confirm whether this trend is robust or simply a consequence of small-number statistics.

For giant stars, a different behaviour is observed. As shown in Fig. 22 (panel *i*), the C/O ratio displays a moderate negative correlation with planetary mass (PCC = -0.34) among hosts of high-mass planets,

indicating a decrease in C/O with increasing planet mass. In contrast, the N/O ratio exhibits a stronger positive correlation (PCC = 0.39; panel *j*), suggesting enhanced nitrogen enrichment in giants hosting more massive planets. These differences reflect the impact of stellar evolution on surface nitrogen enrichment and carbon depletion, which, in turn, affect the C/O and N/O ratios.

Figure 24 shows the abundances of α-elements: magnesium and silicon ([Mg/Fe] and [Si/Fe]) together with the Mg/Si ratio versus planetary mass for all stars in our sample. The same symbol scheme is used as in Fig. 23. Both Mg and Si show weak positive correlations with planetary mass (PCC = 0.08 and 0.19, respectively) towards stars hosting high-mass planets. The Mg/Si ratio, however, exhibits a weak negative correlation with a PCC of $= -0.15$. This behaviour is particularly evident among high-mass planet hosts and may have mineralogical consequences, since Mg/Si determines the relative proportions of olivine- and pyroxene-type silicates available for planet building.

7.1.2 *n*-capture elements

The relation between *n*-capture element abundances and planetary masses was investigated for a combined sample of 160 PHS. As in the CNO analysis, host stars were divided into dwarfs and giants to account for evolutionary effects. For multiplanet systems, only the most massive companion was considered; however, tests including all planets yielded consistent results (see Fig. 26). Figure 25 shows the distribution of *n*-capture element abundances relative to iron as functions of planetary mass for the investigated stars. Dwarfs and giants are represented by circles and triangles, respectively. Linear regressions were performed separately for dwarfs, giants, and the full sample, with the strength of each relation quantified by the PCC values. These values are presented in Table 9.

Light s-process elements (Sr, Y, Zr). Strontium shows no significant dependence on planet mass, with PCC values close to zero across all subsamples (e.g. PCC = 0.01 for the full sample). A very weak depletion trend is observed in dwarf hosts of massive planets (PCC = -0.17), though it is not statistically significant. This weak or absent correlation in Sr is consistent with previous findings by Delgado Mena et al. (2018).

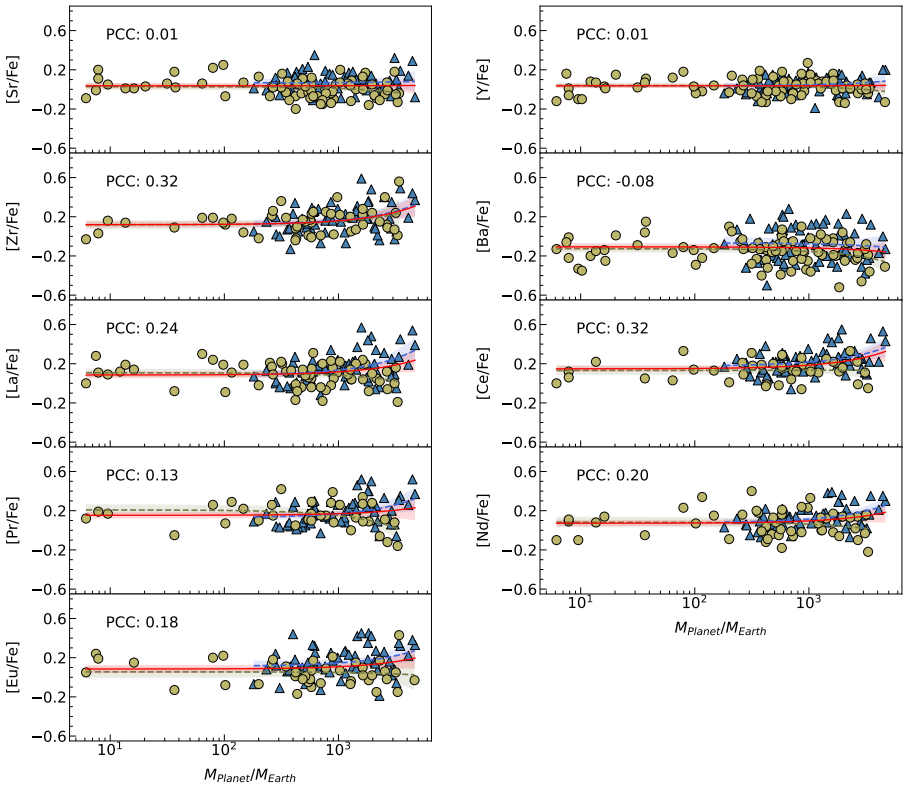

Figure 25: Abundances of neutron-capture elements [El/Fe] shown as functions of planet masses for stars with single planets or the highest-mass planet in multiplanetary systems. All symbols have the same meaning as in Fig. 17. Refer to the text for more information.

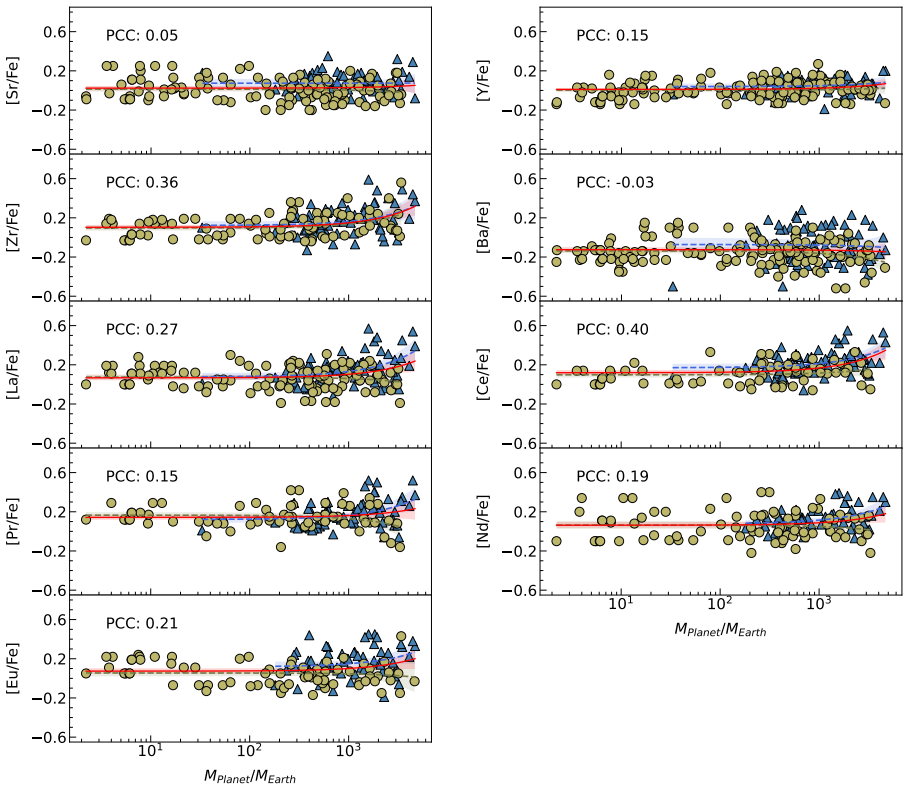

Figure 26: Abundances of neutron-capture elements [El/Fe] shown as functions of planet masses for all investigated planetary systems. All symbols have the same meaning as in Fig. 17. Refer to the text for more information.

Table 9: Pearson correlation coefficient (PCC) values representing the strength and direction of the linear relationship between stellar abundances and planet masses for both dwarf and giant stars, as well as for the entire sample.

Formation	[El/Fe]	All planets			Single/massive planet		
		All stars	Dwarfs	Giants	All stars	Dwarfs	Giants
light *s*-process	[Sr/Fe]	0.05	−0.08	0.00	0.01	−0.17	0.03
	[Y/Fe]	0.15	0.05	0.13	0.01	−0.15	0.14
	[Zr /Fe]	0.36	0.31	0.33	0.32	0.28	0.32
heavy *s*-process	[Ba/Fe]	−0.03	−0.17	−0.04	−0.08	−0.21	−0.06
	[La/Fe]	0.27	−0.10	0.43	0.24	−0.19	0.41
	[Ce/Fe]	0.40	0.15	0.39	0.32	0.01	0.38
mixed *r*+*s*	[Pr/Fe]	0.15	−0.26	0.36	0.13	−0.41	0.34
	[Nd/Fe]	0.19	−0.09	0.38	0.20	−0.14	0.38
r-process	[Eu/Fe]	0.21	−0.07	0.25	0.18	−0.06	0.26

Yttrium also displays negligible correlations, with PCC values of 0.01 for the full sample, −0.15 for dwarfs, and 0.14 for giants. In contrast, zirconium behaves differently, with [Zr/Fe] showing a consistently positive correlation with planetary mass with PCC values ranging from 0.32 to 0.36 across subsamples. This trend is more pronounced in giant hosts and suggests that Zr enrichment may be linked to the presence of massive companions. The result contrasts with the negative correlations reported by Swastik et al. (2022). The discrepancy may arise from differences in the adopted Zr II spectral lines used in the studies or from subtle influences of Galactic chemical evolution, both of which can alter the inferred abundance-planet mass relations.

Heavy s-process elements (Ba, La, Ce). Barium is distinguished by its negative correlation with planetary mass. For the full sample, [Ba/Fe] yields a PCC of −0.08, with dwarf hosts exhibiting more negative values (PCC = −0.21). This indicates a mild depletion of Ba in stars hosting massive planets, consistent with previous reports of Ba deficiencies in PHS (da Silva et al. 2015; Mishenina et al. 2016; Delgado Mena et al. 2018). In contrast, lanthanum and cerium show clear positive correlations with planetary mass. Among giant hosts, the PCC values reach 0.41 for La and 0.38 for Ce, representing some of the strongest correlations identified in this study. These findings suggest that enrichment in heavy

s-process elements may be associated with the presence of massive planets, particularly in evolved stars.

Mixed r+s-elements (Pr, Nd). Praseodymium and neodymium follow the same behaviour as La and Ce in giant stars, with moderate positive correlations (PCC = 0.34 and 0.38, respectively). In dwarfs, however, Pr shows a strong negative slope (PCC = -0.41), highlighting a clear contrast between evolutionary stages. Nd in dwarfs also shows a negative correlation but the strength of the correlation is not significant (PCC =-0.14).

r-process element (Eu). Europium, produced almost entirely by the *r*-process, exhibits weak positive correlations with planetary mass in the overall sample (PCC = 0.18) and in giants (PCC = 0.26). In dwarfs, the slope is slightly negative (PCC = -0.07). These results broadly follow the behaviour of La and Ce, but with a weaker overall strength, suggesting that Eu is less directly linked to planet mass.

Taken together, these results point toward a possible connection between the abundances of *n*-capture elements in giant stars and the masses of their planetary companions. Most of the examined elements, particularly Zr, La, Ce, Pr, Nd, and Eu, exhibit positive correlations with increasing planet mass, with the strongest signals found in giant hosts. This systematic behaviour suggests that the presence of more massive planets may be associated with enhanced enrichment in heavy *n*-capture species, possibly reflecting the combined effects of stellar evolution and chemical history.

Two elements stand out as exceptions to this general trend. Both barium and strontium consistently show negative correlations with planet mass across dwarf, giant, and the combined star samples. The depletion of these elements in high-mass planet hosts has been noted in earlier works (da Silva et al. 2015; Mishenina et al. 2016; Delgado Mena et al. 2018), and their persistence as outliers here underlines the complexity of the abundance-planet connection. The contrasting behaviour between the majority of *n*-capture elements, which rise with companion mass, and Ba and Sr, which decline, suggests that different nucleosynthetic pathways or Galactic chemical evolution effects may be influencing these species in distinct ways.

7.2 Stellar age as a function of planet mass

Over billions of years, the Milky Way has undergone significant chemical enrichment, as successive generations of stars produced and dispersed heavy elements into the interstellar medium. This gradual increase in metals enriched the gas and dust available for forming new stars and planetary systems. Consequently, the physical conditions within the protoplanetary disks around young stars have not been constant throughout Galactic history. Since metals are critical for building solid planetary cores, the age of a star within the Galaxy may influence the types and masses of planets that form around it, with older stars potentially hosting different planetary populations than younger, metal-rich stars. We explored the relationship between stellar age and planetary mass to assess whether the epoch of planet formation imprints measurable signatures on host populations.

Previous studies have suggested that stars hosting small planets are, on average, older than those hosting giant planets ($M_P \geq 0.3\,M_J$; Swastik et al. 2024). Motivated by this, the present analysis investigates whether the ages of PHS in our sample exhibit any dependence on planetary mass. Figure 27 shows stellar ages as a function of planetary mass for the sample of 149 stars, colour-coded by [Fe/H], Mg/Si, and planetary orbital period (in days). The overall distribution reveals no statistically significant correlation, with a linear regression yielding a PCC of -0.07. This indicates only a weak and statistically marginal tendency for stars hosting more massive planets to be younger, though additional data are required to confirm this trend.

Despite the overall flat distribution, several systematic tendencies emerge in our sample. As shown in Fig. 27, stars hosting low-mass, short-period planets tend to be older and more metal-poor, consistent with the idea that such planets formed during earlier phases of Galactic chemical evolution (see also Swastik et al. 2024). In contrast, long-period giant planets are found around stars spanning a wide range of ages, from young to old systems, suggesting that their formation conditions are less tightly linked to stellar age. Notably, systems with short-period, young giant planets tend to exhibit lower Mg/Si ratios compared to the rest of the sample (see also Fig. 24).

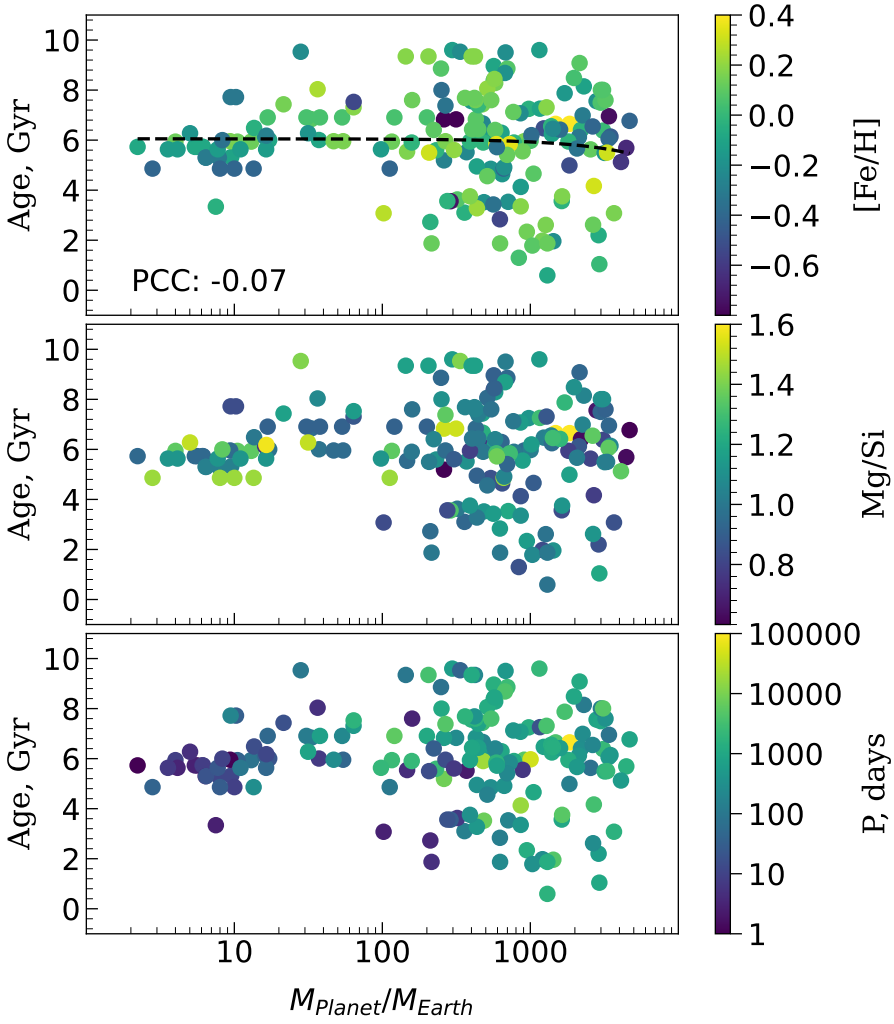

Figure 27: Distribution of stellar age versus planet mass colour-coded by [Fe/H] (top panel), Mg/Si (middle panel) & orbital period of the planets (bottom panel). Refer to the text for more information.

8 Summary, conclusions and future outlook

Exoplanet science has entered an era where large statistical samples of planets become available, yet the precise links between stellar and planetary properties remain incompletely understood. Stellar chemical abundances serve as "fossil records" of the environments in which planetary systems formed. They influence both the mineralogy of planetary interiors and the volatile inventories of exoplanet atmospheres. Furthermore, abundance ratios such as C/O, N/O, and Mg/Si have been proposed as key indicators of where and how planets assemble in protoplanetary disks. The central objective of this thesis has been to observe and explore the spectroscopic signatures of chemical elements in stars known to host planets, with particular focus on light elements (C, N), α-elements (O, Mg, Si), and neutron-capture elements (Sr, Y, Zr, Ba, La, Ce, Nd, Pr, Eu). These studies provide crucial insights into the interplay between stellar composition, Galactic chemical evolution, and the processes that govern the formation and evolution of exoplanetary systems.

This thesis advances the field by providing a uniform and homogeneous spectroscopic analysis of planet-host stars based on high-resolution observations. Observational data were obtained using the high-resolution Vilnius University Echelle Spectrograph at the Molėtai Astronomical Observatory. The thesis is a compilation of three complementary scientific papers. In Paper I, a pilot study was conducted on 25 planet-host stars to determine the abundances of C, N, O, Mg, and Si, as well as their key ratios (C/O, Mg/Si). This initial work established the methodology and demonstrated the potential links between stellar chemistry and planetary systems. In Paper II, the analysis was extended to a significantly larger combined sample of 149 planet-host stars, including 83 main-sequence stars or dwarf stars and 66 evolved giant stars, allowing robust statistical assessment of elemental trends and their correlations with stellar and planetary parameters. Finally, in Paper III, the investigation was extended to include *n*-capture elements produced by the *s*- and *r*-processes (Sr, Y, Zr, Ba, La, Ce, Nd, Pr, and Eu) in 160 planet-host stars, including 86 dwarf stars and 74 giant stars, providing a comprehensive view that incorporates both light and heavy-element chemistry.

The determination of accurate stellar atmospheric parameters (effec-

tive temperature, $T_{\rm eff}$; surface gravity, log g; microturbulence velocity, $v_{\rm t}$; and metallicity [Fe/H]) was a crucial first step in this thesis. By uniformly applying the classical equivalent width approach, we derived a consistent set of parameters for all planet-host stars across the three studies. The main atmospheric parameters for our full sample of 160 PHS span the following ranges: $T_{\rm eff}$ between 4000 and 6680 K; log g range from 1.3 to 3.5 for giant stars and from 3.6 to 4.7 for dwarf stars; [Fe/H] varies from -0.76 to 0.45 dex, with an average of -0.09 ± 0.24 dex. The average uncertainties are about 50 ± 15 K in $T_{\rm eff}$, 0.20 ± 0.05 dex in log g, 0.09 ± 0.02 dex in [Fe/H], and 0.25 ± 0.08 km s^{-1} in $v_{\rm t}$.

The parameter distributions showed that the majority of the sample consists of solar-type F, G, and K dwarfs, complemented by a significant number of evolved giant hosts. Apart from the main atmospheric parameters, we also computed stellar kinematic and orbital parameters for our combined stellar samples of Paper I and Paper II to place the host stars in their Galactic context. The galactic space velocities, U, V, W, and orbital parameters: mean galactocentric distance, $R_{\rm mean}$, maximum vertical distance from the Galactic plane, $|z_{\rm max}|$, and eccentricity, e were computed using *Gaia* DR3 astrometry combined with radial velocities. $R_{\rm mean}$ values for this sample varied between 5.79 to 9.85 kpc, with a mean of 7.80 kpc. The maximum $|z_{\rm max}|$ value reached 1.90 kpc with the average of 0.30 kpc. We also estimated the ages and masses of the stars, based on Bayesian isochrone fitting with UniDAM, as well as disc probability ratios to group our stars into thin or thick disc stars. Most planet hosts in the sample exhibit thin-disc kinematics, while a smaller fraction of stars show thick-disc characteristics. Importantly, these dynamical and age diagnostics reveal that planet-host stars are not confined to a single Galactic population, but rather span the chemical and kinematic diversity of the Milky Way disc. This underscores the conclusion that planet formation has occurred throughout much of the Galaxy's evolutionary history, albeit with varying efficiency depending on metallicity and chemical composition.

The elemental abundances investigated in this thesis were derived using a differential line-by-line spectral synthesis approach based on high-resolution VUES spectra. After determining stellar atmospheric parameters through the equivalent width analysis of Fe I and Fe II lines,

we modelled individual spectral features using the TURBOSPECTRUM code and MARCS model atmospheres under the assumption of local thermodynamic equilibrium and compared them to the observed spectra. Molecular features of C_2 and $^{12}C^{14}N$ were employed to derive carbon and nitrogen abundances, while the forbidden [O I] line at 6300 Å provided the oxygen abundance. Magnesium and silicon abundances were determined from carefully selected Mg I and Si I lines, consistent with the Gaia-ESO Survey line list. For the *n*-capture elements, hyperfine structure and isotopic splitting were explicitly accounted for, particularly in the analysis of Ba II, La II, Pr II, Nd II, and Eu II lines, to obtain accurate abundance measurements. Each spectral line was synthesised and fitted to the observed stellar spectra, thereby minimising systematic errors from atomic data uncertainties and atmospheric modelling. NLTE corrections for key elements (e.g. Mg, Sr, Y, Ba, Eu) were evaluated where applicable.

- The analysis of the derived abundances reveals that PHS follow the general trends of Galactic chemical evolution. In dwarf stars, [C/Fe] and [O/Fe] ratios decrease with increasing metallicity, while [N/Fe] remains close to the solar value across the metallicity range, with an increase in nitrogen abundance observed at sub-solar metallicities. These patterns confirm that carbon and oxygen production in massive stars declines relative to iron at higher [Fe/H], consistent with the delayed iron enrichment from Type Ia supernovae.

  Compared to dwarfs of similar metallicity, giants have carbon abundances lower by about 0.2 dex and nitrogen abundances higher by roughly 0.2 dex, while oxygen remains nearly unchanged. These patterns reflect internal mixing processes that occur during stellar evolution, which bring material processed in the stellar interior to the surface, depleting carbon and enriching nitrogen. As a result, planet-hosting giants tend to exhibit lower C/O ratios and higher N/O ratios than dwarfs. The [N/Fe] abundances of giant planet hosts exhibit a mild increase with metallicity, and the N/O ratio grows with [Fe/H]. The combined A(C+N+O) abundances in giants increase steadily with increasing [Fe/H], displaying very little scatter and indicating that these evolved stars are chemically

homogeneous. We acknowledge the necessity for additional homogeneous nitrogen abundance data to analyse nitrogen trends in planet-hosting stars.

- A comparison between PHS and the reference sample without detected planets shows broadly similar abundance patterns, with only subtle differences. Among dwarfs with super-solar metallicities, PHS tend to exhibit slightly lower [C/Fe] and [O/Fe] ratios than comparison stars, though these differences remain within the uncertainties. At sub-solar metallicities, there is no significant difference in [C/Fe] and [O/Fe] abundances between planet hosts and comparison samples.

  Statistical analyses using the K-S and A-D tests indicate no significant differences in the C/O or N/O ratios between planet host and non-host dwarfs.

  For giants, PHS show reduced scatter in carbon and oxygen abundances and a modestly lower mean C/O ratio compared to single stars, consistent with the overall trends of Galactic chemical evolution.

  N/O ratio in planet host giants is in line with the comparison sample. Comparing the A(C+N+O) abundances in giant planet hosts with the comparison sample, we found that the CDFs for A(C+N+O) are closely aligned, indicating no clear separation between them.

  Within the thin disc population, there is a possible indication of chemical distinctions between stars hosting giant planets and those without detected companions. However, confirming these trends will require larger and more statistically robust samples.

- Magnesium and silicon, the two α-elements examined, show behaviour consistent with Galactic chemical evolution: both [Mg/Fe] and [Si/Fe] decline with increasing metallicity. However, planet-hosting stars exhibit a notable overabundance of Mg and Si compared to the comparison sample, particularly at lower metallicities. This α-element enhancement suggests that refractory materials may play a role in the planet-formation environment, potentially providing more solid material for the assembly of rocky cores in

the early protoplanetary disc. The Mg/Si ratio, a key indicator of silicate mineralogy, appears on average marginally lower in stars with planets than in stars without detected companions. Statistical tests confirm that this difference becomes significant for hosts of high-mass planets, hinting that Mg- and Si-rich environments could influence the composition or structure of the resulting planetary systems.

- When examining possible correlations between stellar abundances and planetary mass, a weak negative trend was observed between [C/Fe], [N/Fe], and [O/Fe] and the planet mass in dwarf hosts. In contrast, giant stars reveal a weak positive correlation between [C/Fe] and planet mass (PCC = 0.13) and a stronger positive trend between [N/Fe] and planetary mass, with a PCC of 0.60. [O/Fe] shows a moderate positive correlation (PCC = 0.30).

  For abundance ratios, the C/O ratio in dwarfs exhibits a weak positive relation with planet mass (PCC = 0.08), whereas giants hosting high-mass planets show a moderate negative slope (PCC = -0.34). The N/O ratio increases weakly with planet mass in dwarfs (PCC = 0.22) and more strongly in giants (PCC = 0.39).

  For the α-elements, [Mg/Fe] and [Si/Fe] show weak positive correlations with planet mass (PCC = 0.08 and 0.19, respectively) more pronounced in stars hosting high-mass planets, while the Mg/Si ratio exhibits a weak negative trend (PCC= -0.15) more pronounced in stars hosting high-mass planets, suggesting that higher-mass planetary systems may be associated with relatively lower Mg/Si ratios.

- Among *n*-capture elements, first-peak *s*-process elements, Sr, Y, and Zr, display behaviours consistent with their nucleosynthetic origin in the weak *s*-process of low- and intermediate-mass AGB stars. While [Sr/Fe] and [Y/Fe] remain broadly aligned with Galactic trends and show no significant enhancement in PHSs, [Zr/Fe] appears systematically enhanced in planet hosts relative to the comparison sample at a given metallicity.

  The [El/Fe] ratios of Sr, Y, and Zr increase toward lower [Fe/H] and lower [Y/Mg], with the Zr enrichment being the most pronounced.

These results suggest that light *s*-process elements are primarily governed by standard Galactic enrichment, though zirconium may retain an imprint of planet formation or local enrichment effects.

For the second-peak *s*-process elements Ba, La, and Ce, we found that barium exhibits nearly solar [Ba/Fe] values across the metallicity range and shows no planet-related anomalies, consistent with the findings for comparison stars. In contrast, lanthanum and cerium show a modest but systematic [La/Fe] and [Ce/Fe] overabundance in planet-hosting stars, especially at sub-solar metallicities. These enhancements may indicate that AGB-star contributions to the natal material of planet hosts were slightly higher, possibly favouring dust-rich environments conducive to planet formation.

The mixed *r*+*s* elements Pr, Nd, and the *r*-process-dominated element Eu, follow the canonical Galactic trends of increasing [El/Fe] with decreasing metallicity. Their average abundance ratios in PHSs are indistinguishable from those of comparison stars within uncertainties.

- Analysis of [El/Fe] ratios as a function of planetary mass reveals that, overall, the abundances of *n*-capture elements in PHS show only a weak dependence on the masses of their planetary companions. Nevertheless, some systematic trends emerge when different nucleosynthetic groups and stellar evolutionary stages are considered. Among the light *s*-process elements, Sr and Y show no statistically significant correlation with planet mass, though a subtle depletion trend may still be present in dwarf stars hosting massive planets particularly when considering the most massive planet in multiplanetary systems. Zirconium, in contrast, consistently shows a positive correlation with planetary mass across all cases, implying that stars with more massive planets tend to be enriched in Zr. Barium, meanwhile, shows slightly negative slopes that may suggest mild depletion in systems with higher-mass planets, though the effect remains within typical abundance uncertainties. For heavier *n*-capture elements such as La, Ce, Pr, Nd, and Eu, moderate to strong positive correlations are observed, particularly among giant stars. These consistent positive trends may indicate

a potential link between the enrichment of these heavy *s*-process elements and the formation or presence of massive planets.

- The distribution of abundance differences between our stars with planets and carefully selected comparison stars (Δ[El/H]) versus condensation temperature shows a distinct positive skewness for the overall sample, implying a general enrichment of refractory elements in PHS relative to volatile ones when compared with their non-host stellar twins. This trend supports the hypothesis that PHS are, on average, more refractory-rich, consistent with the sequestration of refractories into planetary material and subsequent chemical signatures in the host star's photosphere.

  However, when looking at the dwarf star subsample, the slope distribution shifts closer to zero, suggesting less significant trends in abundance differences versus $T_{\rm cond}$.

  Furthermore, although the Δ[El/H]–$T_{\rm cond}$ slopes show no strong correlations with individual stellar or planetary parameters, the results reveal subtle systematic tendencies: older dwarf stars with multiple planets tend to exhibit smaller or even negative slopes, whereas younger dwarf stars display larger positive slopes. This may indicate that chemical signatures linked to planet formation become less pronounced with stellar age or that younger stellar populations have retained higher refractory-to-volatile ratios from the interstellar medium.

Future aspects of the research The results presented in this thesis mark significant progress in understanding the "star-planet" connection. The correlations uncovered among the light, α, and *n*-capture elements open several promising avenues for future research. The next steps in this research will aim to refine the interpretation of these chemical signatures, extend the element coverage, and strengthen the links between stellar chemistry and planetary system formation. Future research should focus on improving both the precision and completeness of elemental abundance measurements. Although this thesis employed a homogeneous spectroscopic approach within the LTE framework and accounted for NLTE effects for selected elements, future investigations should aim to

implement a comprehensive 3D and NLTE analysis for all key elements, particularly those known to be strongly affected by such effects. Incorporating these advanced corrections will reduce systematic uncertainties, especially for giants and metal-poor hosts. Moreover, expanding the current dataset to a larger and more diverse stellar sample, including thick-disc, metal-poor, and halo populations, will help establish whether the observed chemical patterns in PHS are universal or shaped by their Galactic environment and stellar population. Another important step involves broadening the chemical inventory beyond the elements studied in this thesis. Adding elements like lithium to the investigation will help trace stellar mixing, accretion, and possible signatures of planet engulfment. Among heavy elements, future work should include additional heavy *s* and *r*-process elements such as molybdenum and samarium. Similarly, a detailed mapping of iron-peak and refractory elements such as chromium, cobalt, nickel, copper, and zinc will clarify whether the observed Δ[El/H]–$T_{\rm cond}$ slopes reflect true refractory enrichment or local dust-to-gas variations during star formation.

The correlations between certain heavy element abundances and planetary masses observed in this work suggest that chemistry may influence planet formation efficiency or core composition. To test this hypothesis, future studies should integrate homogeneous exoplanet data. Combining future spectroscopic results with precise planetary parameters from TESS, PLATO, and JWST will enable more robust analyses of how individual elements, or specific abundance ratios, vary with planetary mass, multiplicity, and orbital configuration. Cross-matching detailed abundances with kinematic data from *Gaia* DR4 and subsequent releases will allow the chemical and kinematic histories of PHS to be traced simultaneously.

9 Acknowledgements

This research has made use of the NASA Exoplanet Archive, operated by the California Institute of Technology under contract with the National Aeronautics and Space Administration's Exoplanet Exploration Program, and the SIMBAD database, operated at CDS, Strasbourg, France. I also extend my appreciation to Vilnius University's Molėtai Astronomical Observatory for granting observation time for this project, which was partially funded by the Europlanet Telescope Network programme of the Europlanet 2024 Research Infrastructure project. Europlanet 2024 RI has received funding from the European Union's Horizon 2020 research and innovation programme under grant agreement No. 871149.

I want to express my sincere gratitude to my supervisor, Dr. Edita Stonkutė, for her guidance, patience, and continuous support throughout this work, and to Prof. Gražina Tautvaišienė for her mentorship and for providing an inspiring research environment at the Institute of Theoretical Physics and Astronomy, Vilnius University. I would also like to thank my collaborators and colleagues: Dr. Arnas Drazdauskas, Dr. Šarūnas Mikolaitis, Dr. Renata Minkeviciūtė, Dr. Carlos Viscasillas Vázquez, Dr. Markus Ambrosch, Barkha Bale, Bruno Ćurjurić, and the whole "Astrospectroscopy and exoplanets" research group for their cooperation, discussions, and friendship. Special thanks to Barkha for being a friend more than a colleague.

My deepest gratitude goes to my family, especially my parents and brother. Their endless support, sacrifices, and belief in me made this journey possible. Without them, this journey would not have been possible. This work is dedicated to them with the deepest gratitude. I would also like to express my heartfelt appreciation to Arpine and her parents for their love and constant encouragement. During the most challenging moments of this journey, they were always there with support and understanding. Finally, I am grateful to all my friends in Lithuania who shared these years of my PhD journey with me.

Santrauka (Summary in Lithuanian)

Tyrimo temos apžvalga ir mokslinė problematika

Egzoplanetų atradimas iš esmės transformavo šiuolaikinę astrofiziką ir skatina mokslininkus ieškoti galimo ryšio tarp žvaigždžių ir jų planetų. Detali žvaigždžių atmosferų cheminė sudėtis atskleidžia proplanetinio disko sudėtį, kuri gali suteikti įžvalgų apie planetų formavimąsi, jų vidinę struktūrą ir atmosferų sudėtį (Madhusudhan et al. 2012; Bitsch & Battistini 2020; Dorn et al. 2019). Nepaisant pažangos šioje srityje, esminiai klausimai lieka neišspręsti. Nors žinoma, kad planetos milžinės linkusios formuotis prie metalingų žvaigždžių (Gonzalez 1997; Santos et al. 2001; Fischer & Valenti 2005), ši tendencija nėra stebima sistemose su mažos masės planetomis (Ghezzi et al. 2010; Sousa et al. 2011; Buchhave et al. 2012).

Naujausi žvaigždžių atmosferų tyrimai koncentruojami ne tik į geležies gausas, bet įtraukia ir lakiuosius bei α-elementus (C, N, O, Mg, Si), kurie yra esminiai planetų minerologijai, atmosferų cheminei sudėčiai ir proplanetinio disko kondensacijos procesams (Delgado Mena et al. 2010; Mishenina et al. 2016; Suárez-Andrés et al. 2016, 2017, ir kt.). C/O ir Mg/Si santykiai yra ypatingai svarbūs. Teoriniai modeliavimai rodo, kad, esant C/O santykiui didesniam už 0,80, planetos turėtų būti turtingos silikatais (Brewer & Fischer 2016), tuo tarpu Mg/Si santykis yra atsakingas už mantijos minerologiją (Santos et al. 2015). Vis dėlto šios tendencijos nėra visiškai aiškios dėl mažų imčių ir nevienodų gausų nuatatymo metodų.

Neutronų pagavimo elementų, gaminamų tiek *s*-, tiek *r*- procesų metu (Busso et al. 2001; Pian et al. 2017; Côté et al. 2018), gausos nustatytos žvaigždžių atmosferose taip pat gali atskleisti cheminius pėdsakus, susijusius su planetų formavimusi. Tačiau šių elementų gausų tendencijos žvaigždėse su planetomis lieka dviprasmiškos. Kai kuriuose tyrimuose nurodomi sistematiniai skirtumai, pavyzdžiui, „Barium puzzle“ – bario gausos perteklius jaunuose spiečiuose (Reddy & Lambert 2017), arba Ba gausos trūkumas žvaigždėse su planetomis (Mishenina et al. 2016; Delgado Mena et al. 2018; Swastik et al. 2022).

Papildomų neaiškumų kyla ir dėl nustatytų koreliacijų tarp planetas turinčių ir palyginamųjų žvaigždžių cheminių gausų skirtumų bei elementų kondensacijos temperatūrų ($T_{\rm cond}$). Šios koreliacijos indikuoja, kad cheminiai elementai, pasižymintys aukšta kondensacijos temperatūra, galimai yra užrakinami uolinėse planetose (Meléndez et al. 2009; Ramírez et al. 2010). Tačiau alternatyvūs paaiškinimai, tokie kaip Galaktikos cheminė evoliucija arba dulkių ir dujų segregacija, taip pat išlieka galimi (Adibekyan et al. 2014; Nissen 2015), o šių tendencijų reikšmė planetas turinčioms žvaigždėms tebėra diskusijų objektas.

Dabartines žvaigždžių atmosferų cheminių elementų gausų ir planetų ryšio interpretacijas vis dar riboja nuolatiniai iššūkiai. Daugelyje tyrimų naudojamos nedidelės arba heterogeninės imtys, taikomi skirtingi cheminių elementų gausų analizės metodai arba remiamasi nevienodos kokybės spektrais, o visa tai nulemia reikšmingas sistematines paklaidas. Be to, žvaigždžių be aptiktų planetų palyginimo imtys ne visada atrenkamos ar analizuojamos vienodai, kaip ir planetas turinčių žvaigždžių. Dėl šių priežasčių dažnai sudėtinga nustatyti, ar stebimi cheminių gausų pasiskirstymai iš tikrųjų atspindi planetų formavimosi procesus, ar jie kyla dėl platesnio masto reiškinių, tokių kaip Galaktikos cheminė evoliucija, žvaigždžių amžius, jų kinematika ar aplinkos veiksniai.

Šioje disertacijoje siekiama spręsti išvardytus iššūkius, atliekant homogeninę 160 ryškių planetas turinčių žvaigždžių didelės skiriamosios gebos spektrų analizę, pagrįstą stebėjimais, atliktais naudojant Molėtų astronomijos observatorijos VUES spektrografą ir 1,65 m teleskopą. Darbas remiasi trimis recenzuotomis publikacijomis:

- I publikacijoje pateikta anglies, azoto, deguonies, magnio ir silicio cheminių gausų analizė 25 ryškioms planetas turinčioms žvaigždėms.
- II publikacijoje pateikta išplėsta imtis iki 149 žvaigždžių su planetomis ir daugiausia dėmesio skirta tam pačiam cheminių elementų rinkiniui, nagrinėtam I publikacijoje.
- III publikacijoje, kurioje pateikta 160 žvaigždžių su planetomis imtis ir devynių neutronų pagavimo proceso cheminių elementų (Sr, Y, Zr, Ba, La, Ce, Pr, Nd ir Eu) gausų analizė.

Šios trys publikacijos kartu sudaro didžiausią homogeninį šiaurinio dangaus planetas turinčių žvaigždžių cheminių gausų duomenų rinkinį, gautą naudojant VUES spektrografą. Šie rezultatai, analizuojami kartu su žvaigždžių metalingumu, amžiumi, kinematika ir planetų parametrais, leidžia pateikti patikimas įžvalgas apie cheminius ryšius tarp žvaig-ždžių ir jų planetų bei išplečia supratimą apie Galaktikos cheminę evoliuciją.

Darbo tikslas ir uždaviniai

Šio darbo tikslas yra ištirti galimą ryšį tarp žvaigždžių ir jų planetų, analizuojant planetas turinčių žvaigždžių atmosferų cheminę sudėtį. Taikant homogeninę didelės skiriamosios gebos ryškių F-, G- ir K-spektrinės klasės žvaigždžių su patvirtintomis planetomis spektroskopinę analizę, nagrinėjama, kaip lengvųjų elementų (C, N), α elementų (O, Mg, Si) ir neutronų pagavimo elementų (Sr, Y, Zr, Ba, La, Ce, Pr, Nd ir Eu) gausos yra susijusios su žvaigždžių ir planetų savybėmis. Svarbi šio darbo užduotis yra nustatyti, ar planetas turinčios žvaigždės pasižymi sisteminiais cheminiais skirtumais, palyginti su žvaigždėmis be aptiktų planetų, ir ar tokie skirtumai yra žvaigždžių formavimosi pasėkmė, ar juos lemia planetų formavimosi procesai.

Šiam tikslui pasiekti darbo metu buvo suformuluoti ir įgyvendinti pagrindiniai uždaviniai.

- Remiantis NASA egzoplanetų archyvo ir TESS katalogų duomenimis sudarytas homogeninis šiaurinio dangaus planetas turinčių žvaigždžių sąrašas. Naudojant Molėtų astronomijos observatorijos VUES spektrografą, gauti šių žvaigždžių aukštos skiriamosios gebos spektrai, taip pat sudaryta palyginamoji planetų neturinčių žvaigždžių imtis, stebėta tuo pačiu prietaisu ir analizuota taikant tuos pačius metodus.

- Žvaigždžių atmosferų parametrai apskaičiuoti naudojant klasikinį ekvivalentinių pločių metodą, o pagrindinių cheminių elementų gausos nustatytos taikant spektrinės sintezės metodą, o daliai elementų atliktos ir NLTE korekcijos.

- Cheminių elementų gausų kitimo dėsningumai ištirti atsižvelgiant į žvaigždžių ir planetų savybes, tokias kaip metalingumas, amžius ir

planetų masė. Be to, analizuoti cheminių gausų skirtumai tarp planetas turinčių ir palyginamųjų žvaigždžių, įvertinant jų pasiskirstymą nuo kondensacijos temperatūros, siekiant identifikuoti galimus aukštos kondensacijos temperatūros elementų pėdsakus atsirandančius planetų formavimosi proceso metu.

Ginamieji teiginiai

1. Žvaigždžių nykštukių su planetomis C ir O gausos yra sistemingai mažesnės nei palyginamosiose žvaigždėse, esant metalingumui didesniam nei Saulės. Žvaigždžių milžinių rezultatai rodo, kad C, N ir O gausos abiejose grupėse iš esmės pasiskirsto panašiai, tačiau planetas turinčios milžinės, esant tam tikram metalingumui, pasižymi šiek tiek mažesne [C/Fe] gausa. C/O ir N/O santykiai didėja didėjant metalingumui, tačiau statistiškai reikšmingų skirtumų tarp planetas turinčių ir palyginamųjų žvaigždžių nenustatyta. Mg ir Si gausos yra padidėjusios planetas turinčiose žvaigždėse, ypač esant mažam metalingumui. Tuo tarpu Mg/Si santykis šiose žvaigždėse yra sistemingai mažesnis, o žvaigždėms, turinčioms didelės masės planetas, Mg/Si santykio pasiskirstymas skiriasi statistiškai reikšmingai.

2. Žvaigždėse nykštukėse nustatyta silpna neigiama koreliacija tarp [C/Fe], [N/Fe], [O/Fe] ir planetų masės. Tuo tarpu žvaigždėse milžinėse atvirkščiai - stebima silpna koreliacija tarp planetos masės ir [C/Fe], [O/Fe] ir [N/Fe]. C/O ir N/O žvaigždėse nykštukėse didėja, o milžinėse C/O ir N/O santykiai pasižymi priešingais nuo planetų masės pasiskirstymais. [Mg/Fe] ir [Si/Fe] rodo silpną didėjimą didėjant planetų masei. Mg/Si santykis pasižymi nedidele neigiama koreliacija, kuri ryškiausiai pasireiškia didelės masės planetų sistemose.

3. Milžinių suminė A(C+N+O) gausa didėja didėjant [Fe/H], kaip ir numato Galaktikos cheminės evoliucijos modeliai. Lyginant A(C+N+O) pasiskirstymą tarp planetas turinčių ir palyginamųjų žvaigždžių, reikšmingų skirtumų nenustatyta. Plonojo disko žvaigždžių populiacijoje pastebima galima skirtis, t.y. milžinės su masyviomis planetomis rodo kiek kitokį A(C+N+O) gausų pasiskirstymą.

4. Neutronų pagavimo elementų gausos planetas turinčių žvaigždžių atmosferose atitinka Galaktikos cheminės evoliucijos modelius. Rezultatai rodo, kad lengvųjų *s*-proceso elementų [Sr/Fe], [Y/Fe] ir [Zr/Fe] gausos auga link mažesnių metalingumų. Antrojo piko *s*-proceso elemento Ba gausa nustatyta nepadidėjusi esant mažesniam nei Saulės metalingumui, o La ir Ce gausos didėja mažėjant [Fe/H]. Žvaigždžių su planetomis atmosferose La ir Ce gausos yra šiek tiek padidėjusios. *s*- ir *r*-procesų elementų Pr, Nd ir *r*-proceso elemento Eu gausos didėja, mažėjant metalingumui.

5. Sr, Y ir Ba reikšmingų koreliacijų su planetų mase nenustatyta. Tuo tarpu Zr gausa koreliuoja su planetų mase, labiau matomą žvaigždėse nykštukėse. Žvaigždžių milžinių imtyje La, Ce Pr ir Nd gausos koreliuoja su planetų mase. Eu gausa taip pat rodo silpną teigiamą koreliaciją su planetų mase. Šiuos dėsningumus būtina vertinti kritiškai, nes Galaktikos cheminės evoliucijos procesai gali iškreipti arba užmaskuoti tikruosius, su planetomis susijusius cheminių elementų gausų pokyčius.

6. Žvaigždės rodo teigiamus Δ[El/H]-$T_{\rm cond}$ polinkius, o tai reiškia didesnę uolinių elementų gausą, palyginti su lakiųjų elementų gausomis. Šis efektas mažesnis žvaigždėse nykštukėse, kurioms nustatytos silpnesnės planetų formavimosi paliktos cheminės žymės atmosferose. Tai leidžia manyti, kad planetų formavimasis, ypač metalingose ir daugiaplanetėse sistemose, gali palikti subtilius, bet pastebimus cheminius pėdsakus žvaigždžių atmosferose.

1. Įvadas

Egzoplanetų tyrimai prasidėjo nuo pirmųjų jų atradimų šalia pulsaro (Wolszczan & Frail 1992) ir Saulės tipo žvaigždės (Mayor & Queloz 1995). Pažanga tiek antžeminiuose radialinio greičio tyrimuose, tiek kosminėse tranzitų misijose, tokiose kaip Kepler (Borucki et al. 2010) ir TESS (angl. Transiting Exoplanet Survey Satellite) (Rinehart et al. 2015), išplėtė patvirtintų egzoplanetų sąrašą iki daugiau kaip 6,000 objektų. Artimiausiais metais jų skaičius dar labiau augs, kai pradės veikti naujos kartos kosminiai teleskopai, pavyzdžiui, PLATO (angl. Planetary Transits and Oscillations of Stars) (Rauer et al. 2024), ARIEL

(angl. Atmospheric Remote-sensing Infrared Exoplanet Large-survey) (Tinetti et al. 2022) arba antžeminis E-ELT (angl. European Extremely Large Telescope) (de Zeeuw et al. 2014). Tokie spartūs atradimai lėmė, kad dėmesys vis labiau krypsta nuo pačių egzoplanetų paieškų link jų fizikinių, cheminių ir statistinių savybių tyrimų (Udry & Santos 2007; Winn & Fabrycky 2015). Šioje disertacijoje keliama mokslinė problema: ar planetų buvimas ir jų savybės palieka aptinkamus cheminius pėdsakus žvaigždžių atmosferose?

Aukštos skiriamosios gebos žvaigždžių spektroskopija yra esminis įrankis, leidžiantis tiksliai nustatyti žvaigždžių atmosferų cheminę sudėtį, analizuojant atskiras spektrines sugerties linijas (Gray 2005). Šie cheminiai pėdsakai veikia tarsi proplanetinių diskų, kuriuose formavosi planetos, fosilijų įrašai. Spektrinių linijų formavimasis, priklausantis nuo elektronų perėjimų, spinduliuotės pernašos, sužadinimo ir jonizacijos pusiausvyrų bei termodinaminių sąlygų žvaigždžių atmosferose, suteikia informaciją apie žvaigždžių parametrus, tokius kaip temperatūra, slėgis, gravitacijos pagreitis paviršiuje, mikroturbulentinis greitis ir, svarbiausia, cheminių elementų gausos.

Tikslus spektrinių linijų interpretavimas priklauso nuo aukštos kokybės atominių duomenų iš tokių duomenų bazių kaip VALD (Piskunov et al. 1995) ar NIST (Kramida et al. 2023), atmosferų modelių, pavyzdžiui MARCS (Gustafsson et al. 2008), ATLAS9 (Kurucz 1993) ar PHOENIX (Husser et al. 2013), bei atidaus dėmesio tokiems procesams kaip sužadinimo ir jonizacijos pusiausvyra, linijų išplitimas ar blendavimas. Daugeliui elementų reikalingos papildomos linijų išplitimo korekcijos, atsiradusio dėl hipersmulkiosios struktūros arba izotopų poslinkio (McWilliam 1998; Sneden et al. 2002), gausų nustatymui gali prireikti NLTE korekcijų, kai LTE prielaidos nepasiteisina (Asplund 2005; Mashonkina et al. 2011; Lind et al. 2012).

Šiuolaikiniai spektrografai, tokie kaip HARPS (Mayor et al. 2003), UVES (Dekker et al. 2000), HIRES (Vogt et al. 1994), ESPRESSO (Pepe et al. 2021), ar VUES (Jurgenson et al. 2016), suteikia tiksliam žvaigždžių atmosferų parametrų nustatymui ir gausos analizei reikalingą spektrinę skiriamąją gebą ir stabilumą. O duomenų redukcijos programinių paketų pagalba atliekami pagrindiniai veiksmai, įskaitant plokščiojo lauko korekciją, bangos ilgių priskyrimą (pavyzdžiui, naudojant ThAr

lempas), ir eilių sujungimą. Tuomet cheminių elementų gausų analizė paprastai atliekama naudojant ekvivalentinių pločių arba spektrinės sintezės metodus, pasitelkus plačiai naudojamus įrankius, tokius kaip MOOG (Sneden 1973), SME (Valenti & Piskunov 1996) ar iSpec (Blanco-Cuaresma et al. 2014).

Žvaigždės ir planetos ryšys

Svarbus empirinis atradimas, nagrinėjant žvaigždžių ir planetų ryšį, yra priklausomybė tarp žvaigždžių metalingumo ir planetų milžinių susidarymo tikimybės. Kitaip tariant, didelės masės planetos daug dažniau formuojasi aplink žvaigždes, turinčias didesnį metalingumą, nes tokiuose protoplanetiniuose diskuose yra daugiau kietos medžiagos, reikalingos greitam planetų branduolių augimui pagal branduolio akrecijos modelį (Gonzalez 1997; Santos et al. 2001; Fischer & Valenti 2005; Johnson et al. 2010, ir kt.). Tuo tarpu mažos masės planetos gali efektyviai formuotis labai plačiame metalingumo intervale (Ghezzi et al. 2010; Sousa et al. 2011; Buchhave et al. 2012), todėl siekiant visapusiškai suprasti planetų formavimosi procesus būtina nagrinėti ne tik geležies, bet ir kitų cheminių elementų gausas.

Šiame kontekste lakieji ir α-elementai, tokie kaip C, N, O, Mg ir Si, vaidina lemiamą vaidmenį apsprendžiant planetų formavimosi būdą ir jų sudėtį (pvz., Bitsch & Battistini 2020; Bitsch & Mah 2023). Šių elementų gausos, išreikštos santykiais C/O, N/O ir Mg/Si, turi įtakos kondensacijos sekoms, mineralogijai ir atmosferos savybėms. Be to, tai turi įtakos tam, ar protoplanetiniame diske planetos formuojasi iki įvairių anglies, azoto ir deguonies molekulių ledo linijų, ar už jų, o tai yra labai svarbu reguliuojant kietųjų dalelių prieinamumą planetoms formuojantis (Öberg et al. 2011; Schneider & Bitsch 2021; Ohno & Fortney 2023). Ypač svarbus yra Mg/Si santykis, nes jis nulemia silikatų mineralogiją, kuri tiesiogiai siejasi su planetų mantijų sudėtimi (Bond et al. 2010).

Ankstyvieji tyrimai, kurie analizavo lengvuosius elementus, nerado anglies gausos skirtumų tarp žvaigždžių su planetomis ir palyginamųjų žvaigždžių (Ecuvillon et al. 2004b, 2006). Vėlesnės, didesnėmis imtimis paremtos analizės parodė, kad žvaigždės su planetomis gali būti šiek tiek praturtintos anglimi (Suárez-Andrés et al. 2017). Pastebėta, kad mažos masės planetas turinčios žvaigždės gali pasižymėti didesniu [C/Fe] esant

mažesniam nei Saulės metalingumui, tačiau prie metalingų žvaigždžių ši tendencija neaptikta (Delgado Mena et al. 2021). Deguonies gausa žvaigždėse su mažos masės planetomis rodo panašius požymius, tačiau dėl didelių neapibrėžčių nebuvo galima pateikti tvirtų išvadų (Delgado Mena et al. 2021; Biazzo et al. 2022). Šiek tiek didesnės azoto gausos taip pat nustatytos žvaigždėse su mažos masės planetomis (Suárez-Andrés et al. 2016).

Alfa elementų atveju buvo nustatyta, kad storojo disko žvaigždės su planetomis dažnai turi padidintą magnio ir silicio gausą (Adibekyan et al. 2012a). Manoma, kad šis padidėjimas gali kompensuoti mažesnę geležies gausą planetų formavimuisi (Bashi & Zucker 2019). Taip pat manoma, kad planetų Mg/Si santykis paprastai atspindi jų žvaigždžių Mg/Si santykį (Thiabaud et al. 2015).

Neutronų pagavimo (*n*-pagavimo) elementai daugiausia susidaro dviejų procesų metu. Lėtojo – *s*-proceso metu, vykstančiame AGB etapo ir kai kuriose masyviose žvaigždėse, formuojasi tokie elementai kaip Sr, Y, Zr (pirmasis pikas) ir Ba, La, Ce, Pr, Nd (*s*-proceso antrasis pikas). Tuo tarpu greitojo *n*-pagavimo arba *r*-proceso, vykstančio supernovų sprogimuose ir neutroninių žvaigždžių susiliejimuose, metu susidaro tokie elementai kaip europis (Karakas & Lattanzio 2014; Cseh et al. 2022; Cowan et al. 2021; Travaglio et al. 1999; Bisterzo et al. 2014; Prantzos et al. 2020). Šių elementų gausos atspindi Galaktikos cheminės evoliucijos istoriją ir gali turėti įtakos planetinėms sistemoms. Ankstyvieji tyrimai parodė, kad žvaigždės su planetomis turi didesnę šių elementų gausą (Bond et al. 2008). Tačiau vėlesni darbai atskleidė kiek sudėtingesnį vaizdą, ypač bario atveju: literatūroje pranešta ir apie Ba perteklių, ir apie jo trūkumą (da Silva et al. 2015; Mishenina et al. 2016; Delgado Mena et al. 2018). Tai rodo, kad šių elementų gausų interpretacijai svarbus žvaigždžių populiacijos kontekstas.

Cheminių elementų gausos gali atspindėti planetų formavimosi procesus, ypač tada, kai jos siejamos su kondensacijos temperatūra ($T_{\rm cond}$), tai yra temperatūra, kuriai esant cheminiai elementai protoplanetiniuose diskuose pereina iš dujų į kietą būseną. Uoliniai elementai kondensuojasi esant aukštoms temperatūroms (apie $\gtrsim$1200 K), o lakieji elementai – daug žemesnėms (apie $\lesssim$200 K). Tuomet, žvaigždžių su planetomis ir palyginamųjų žvaigždžių gausų skirtumų Δ[El/H] priklausomybės

nuo $T_{\rm cond}$ polinkiai yra interpretuojami kaip galimi planetų formavimosi požymiai. Uolinių elementų sumažėjimas gali reikšti, kad jie buvo „sunaudoti" planetų formavimuisi, o jų perteklius, kad jie pateko į žvaigždės atmosferą (Meléndez et al. 2009; Adibekyan et al. 2016; Yun et al. 2024). Nors šie ryšiai plačiai tyrinėjami, gauti rezultatai vis dar nėra nuoseklūs dėl skirtingų analizės metodų ir ribotų imčių (Mishenina et al. 2016; Delgado Mena et al. 2018; Swastik et al. 2022; da Silva et al. 2024).

2. Stebėjimų duomenys ir analizės metodai

Ši disertacija parengta remiantis aukštos skiriamosios gebos spektroskopiniais stebėjimais, analizuojant ryškių šiaurės pusrutulio F, G ir K spektrinių klasių žvaigždžių su planetomis (V$\leq$8.5 mag) spektrus. Šios žvaigždės atrinktos iš NASA egzoplanetų archyvo pagal griežtus kriterijus ir apima tiek pagrindinės sekos nykštukes, tiek ir evoliucionavusias žvaigždes milžines. Galutinę imtį sudarė 160 žvaigždžių su planetomis, kolektyviai turinčių 222 patvirtintas planetas.

Stebėjimai buvo atlikti 2021 – 2024 m. naudojant Vilniaus universiteto ešele spektrografą VUES (Jurgenson et al. 2016), prie 1.65 m teleskopo Molėtų astronomijos observatorijoje. Šiame darbe analizuoti $R \sim 36,000$ ir $68,000$ spektrinės gebos spektrai, o jų ekspozicijų trukmės stebint parinktos taip, kad būtų pasiekti 75–200 S/N santykiai. Homogeniškai apdoroti, sukalibruoti ir normalizuoti VUES spektrografo spektrai leido tiksliai nustatyti žvaigždžių parametrus ir cheminių elementų gausas. Be to, į analizę buvo įtrauktas homogeniškas žvaigždžių be aptiktų planetų palyginamasis rinkinys iš ankstesnių tyrimų (Mikolaitis et al. 2019; Stonkutė et al. 2020; Tautvaišienė et al. 2022). Tai leido patikimai įvertinti cheminių gausų skirtumus tarp žvaigždžių su planetomis ir palyginamųjų, pasitelkiant vienodus stebėjimo ir analizės būdus.

2.1 Žvaigždžių kinematinės savybės ir amžius

Galaktiniai žvaigždžių erdviniai greičiai (U, V, W), vidutinis galaktocentrinis atstumas ($R_{\rm mean}$), didžiausias žvaigždės nuokrypis nuo Galaktikos plokštumos ($|z_{\rm max}|$) ir orbitų ekscentricitetai (e) apskaičiuoti kiekvienai

žvaigždei naudojant *galpy* paketą[6] (Bovy 2015), kuris skaitmeniškai integruoja žvaigždžių orbitas realistiškame Galaktikos gravitaciniame potenciale *MilkyWayPotential2014*. Žvaigždžių atstumai paimti iš Bailer-Jones et al. (2021), savieji judėjimai ir koordinatės – iš *Gaia* EDR3 katalogo (Gaia Collaboration et al. 2016, 2021; Lindegren et al. 2021; Seabroke et al. 2021), o reikalingi radialiniai greičiai daugiausia nustatyti šiame darbe. Visus įvesties duomenis perkėlus į galaktocentrinę koordinačių sistemą, pritaikytos Saulės padėties ir judėjimo korekcijos pagal Bovy et al. (2012). Tuomet, žvaigždžių orbitos integruotos 5 mlrd. m., siekiant nustatyti jų kinematinius ir orbitinius parametrus. Paklaidos įvertintos atliekant 1 000 Monte Karlo realizacijų kiekvienai žvaigždei. Visi įvesties dydžiai buvo atsitiktinai varijuojami pagal Gauso pasiskirstymą, o gauti išsibarstymai priimti kaip paklaidų reikšmės.

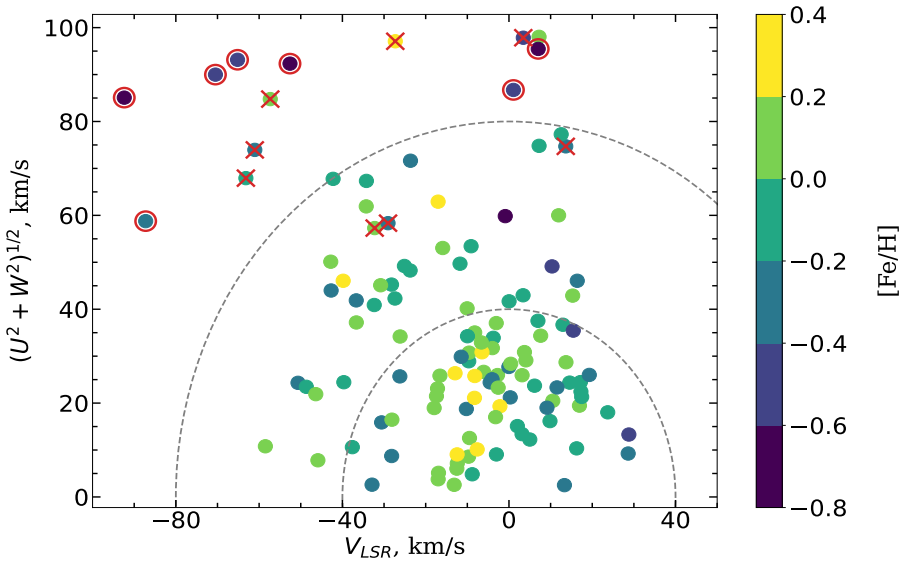

28 pav.: Analizuotų žvaigždžių Toomre diagrama. Simboliai nuspalvinti pagal metalingumą, [Fe/H]. Brūkšninės linijos žymi pastovią suminio erdvinio greičio ($v_{\rm tot} = (U^2_{\rm LSR} + V^2_{\rm LSR} + W^2_{\rm LSR})^{1/2}$) vertę ties 40 ir 80 km s^{-1}. Raudonai apibrėžtos žvaigždės priskirtos storojo disko populiacijai, o "x" pažymėtos tarpinės plonojo-storojo disko žvaigždės.

Žvaigždžių priklausomybė tam tikrai Galaktikos disko populiacijai nustatyta apskaičiuojant storojo ir plonojo disko tikimybės santykį

[6] http://github.com/jobovy/galpy

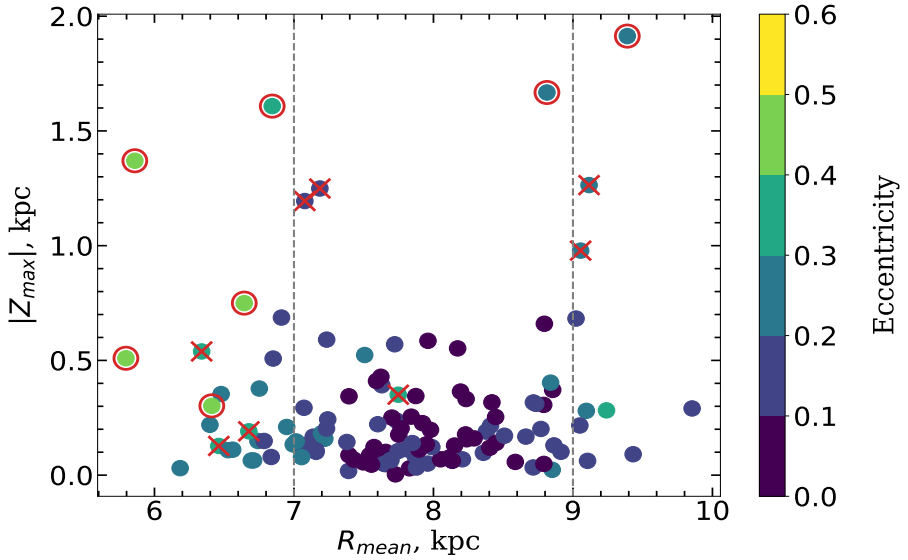

29 pav.: Stebėtų žvaigždžių vidutinio galaktocentrinio atstumo ($R_{\rm mean}$) ir maksimalaus atstumo nuo Galaktikos plokštumos $|z_{\rm max}|$ pasiskirstymas. Simboliai nuspalvinti pagal žvaigždžių orbitų ekscentricitetą. Vertikalios brūkšninės linijos žymi Saulės aplinką (7 kpc $< R_{\rm mean} <$9 kpc).

(TD/D), kaip aprašyta Bensby et al. (2003, 2014). Šis santykis gaunamas iš erdvinių greičių *U, V, W* komponentų, atsižvelgiant į Saulės judėjimą. Gauta TD/D reikšmė parodo, kiek tikėtina, kad žvaigždė priklauso storajam diskui, palyginti su plonuoju disku. Vadovaujantis Bensby et al. (2003) klasifikavimo schema, žvaigždės su TD/D $\leq$ 0,2 priskiriamos plonajam diskui, žvaigždės su TD/D $\geq$ 5 laikomos storojo disko nariais, o tarpinės reikšmės priskiriamos tarpinei (pereinamajai) populiacijai.

Žvaigždžių kinematinės savybės taip pat nagrinėtos pasitelkiant Toomre diagramą, kurioje $\sqrt{U^2+W^2}$ pavaizduota kaip funkcija nuo žvaigždės sukimosi greičio Saulės LRS atžvilgiu, $V_{\rm LSR}$ (žr. 28 pav.). Toomre diagrama atskleidė skirtumus tarp plonojo disko žvaigždžių, kurios pasižymi mažais erdviniais greičiais, ir storojo disko žvaigždžių, turinčių didesnius suminius greičius bei labiau neigiamus $V_{\rm LSR}$. Pastovaus suminio greičio kontūrai rodo, kad didžioji dalis žvaigždžių su planetomis turi $v_{\rm tot} < 50$ km s^{-1}, tuo tarpu storojo disko žvaigždėms būdingi greičiai viršija 80 km s^{-1}. Šis skirtumas taip pat matomas $R_{\rm mean}$–$|z_{\rm max}|$ pasi-

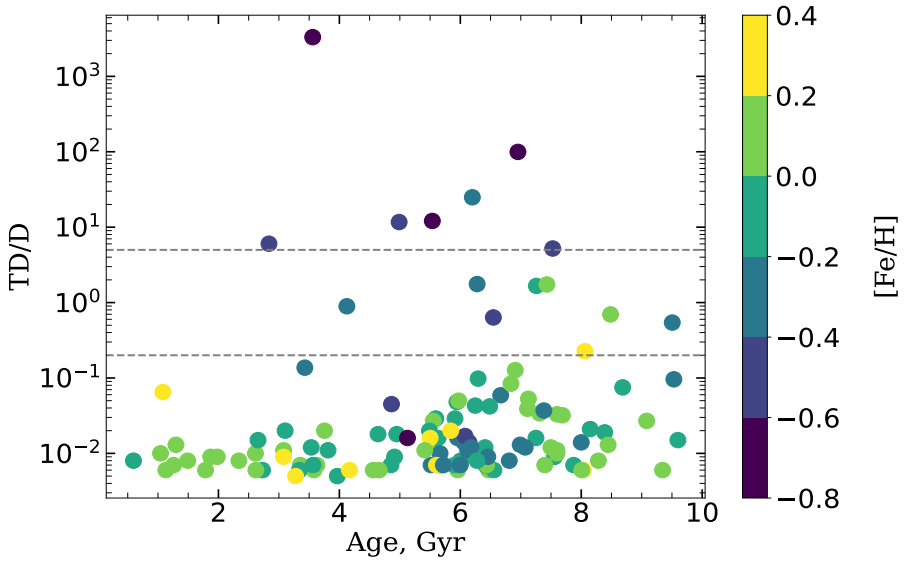

30 pav.: Kinematinių storo ir plono diskų tikimybės santykio (TD/D) pasiskirstymas nuo žvaigždžių amžiaus. Simboliai nuspalvinti pagal žvaigždžių metalingumą, [Fe/H]. Horizontalios punktyrinės linijos skiria ribas tarp plonojo disko, storojo ir tarpinės populiacijos.

skirstyme (žr. 29 pav.), kur žvaigždės su didesnėmis $|z_{\max}|$ ir didesniais ekscentricitetais aiškiai priklauso storajam diskui, o dauguma visų tirtų žvaigždžių yra Saulės aplinkoje ir turi mažas $|z_{\max}|$ vertes.

Žvaigždžių amžiai buvo nustatyti naudojant Bajeso izochronų aproksimacijos įrankį UniDAM (Mints & Hekker 2017, 2018). Jame, spektroskopiškai gauti žvaigždžių parametrai kartu su infraraudonąja fotometrija iš 2MASS (Skrutskie et al. 2006) bei AllWISE katalogų (Cutri et al. 2021) lyginami su PARSEC evoliuciniais trekais (Bressan et al. 2012). Tipinės amžiaus paklaidos siekia 10-30 %, priklausomai nuo žvaigždės evoliucijos etapo.

Analizuojant amžiaus įverčius su TD/D tikimybių santykiais, gaunamas amžiaus pasiskirstymas aiškiai parodo skirtumą tarp dviejų populiacijų: jaunesnių, metalais praturtintų plonojo disko žvaigždžių ir senesnių, kinematiškai „karštesnių“ storojo disko narių. Toks pasiskirstymas visiškai atitinka Galaktikos disko evoliucijos modelių rezultatus (žr. 30 pav.).

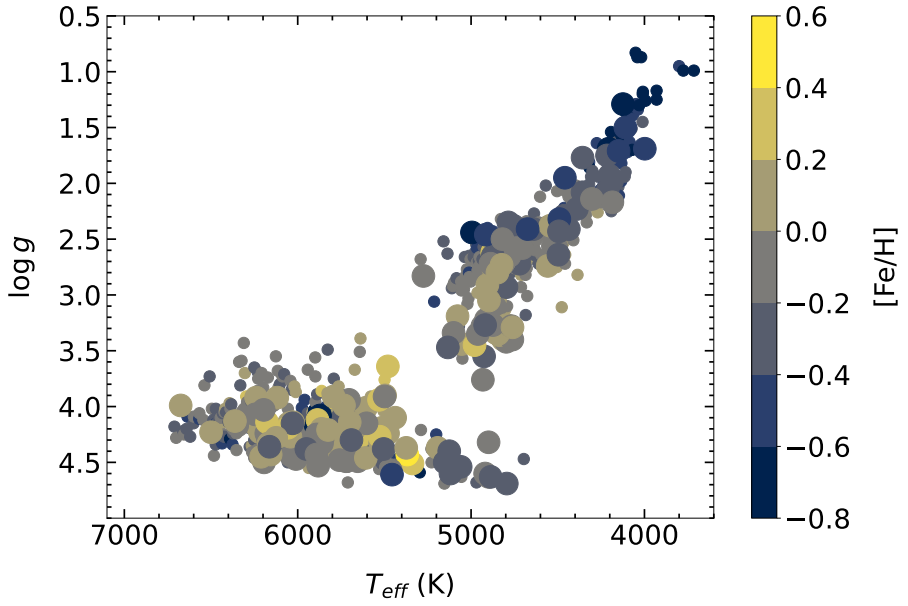

31 pav.: Žvaigždžių, turinčių planetas, efektinės temperatūros ($T_{\rm eff}$) ir paviršiaus gravitacijos (log g) pasiskirstymas. Simboliai nuspalvinti pagal metalingumą, [Fe/H]. Palyginamosios žvaigždės, paimtos iš Tautvaišienė et al. (2021), yra pažymėtos mažesniais simboliais.

2.2 Žvaigždžių atmosferų parametrai

Žvaigždžių atmosferų parametrai (efektinė temperatūra $T_{\rm eff}$ (K), paviršiaus gravitacijos pagreitis log g, mikroturbulentinis greitis $v_{\rm t}$ (km s^{-1}) ir metalingumas [Fe/H]) nustatyti naudojant klasikinį ekvivalentinių pločių metodą. Fe I ir Fe II linijų ekvivalentiniai pločiai išmatuoti su DAOSPEC (Stetson & Pancino 2008), o geriausiai tinkantys parametrai nustatyti apskaičiuojant geležies gausas naudojant MOOG (Sneden 1973) programinį paketą ir 1D LTE MARCS atmosferų modelius (Gustafsson et al. 2008), pasitelkiant sužadinimo ir jonizacijos balanso sąlygas. Žvaigždžių efektinė temperatūra apima platų intervalą (4000–6680 K). Paviršiaus gravitacijos pagreičio vertės aiškiai skiria milžines (1,3 – 3,5, vidurkis $2,8 \pm 0,6$) nuo nykštukių (3,6 – 4,7, vidurkis $4,2 \pm 0,2$). Metalingumas svyruoja nuo $-0,76$ iki 0,45, o vidurkis yra $-0,09 \pm 0,24$.

31 pav. $T_{\rm eff}$ ir log g diagramoje pavaizduotos planetas turinčios žvaigždės, o palyginamosios žvaigždės, paimtos iš Tautvaišienė et al. (2021), pavaizduotos mažesniais simboliais. Kaip matyti, imtis yra

maždaug tolygiai pasiskirsčiusi tarp evoliucionavusių ir pagrindinės sekos žvaigždžių.

2.3 Cheminių elementų gausos

Elementų gausos nustatytos lyginant sintetinius spektrus, apskaičiuotus naudojant TURBOSPECTRUM kodą (Alvarez & Plez 1998) ir 1D LTE MARCS atmosferų modelius, (Gustafsson et al. 2008), su stebėtais žvaigždžių spektrais. Analizei buvo taikytas griežtai homogeniškas, diferencialinės analizės metodas Saulės atžvilgiu, naudojant Saulės gausas iš Grevesse et al. (2007). Toks metodas leidžia sumažinti sistematines paklaidas, atsirandančias dėl atominių duomenų netikslumų, spinduliuotės pernašos prielaidų ir instrumentinių efektų. Vienodai taikoma visai žvaigždžių imčiai, ši metodika užtikrina tikslius ir nuoseklius tiek lengvųjų, tiek *n*-pagavimo elementų gausų įverčius. Prireikus buvo taikytos NLTE korekcijos ar korekcijos dėl hipersmulkiosios struktūros ir izotopinio išplitimo, ypač analizuojant *n*-pagavimo elementus.

Anglies gausa nustatyta iš C_2 molekulinių juostų ties 5135 Å ir 5635 Å (Brooke et al. 2013; Ram et al. 2014), azoto iš $^{12}C^{14}N$ molekulinių juostų 6470-6485 Å ir 7980-8005 Å regionuose (Sneden et al. 2014). Deguonies gausa nustatyta iš draustinės [O I] 6300 Å linijos, patikimos F, G, K spektrinės klasės žvaigždėse, kadangi ji nėra jautri NLTE ir 3D efektams (Amarsi et al. 2021). Ni I blenda ties šiuo bangos ilgiu įskaityta naudojant osciliatorių stiprius iš Johansson et al. (2003). Kadangi anglies ir deguonies gausos yra stipriai susijusios per CO molekulės susidarymą vėsiose žvaigždžių atmosferose, jų gausa buvo nustatyta iteracijos būdu siekiant molekulinės pusiausvyros sąlygų. Pirmiausia nustatomas deguonis iš [O I] linijos, po to anglis nustatoma iš C_2 linijų, naudojant atnaujintą deguonies gausos vertę, ir šis ciklas kartojamas tol, kol pasiekiama pusiausvyra. Užfiksavus anglies ir deguonies gausas, azotas nustatytas iš CN molekulinių linijų, tokiu būdu užtikrinant homogenišką C, N ir O gausų nustatymą visai žvaigždžių imčiai.

Devyni neutronų pagavimo elementai (Sr, Y, Zr, Ba, La, Ce, Pr, Nd, and Eu) gauti naudojant tą patį sintetinių spektrų metodą, spektro linijas pasirinkus iš *Gaia*-ESO apžvalgos linijų sąrašo 5 versijos (Heiter et al. 2021). Siekiant užtikrinti linijų patikimumą F, G, K spektrinės klasės žvaigždėms atrinktos tik tos linijos kurios buvo identifikuotos kaip pa-

tikimos. Spektrinių linijų kalibravimas pagal Saulės spektro sugerties linijas atliktas naudojant Kurucz (2005) Saulės spektrą ir Grevesse et al. (2007) Saulės gausas, o kalibruotų linijų sąrašas papildomai patvirtintas VUES Saulės spektrui, atkuriant gausas su mažesniu nei 0,05 dex nuokrypiu. Hipersmulkioji struktūra ir izotopinis poslinkis įtraukti, atitinkamų elementų gausų nustatymams, ypač Ba, La, Pr, Nd ir Eu, kur šie efektai reikšmingai veikia linijų profilius. Turint kelias to paties elemento linijas, galutinė gausa laikomas atskirų nustatymų vidurkis.

2.4 Nukrypimai nuo lokalios termodinaminės pusiausvyros

Gausų analizė atlikta naudojant 1D LTE modelius, o pagrindiniams elementams (Mg, Sr, Y, Ba, Eu) papildomai įvertinti ir NLTE efektai, taikant 2020 m. Turbospectrum versiją ir *calculate_nlte_correction_line* komandą iš TSFitPy (Gerber et al. 2023). Didžiausi NLTE poveikiai nustatyti stronciui: Sr I 4607 Å linijai reikėjo didėjančių teigiamų korekcijų mažėjant metalingumui, o 7070 Å linijai korekcijos beveik nebuvo būtinos. Itrio linijos dažniausiai rodė mažas pataisas, kurios vidutiniškai išliko artimos nuliui. Didžiausi neigiami NLTE efektai gauti bariui, ypač stiprioms Ba II linijoms ties 6141 ir 6496 Å. Eu II 6645 Å linija rodė tik nedidelį poveikį (iki –0,05 dex), o Mg gausos jautrumas NLTE poveikiui buvo minimalus. Literatūroje pateiktos labai mažos NLTE pataisos Pr II (Shaltout et al. 2020), o Nd NLTE efektai, nors reikšmingi karštose A–Ap žvaigždėse (Mashonkina et al. 2005), mūsų vėsesnėms F, G, K spektrinės klasės žvaigždėms nėra nustatyti.

3. Lengvųjų ir α-elementų gausų rezultatai

α-elementų [El/Fe] santykio priklausomybė nuo metalingumo rodo kiekvienam elementui būdingas tendencijas, kurios iš esmės dera su Galaktikos cheminės evoliucijos modeliais, tačiau tuo pačiu leidžia pastebėti ir subtilius skirtumus tarp žvaigždžių su planetomis ir palyginamųjų žvaigždžių. Tyrimas rodo, kad žvaigždėse nykštukėse anglies ir deguonies gausos, išreikštos [C/Fe] ir [O/Fe], mažėja didėjant metalingumui. Tai atspindi ankstyvą šių elementų gamybą masyviose žvaigždėse ir vėlesnį praturtinimą geležimi po Ia tipo supernovų. Esant mažesniam nei Saulės metalingumui, tiek C, tiek O gausa būna šiek tiek padidėjusi,

o esant didesniam metalingumui – sumažėja iki Saulės lygio arba dar mažiau. Žvaigždėse su planetomis anglies sumažėjimas yra nedidelis ir statistiškai nereikšmingas, lyginant su žvaigždėmis be patvirtintų planetų. Azotas pasižymi kur kas stabilesne elgsena: [N/Fe] paprastai išlieka artimas Saulės reikšmei. Tik esant mažam metalingumui matomas nežymus jo padidėjimas, tačiau ši tendencija neaiški dėl riboto patikimų matavimų skaičiaus. Rezultatai nerodo jokių indikacijų, kad azoto gausų pokyčiai būtų susiję su planetų formavimusi.

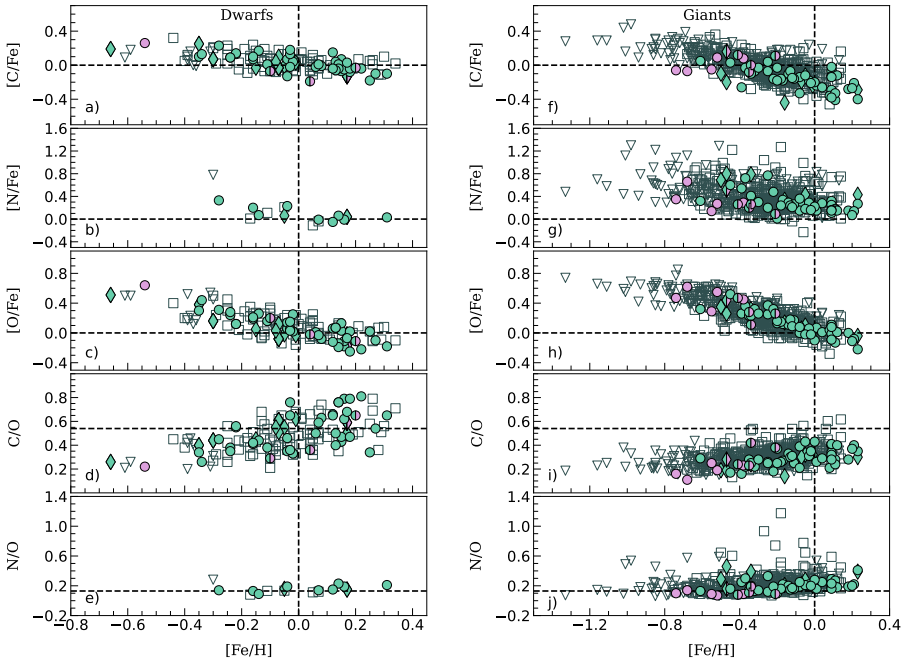

32 pav.: Žvaigždžių su planetomis anglies, azoto ir deguonies santykinė gausa [El/Fe] kartu su C/O ir N/O santykiais kaip funkcija nuo metalingumo [Fe/H]. Kairėje vaizduojami nykštukių rezultatai, dešinėje - milžinių. Plonojo ir storojo disko žvaigždės atitinkamai yra pavaizduotos žalia ir rožine spalvomis, o tarpinės, pereinamosios populiacijos žvaigždės pažymėtos spalvotais simboliais. Planetų turinčios žvaigždės iš I Publikacijos yra pavaizduotos rombais. Palyginamosios žvaigždės, neturinčios patvirtintų planetų ir paimtos iš Stonkutė et al. (2020) ir I publikacijos, yra pažymėtos tuščiaviduriais pilkais kvadratais (plonasis diskas) ir trikampiais (storasis diskas).

Analizuojant milžines, vidinis maišymasis pirmosios drumsties metu žvaigždžių atmosferose sumažina [C/Fe] maždaug per 0,2. [N/Fe] padidėja tiek pat, o tai rodo anglies gamybą azoto sąskaita CNO ciklu.

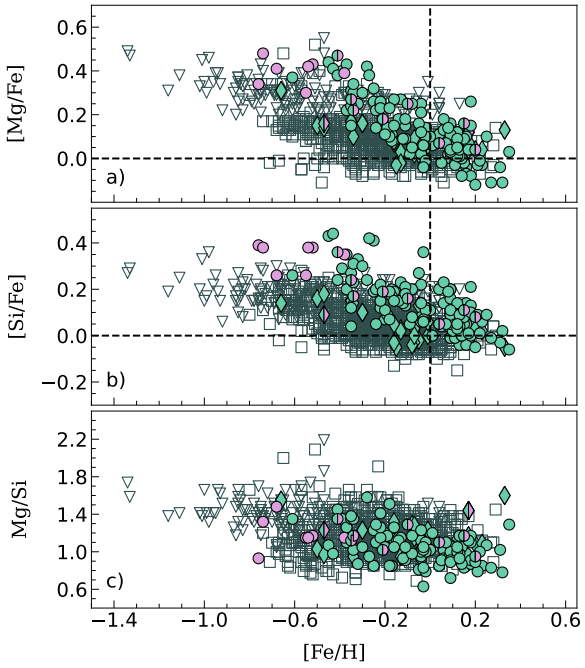

33 pav.: [El/Fe] santykinė magnio ir silicio gausa kartu su Mg/Si santykiu kaip funkcija nuo metalingumo [Fe/H]. Visi simboliai atitinka tokias pat reikšmes kaip ir 32 pav. Duomenys palyginimui (tuščiaviduriai pilki kvadratai plonajam diskui ir trikampiai - storajam diskui) yra paimti iš Mikolaitis et al. (2019) ir Tautvaišienė et al. (2022).

Bendras milžinių C ir N gausų pasiskirstymas yra panašus į palyginamųjų žvaigždžių. [O/Fe] pasiskirstymas tiek nykštukėse, tiek milžinėse yra nuoseklus, nėra jokių sistematinių skirtumų tarp planetas turinčių ir jų neturinčių žvaigždžių. 32 pav. parodytos [C/Fe], [N/Fe], [O/Fe] ir C/O bei N/O vertės, atidėtos nuo metalingumo mūsų imties žvaigždėse su planetomis.

α-elementai magnis ir silicis pasiskirsto panašiai, kaip ir galima būtų tikėtis pagal Galaktikos cheminės evoliucijos modelį (žr. 33 pav.), t. y., [Mg/Fe] ir [Si/Fe] gausos yra padidėjusios ties mažo metalingumo vertėmis ir mažėja artėjant link Saulės metalingumo, pasiekdamos artimas Saulei vertes ties [Fe/H] $\gtrsim$ 0.0.

Pastebėjome, kad žvaigždės, turinčios planetų, ypač esant mažam metalingumui, pasižymi didesnėmis Mg ir Si gausomis nei palyginamosios žvaigždės. Tuo tarpu ties Saulės metalingumu ir didesniu metalingumu

abiejų populiacijų gausos beveik sutampa. Šis padidėjęs α elementų kiekis nemetalingose žvaigždėse su planetomis rodo, kad papildomas Mg ir Si gali kompensuoti mažesnį geležies kiekį planetų formavimosi metu, suteikdamas alternatyvų cheminį kelią planetų susidarymui aplinkoje, kurioje geležies yra mažai.

3.1 C/O, N/O ir Mg/Si santykiai

Elementų santykiai C/O, N/O ir Mg/Si yra ypač svarbūs, nes jie suteikia vertingos informacijos apie žvaigždžių cheminę sudėtį ir medžiagą, iš kurios formuojasi planetos. C/O ir N/O priklausomybės nuo metalingumo pavaizduotos 32 pav.

Mūsų imties žvaigždės nykštukės rodo didėjančią C/O tendenciją didėjant metalingumui, o tarp žvaigždžių su planetomis bei palyginamųjų žvaigždžių reikšmingų skirtumų nestebima. Milžinių C/O santykiai yra sistemingai mažesni nei nykštukių dėl evoliucijoje vykusio medžiagos maišymosi, ir paprastai yra mažesni nei palyginamųjų milžinių. Visos imties žvaigždžių C/O išlieka < 0,8, o tai rodo deguonimi praturtintą planetų formavimosi aplinką.

Nykštukėse N/O santykis paprastai išlieka artimas Saulės vertei, tik šiek tiek didėja priklausomai nuo metalingumo. Tuo tarpu milžinėse N/O santykis yra aiškiai didesnis nei nykštukėse dėl CNO ciklo poveikio. Skirtumų tarp žvaigždžių su planetomis ir palyginamųjų nepastebėta. Mg/Si santykis mažėja didėjant [Fe/H], kas sutampa su Galaktikos cheminės evoliucijos tendencijomis (Adibekyan et al. 2012a; Delgado Mena et al. 2018). Be to, žvaigždės su planetomis esant tam pačiam metalingumui linkusios turėti kiek mažesnes Mg/Si vertes nei palyginamosios žvaigždės.

Norėdami įvertinti, ar gausų santykiai skiriasi tarp žvaigždžių su planetomis ir palyginamosios imties, taikėme dvipusius Kolmogorovo-Smirnovo (K–S) ir Andersono-Darlingo (A–D) statistinius testus. Žvaigždės su planetomis buvo suskirstytos į mažos masės ($M_{\rm p} < 30 M_{\oplus}$) ir didelės masės ($M_{\rm p} > 30 M_{\oplus}$) sistemas. Jei žvaigždė turėjo kelias planetas, ji buvo priskirta grupei tik tuo atveju, jei visos planetos atitiko masės kriterijų, o mišrios masės sistemos buvo įtrauktos į abi kategorijas. Papildomai analizuota ir tik plonojo disko žvaigždžių imtis. Visų rezultatų patikimumui patikrinti atlikome 1000 „bootstrap“ skaičiavimų. Statisti-

10 lentelė: Kolmogorovo-Smirnovo (K–S) testo rezultatai, įvertinantys gausų pasiskirstymų skirtumus žvaigždžių su planetomis ir palyginamųjų žvaigždžių atmosferose.

	$K\text{-}S^{\text{Maža masė}}_{\text{Visa imtis}}$		$K\text{-}S^{\text{Maža masė}}_{\text{Plonasis diskas}}$		$K\text{-}S^{\text{Didelė masė}}_{\text{Visa imtis}}$		$K\text{-}S^{\text{Didelė masė}}_{\text{Plonasis diskas}}$	
	Statistika	*p* reikšmė	Statistika	*p* reikšmė	Statistika	*p* reikšmė	Statistika	*p* reikšmė
C/O_D	0.28	0.39	0.21	0.81	0.23	0.07	0.21	0.17
C/O_G	–	–	–	–	0.22	0.01	0.22	0.02
N/O_G	–	–	–	–	0.11	0.49	0.20	0.06
$A(C+N+O)_G$	–	–	–	–	0.14	0.24	0.23	0.02
Mg/Si	0.19	0.55	0.23	0.38	0.30	$\leq$0.001	0.29	$\leq$0.001
Su 1000 „bootstrap“ iteracijų:								
C/O_D	0.38	0.20	0.34	0.34	0.25	0.13	0.24	0.20
C/O_G	–	–	–	–	0.24	0.03	0.25	0.04
N/O_G	–	–	–	–	0.16	0.21	0.22	0.09
$A(C+N+O)_G$	–	–	–	–	0.18	0.14	0.25	0.05
Mg/Si	0.27	0.30	0.29	0.27	0.31	$\leq$0.001	0.31	$\leq$0.001

Pastaba: Dvipusė K-S statistika ir atitinkamos *p* reikšmės, patvirtintos atliekant 1000 pakartotinių imties iteracijų, naudojant „bootstrap“ metodą. N gausos nustatymas žvaigždėse nykštukėse nėra reprezentatyvus, todėl N/O_D ir $A(C+N+O)_D$ palyginimai šiai imčiai nėra pateikti.

nis reikšmingumas buvo vertinamas naudojant 5 % lygmenį K–S testui ir kritinę ribą $AD_{crit} = 1.961$ A–D testui. Testo statistikos ir *p* reikšmės pateiktos 10 ir 11 lentelėse, o kaupiamosios pasiskirstymo funkcijos (CDF) parodytos 34 pav.

Atlikti statistiniai testai parodė, kad žvaigždžių nykštukių, turinčių mažos masės planetų, C/O santykiai reikšmingai nesiskiria nuo palyginamųjų žvaigždžių, tiek vertinant visą imtį, tiek ją apribojant plonojo disko populiacija. Dėl nepakankamo azoto gausų skaičiaus šiai žvaigždžių grupei neįmanoma patikimai įvertinti N/O santykio. Žvaigždėms nykštukėms, turinčioms didelės masės planetų, taip pat nenustatyta reikšmingų C/O skirtumų, tačiau milžinėms su patvirtintomis planetomis būdingas statistiškai reikšmingas C/O poslinkis, o abu taikyti testai leidžia atmesti nulinę hipotezę. Milžinės su planetomis, vertinant visą imtį, neparodo sisteminių N/O skirtumų, nors plonojo disko pogrupyje identifikuojamas nedidelis, tačiau statistiškai reikšmingas pokytis. Ryškiausias skirtumas nustatytas Mg/Si santykyje: žvaigždės su mažos masės planetomis pasižymi kontrolinei grupei artimomis vertėmis, o žvaigždės, turinčios didelės masės planetų, visose imtyse ir visuose statistiniuose vertinimuose nuosekliai išsiskiria gerokai mažesnėmis Mg/Si reikšmėmis. Tai rodo, kad sumažintas Mg/Si santykis yra tvirtas ir nuoseklus didelės masės

11 lentelė: Andersono-Darlingo (A–D) testo rezultatai, įvertinantys gausų pasiskirstymų skirtumus žvaigždžių su planetomis ir palyginamųjų žvaigždžių atmosferose.

	$A\text{-}D^{\text{Maža masė}}_{\text{Visa imtis}}$		$A\text{-}D^{\text{Maža masė}}_{\text{Plonasis diskas}}$		$A\text{-}D^{\text{Didelė masė}}_{\text{Visa imtis}}$		$A\text{-}D^{\text{Didelė masė}}_{\text{Plonasis diskas}}$	
	Statistika	*p* reikšmė	Statistika	*p* reikšmė	Statistika	*p* reikšmė	Statistika	*p* reikšmė
C/O_D	0.42	0.22	−0.45	≥0.25	1.71	0.06	1.07	0.12
C/O_G	–	–	–	–	4.19	0.01	3.72	0.01
N/O_G	–	–	–	–	−0.56	≥0.25	1.20	0.10
$A(C+N+O)_G$	–	–	–	–	1.15	0.11	4.41	0.01
Mg/Si	−0.42	≥0.25	0.32	≥0.25	29.82	≤0.001	24.87	≤0.001
Su 1000 „bootstrap“ iteracijų:								
C/O_D	1.64	0.14	0.70	0.18	3.00	0.09	2.45	0.10
C/O_G	–	–	–	–	5.72	0.02	5.31	0.03
N/O_G	–	–	–	–	0.76	0.17	2.35	0.09
$A(C+N+O)_G$	–	–	–	–	2.35	0.10	5.84	0.03
Mg/Si	0.87	0.17	1.95	0.13	31.17	≤0.001	26.15	≤0.001

Pastaba: Dvipusė A-D statistika ir *p* reikšmės, patvirtintos 1000 pakartotinių imties atlikimo iteracijų. Kritinė vertė 5 % reikšmingumo lygiui yra 1,961. Elementų $A(C+N+O)_D$ ir N/O_D santykiai žvaigždėse nykštukėse nėra reprezentatyvus dėl ribotų azoto matavimų.

planetų turinčių žvaigždžių cheminis požymis.

3.2 Suminė A(C+N+O) gausa

Norėdami eliminuoti maišymo procesų poveikį evoliucionavusiose žvaigždėse, kurie keičia atskirų C, N ir O elementų gausas, milžinių su planetomis imtyje analizavome bendrą gausą A(C+N+O). Kaip matyti iš 35 pav. *b* dalies, A(C+N+O) didėja didėjant metalingumui, o duomenys pasižymi labai maža sklaida. Ta pati *b* dalis rodo, kad nėra reikšmingos sąsajos tarp absoliučios A(C+N+O) gausos ir planetos masės (PCC = −0,08). *c* dalyje pateikti kaupiamieji pasiskirstymai taip pat nerodo statistiškai reikšmingų skirtumų tarp milžinių, turinčių didelės masės planetas, ir lyginamosios imties, kai vertinama visa populiacija.

4. Neutronų pagavimo elementų gausų rezultatai

Ištyrėme devynių *n*-pagavimo elementų (Sr, Y, Zr, Ba, La, Ce, Nd, Pr, Eu) gausas žvaigždėse su planetomis ir palyginome jas su kontrolinės imties žvaigždėmis. 36 pav. pateikiama šių elementų [El/Fe] priklausomybė nuo [Fe/H], atskirai nykštukėms ir milžinėms, o taškų spalva žymi [Y/Mg] kaip amžiaus indikatorių. Sr, Y, Ba, Eu ir Mg elementams

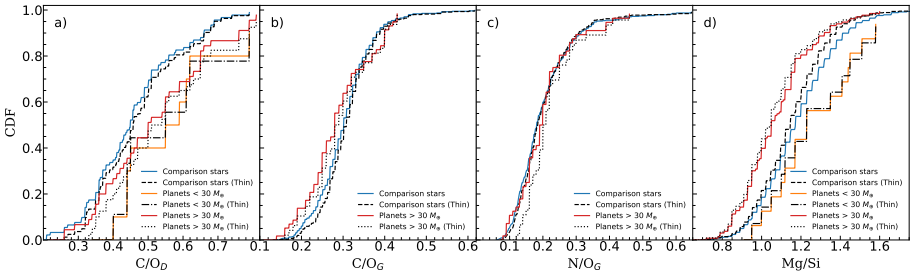

34 pav.: Elementų santykių C/O, N/O ir Mg/Si kaupiamosios pasiskirstymo funkcijos (CDF) žvaigždėms su aptiktomis planetomis ir be jų. *a* dalyje pavaizduotas kaupiamasis C/O pasiskirstymas nykštukėms. Ištisinės oranžinės ir raudonos linijos atitinkamai žymi mažos masės ($M_\mathrm{p} < 30M_\oplus$) ir didelės masės ($M_\mathrm{p} > 30M_\oplus$) planetas, o ištisinė mėlyna linija atitinka palyginamąsias žvaigždes be planetų. Juodos linijos žymi atitinkamas plonojo disko imtis. Dalyse *b* ir *c* pavaizduotas kaupiamasis C/O ir N/O santykių pasiskirstymas žvaigždėms milžinėms, o *d* dalyje pademonstruotas kaupiamasis Mg/Si pasiskirstymas visoms žvaigždėms su planetomis, lyginant su kontroline imtimi.

abiejose imtyse prireikus buvo taikytos NLTE korekcijos.

Pirmojo *s*-proceso piko elementų Sr, Y ir Zr [El/Fe] pasiskirstymai didėja mažėjant [Fe/H] ir [Y/Mg], labiausia tas matoma Zr atveju. Mažo metalingumo srityje Sr ir Y mažėja, o vėliau stabilizuojasi dėl pusiausvyros tarp *s*-proceso gamybos ir SNIa geležies indėlio, tuo tarpu Zr toliau didėja. Jaunesnės, metalingos nykštukės (su didelėmis [Y/Mg] reikšmėmis) pasižymi didesnėmis Sr, Y ir Zr gausomis. Apskritai Sr ir Y pasiskirstymai žvaigždėse su planetomis sutampa su palyginamąja imtimi, o Zr atveju planetas turinčiose žvaigždėse pastebimas šio elemento perteklius, ypač mažo metalingumo intervale.

Antro *s*-proceso piko elementų Ba, La ir Ce, daugiausia susidarančių mažos ir vidutinės masės AGB žvaigždėse, gausos skiriasi priklausomai nuo metalingumo. Bario gausa didėja, mažėjant [Fe/H] esant didesnėms nei Saulės metalingumo reikšmėms, o vėliau priklausomybės nelieka ir galiausiai žemiau [Fe/H]≈–0.2 bario gausa ima mažėti, kas atitinka palyginamųjų žvaigždžių tendencijas ir rodo, kad nėra su planetomis susijusių anomalijų. La ir Ce elgiasi priešingai: jų [El/Fe] didėja mažėjant metalingumui, o planetas turinčios žvaigždės paprastai yra praturtintos šiais elementais. Vis dėlto skirtumai nedideli ir palyginimi su gausų paklaidomis.

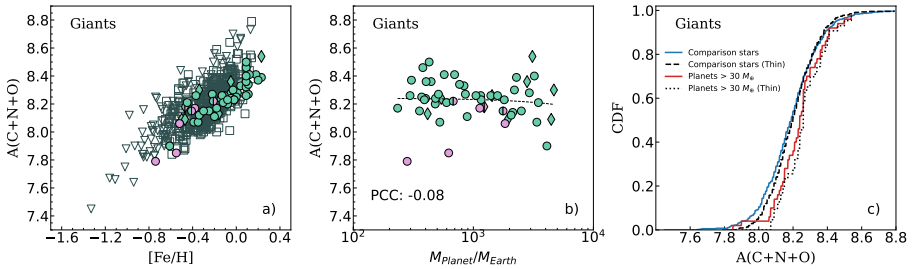

35 pav.: *a* dalyje: A(C+N+O) gausos pasiskirstymas [Fe/H] atžvilgiu. *b* dalyje: ta pati gausa, priklausomai nuo planetų masių žvaigždėms milžinėms. *c* dalyje: kaupiamasis A(C+N+O) pasiskirstymas žvaigždėms milžinėms. Visi simboliai turi tas pačias reikšmes kaip 32 ir 34 pav.

Mišrių *s*- ir *r*-proceso elementų Pr ir Nd santykinės gausos [El/Fe] mūsų imtyje didėja mažėjant metalingumui. Tai rodo ankstyvą *r*-proceso praturtinimą, vėliau papildytą laipsnišku *s*-proceso indėliu iš AGB žvaigždžių. Planetų turinčių žvaigždžių atmosferose šių elementų gausos beveik nesiskiria nuo palyginamųjų. Europis, beveik grynas *r*-proceso elementas, taip pat rodo [Eu/Fe] didėjimą mažėjant metalingumui, o tai siejama su ankstyvu masyvių žvaigždžių indėliu ir vėlesniu Ia tipo supernovoms gaminant Fe. Šie pasiskirstymai sutampa su palyginamųjų žvaigždžių pasiskirstymais, todėl darome išvadą, kad Eu gausas lemia Galaktikos cheminė evoliucija, o ne planetų buvimas.

5. [Y/Mg] cheminis laikrodis

Naujausi tyrimai rodo, kad *s*-proceso ir α-elementų santykis [Y/Mg] stipriai siejasi su žvaigždžių amžiumi dėl skirtingų jų susidarymo laiko skalių: Mg susidaro greičiau II tipo supernovose, o Y – vėliau AGB žvaigždėse. Todėl [Y/Mg] veikia kaip „cheminis laikrodis". Mūsų planetas turinčių nykštukių imtis patvirtina šį ryšį – plonojo disko žvaigždėms gautas [Y/Mg] santykio nuo amžiaus polinkis –0,030 ± 0,008 (žr. 37 pav.), atitinka ankstesnius rezultatus (Tautvaišienė et al. 2021). Storojo disko nemetalingos žvaigždės yra praturtintos magniu, todėl jų [Y/Mg] mažesnis, o tai gali reikšti, kad didesnis Mg kiekis iš dalies kompensuoja mažą geležies gausą planetų formavimosi aplinkoje (žr. pvz., Adibekyan et al. 2012a,b; Bashi & Zucker 2019).

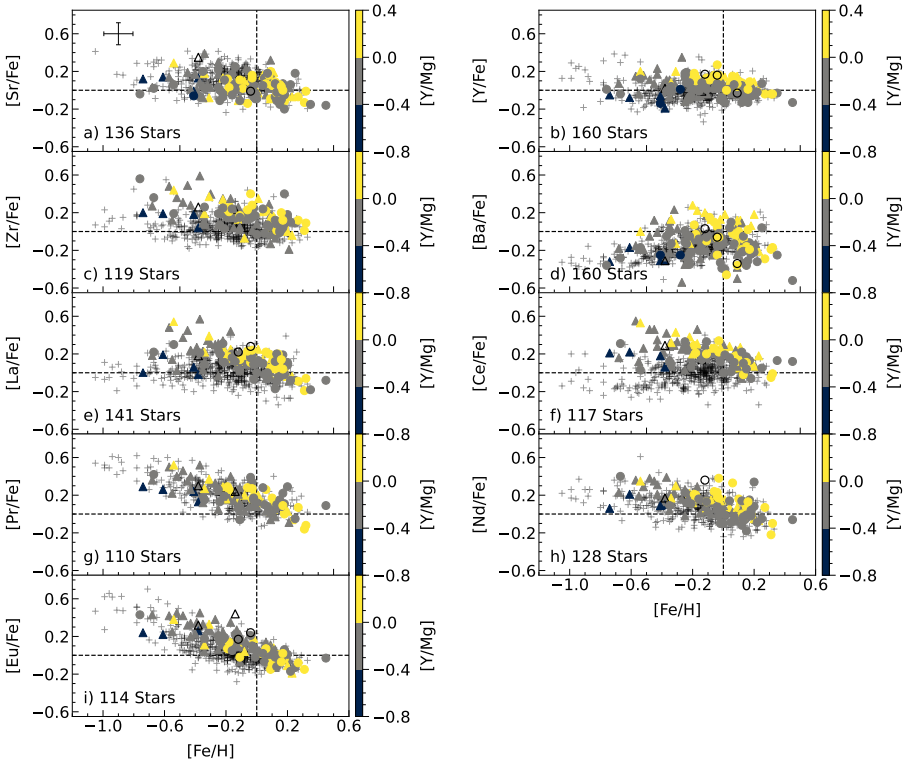

36 pav.: Neutronų pagavimo elementų santykinės [El/Fe] gausos kaip funkcija nuo [Fe/H]. Žvaigždės nykštukės pažymėtos apskritimais, o žvaigždės milžinės ($\log g \leq 3{,}5$) – trikampiais. Žvaigždės nuspalvintos pagal [Y/Mg]. Vidutinės paklaidos yra parodytos *a* dalyje. Palyginamųjų disko žvaigždžių imtis yra pažymėta pliusais ir paimta iš Tautvaišienė et al. (2021).

6. Gausų skirtumų ir kondensacijos temperatūrų priklausomybės

Ryšys tarp žvaigždžių cheminių gausų ir elementų kondensacijos temperatūrų ($T_{\rm cond}$) yra plačiai nagrinėtas kaip galimas planetų formavimosi indikatorius, tačiau ankstesni rezultatai išlieka prieštaringi. Ankstyvieji darbai teigė, kad Saulėje trūksta aukštos kondensacijos temperatūros elementų dėl jų sunaudojimo formuojantis planetoms (Meléndez et al. 2009). Vėlesni tyrimai parodė, kad gausų–$T_{\rm cond}$ ryšiai gali būti įvairūs: nustatyti teigiami, plokšti, neigiami ar kintantys priklausomybių polinkiai (González Hernández et al. 2013; Mack et al. 2014; Liu et al. 2020). Naujesni rezultatai rodo, kad šie ryšiai stipriai priklauso nuo planetų sistemos architektūros (Yun et al. 2024). Pavyzdžiui, žvaigždės su pla-

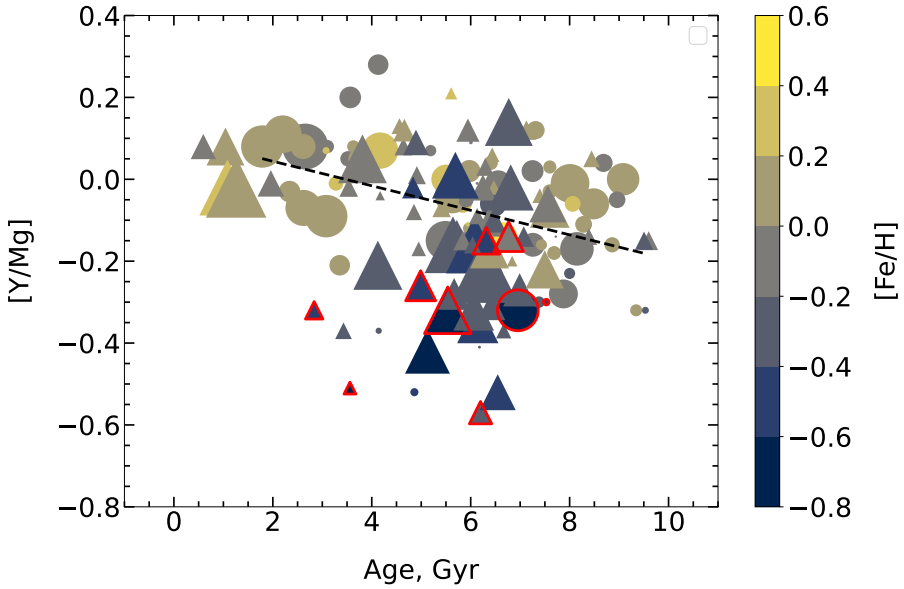

37 pav.: [Y/Mg] NLTE santykis kaip funkcija nuo žvaigždžių amžiaus (milijardais metų, Gyr). Simbolių spalvos pagal [Fe/H]. Visi simboliai turi tą pačią reikšmę kaip ir 36 pav.

netomis milžinėmis paprastai turi mažiau aukštos $T_{\rm cond}$ elementų nei žvaigždės su uolinėmis planetomis, o pastarosiose šių elementų gausos koreliuoja su planetų dydžiu ir sistemoje esančių planetų skaičiumi.

Kiekvienai planetų turinčiai žvaigždei apskaičiavome diferencialines gausas Δ[El/H], lygindami su panašiomis žvaigždėmis iš Tautvaišienė et al. (2021), atrinktomis pagal $T_{\rm eff}$, $\log, g$ ir [Fe/H]. Kondensacijos temperatūros paimtos iš Lodders (2003). Gautus Δ[El/H]–$T_{\rm cond}$ pasiskirstymus atskirai įvertinome nykštukėms ir milžinėms (žr. 38 pav.).

Gautų Δ[El/H]-$T_{\rm cond}$ polinkių pasiskirstymas mūsų imtyje yra teigiamai asimetriškas, o tai rodo, kad daugelis žvaigždžių, turinčių planetas, pasižymi nedideliu aukštos kondensacijos temperatūros elementų praturtinimu, nors nykštukėse šis efektas silpnesnis. Šie priklausomybės polinkiai skirtingoms žvaigždėms skiriasi: kai kurios žvaigždės pasižymi aiškiu praturtinimu aukštos kondensacijos temperatūros elementais, lyginant su lakiaisiais, o kitos turi beveik plokščius ar net neigiamus polinkius. Šis skirtumas pabrėžia, kad elementų gausų ir $T_{\rm cond}$ koreliacijos nėra universalios, o gali priklausyti nuo žvaigždžių ir planetų savybių.

Analizuojant šių polinkių priklausomybę nuo žvaigždžių ir jų planetų

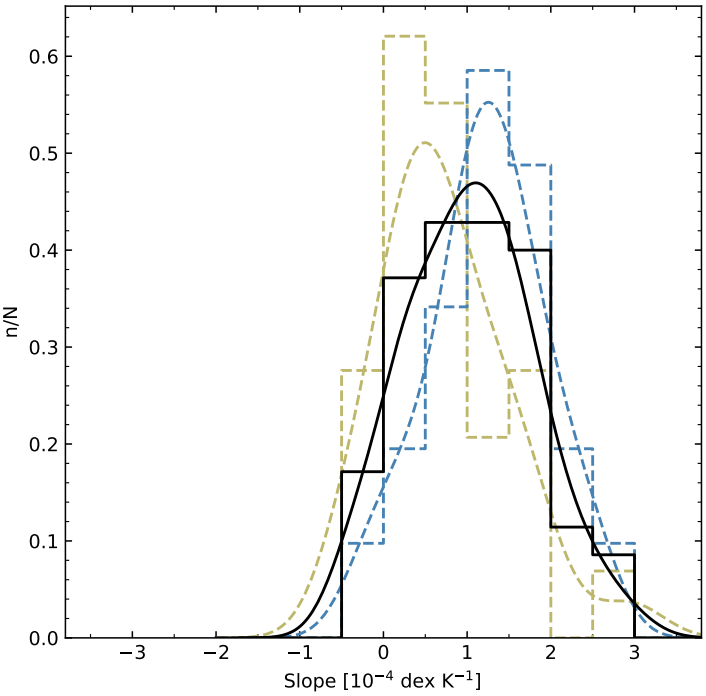

38 pav.: Gausų–T_{cond} pasiskirstymų polinkiai mūsų tirtoms žvaigždėms su planetomis atėmus palyginamąsias žvaigždes. Juoda ištisinė linija žymi visas planetų turinčias žvaigždes, o geltona ir mėlyna punktyrinė linija –žvaigždes nykštukes ir milžines. Pasiskirstymas normalizuotas pagal bendrą žvaigždžių skaičių kiekvienoje grupėje.

savybių, pastebimos tik silpnos koreliacijos (žr. 39 pav.). Žvaigždės, turinčios didesnės masės planetas, didesnius orbitinius spindulius ar masyvesnes sistemas, paprastai pasižymi kiek didesniais teigiamais polinkiais. Tuo tarpu nemetalingos, senesnės arba dinamiškai karštesnės žvaigždės (turinčios didesnes $|z_{\mathrm{max}}|$ reikšmes) dažniausiai rodo plokščius arba neigiamus polinkius. Žvaigždžių amžiaus tendencija leidžia manyti, kad aukštos kondensacijos temperatūros elementų praturtinimas gali būti labiau būdingas jaunesnėms sistemoms arba toms, kuriose yra masyvesnių planetų, o senesnėse ar dinamiškai karštesnėse žvaigždėse lakiųjų ir aukštos kondensacijos temperatūros cheminių elementų gausos, atrodo, esą labiau subalansuotos.

Apibendrinant galima teigti, kad Δ[El/H]–T_{cond} polinkių įvairovė liudija apie įvairių procesų poveikį žvaigždžių atmosferų gausų skirtu-

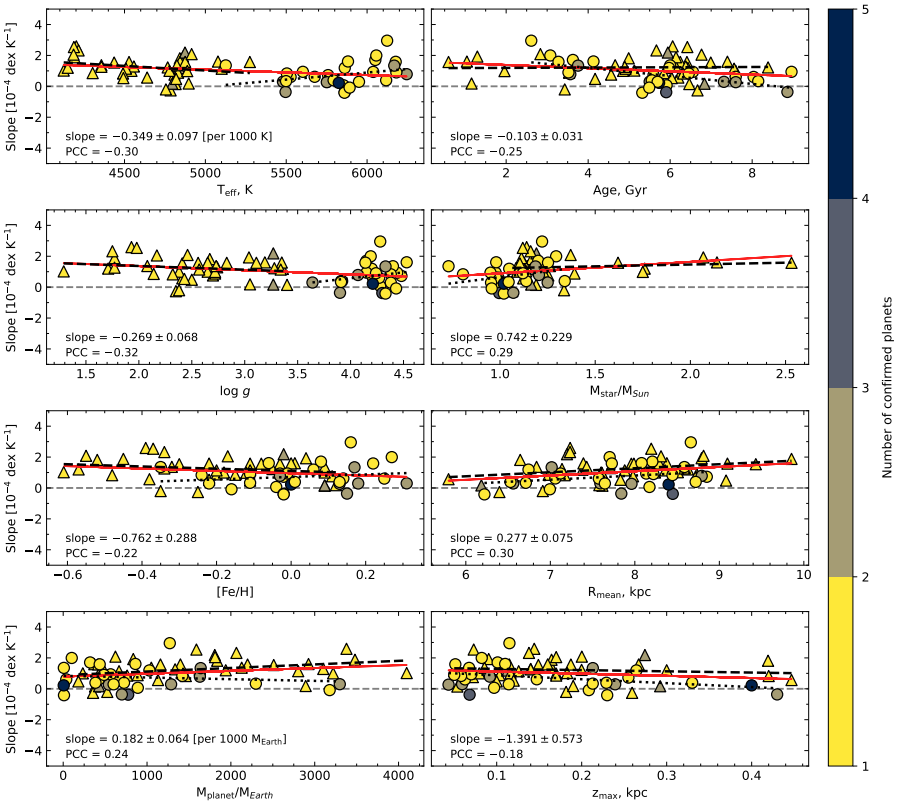

39 pav.: Elementų gausų ir T_{cond} priklausomybių polinkiai kaip funkcija nuo žvaigždžių parametrų ir planetų masių. Simboliai nuspalvinti pagal patvirtintų planetų skaičių ir yra tokie pat kaip 36 pav. Raudona linija žymi duomenims pritaikytas tiesinės regresijas. Polinkių ir Pearson koreliacijos koeficientų vertės yra pateiktos kiekvienos skilties apatiniame kairiajame kampe. Daugiau informacijos rasite tekste.

mui, įskaitant disko evoliuciją, uolinės medžiagos akreciją bei uolinių elementų sunaudojimą planetų formavimosi metu. Tuo tarpu plokšti arba neigiami priklausomybių polinkiai rodo, kad šios priklausomybės nėra universalūs planetinių sistemų požymiai ir gali atspindėti pirminius dulkių ir dujų santykio skirtumus žvaigždėdaros aplinkoje (Soliman & Hopkins 2025). Dėl to tokie gausų pokyčiai tam tikrais atvejais gali būti visiškai nesusiję su planetomis sistemoje.

7. Ryšys su planetų masėmis

Ištyrėme, kaip žvaigždžių cheminės gausos siejasi su jų planetų masėmis, o planetų parametrus pagrinde surinkome iš NASA egzoplanetų archyvo. Objektų, kurių masė viršija maždaug $\sim$13 M_J, nenaudojome siekdami išvengti rudųjų nykštukių įtraukimo. Atsižvelgiant į galimus evoliucijos efektus, imtis buvo suskirstyta į žvaigždes, turinčias mažos masės ir didelės masės planetas. Gausų ir planetų masių priklausomybės tendencijoms įvertinti buvo taikytos tiesinės regresijos ir apskaičiuoti Pearson koreliacijos koeficientai (PCC). Sistemose, kuriose aptinkama daugiau nei viena planeta, reprezentatyvia buvo laikoma didžiausios masės planeta.

7.1 CNO ir α-elementai

C, N ir O gausų priklausomybės nuo planetų masių, išreikštos santykiu su geležimi, kartu su C/O ir N/O santykiais, pateikiamos 40 pav. Tarp planetas turinčių žvaigždžių nykštukių anglies, azoto ir deguonies gausos rodo tik silpnas neigiamas koreliacijas su planetos mase, o tai atitinka ankstesnių tyrimų išvadas, kad nykštukių cheminės gausos tik silpnai siejasi su planetų masėmis (Suárez-Andrés et al. 2017; Tautvaišienė et al. 2022). Tuo tarpu žvaigždėse milžinėse anglis pasižymi nedidele teigiama koreliacija (PCC = 0,13), azotas sistemose su masyviomis planetomis yra akivaizdžiai padidėjęs (PCC = 0,60), o deguonis rodo vidutinio stiprumo teigiamą koreliaciją (PCC = 0,30). Šie rezultatai rodo, kad žvaigždžių evoliucija ir masyvių planetų buvimas gali turėti reikšmingos įtakos evoliucionavusių žvaigždžių CNO gausoms.

Nustatėme, kad nykštukinėse žvaigždėse C/O santykis rodo labai silpną teigiamą koreliaciją (PCC = 0,08) su planetų mase. Priešingai, N/O santykis šiek tiek padidėja žvaigždėse, turinčiose masyvias planetas (PCC = 0,22), nors šio rezultato interpretaciją riboja negausūs azoto matavimai mažos masės planetų sistemose. Žvaigždėse milžinėse C/O santykis, didėjant planetų masėms, pasižymi neigiama koreliacija (PCC = $-$0,34), o N/O santykis rodo stipresnę teigiamą koreliaciją (PCC = 0,39) didelės masės planetas turinčiose sistemose. Tai atspindi evoliucinį anglies sumažėjimą ir azoto pagausėjimą šiose žvaigždėse.

41 pav. pateiktas α-elementų Mg ir Si pasiskirstymas kartu su Mg/Si

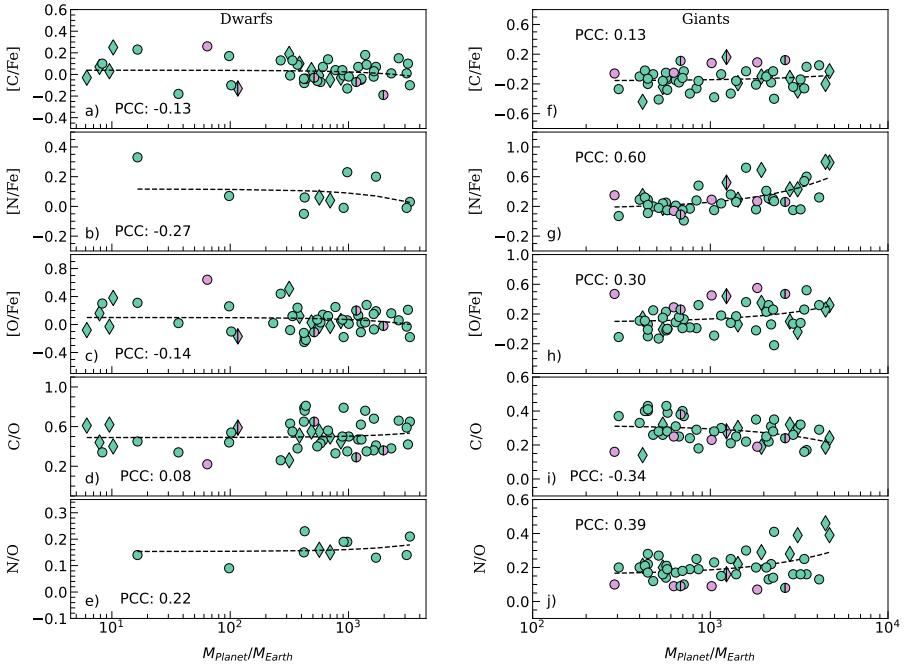

40 pav.: [C/Fe], [N/Fe], [O/Fe] santykinės gausos ir C/O, N/O santykiai pavaizduoti kaip funkcija nuo planetų masių tirtose nykštukėse (kairė pusė) ir milžinėse (dešinė pusė). Sistemoje esant ne vienai planetai, atsižvelgiama tik į masyviausią planetą. Visi simboliai turi tą pačią reikšmę kaip ir 23 pav.

santykiu nuo planetos masės. Tiek [Mg/Fe], tiek [Si/Fe] rodo silpną teigiamą koreliaciją (atitinkamai PCC = 0,08 ir 0,19), o Mg/Si santykis pasižymi nedidele neigiama koreliacija (PCC = $-0{,}15$), ypač žvaigždėse, turinčiose didelės masės planetas. Šie rezultatai gali būti reikšmingi silikatų mineralogijai, nes Mg/Si santykis lemia olivino ir pirokseno pusiausvyrą planetų formavimosi metu.

7.2. Neutronų pagavimo proceso elementai

Taip pat išanalizavome *n*-pagavimo elementų gausų (geležies atžvilgiu) ir planetų masių sąryšį, naudodami visą 160 žvaigždžių imtį (žr. pav. 42). Kaip ir CNO bei α-elementų analizėje, sistemose su keliomis planetomis buvo atsižvelgiama tik į masyviausią planetą.

Stroncio ir itrio elementų gausos nerodo reikšmingos koreliacijos su planetų masėmis visoje imtyje; jų PCC reikšmės išlieka artimos nuliui.

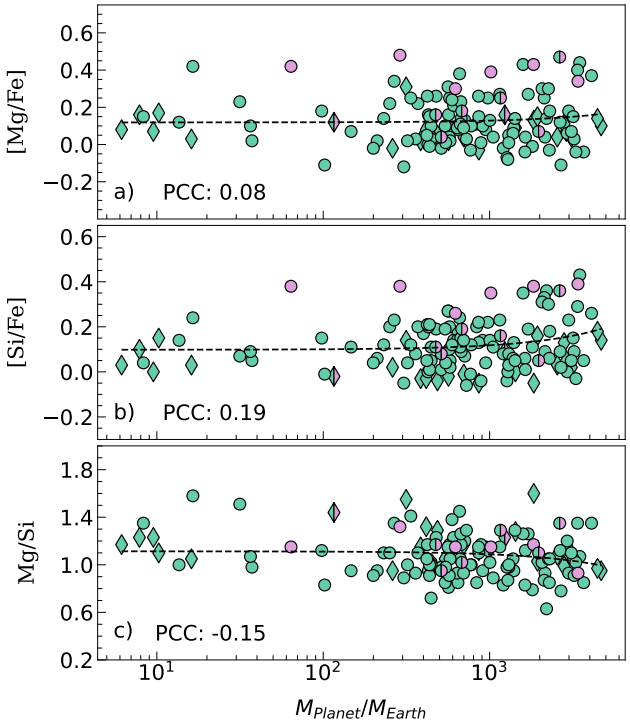

41 pav.: [Mg/Fe], [Si/Fe] santykinės gausos ir jų santykis Mg/Si pavaizduoti kaip funkcija nuo planetų masių visose tirtose žvaigždėse. Sistemoje esant ne vienai planetai, atsižvelgiama tik į masyviausią planetą. Visi simboliai turi tą pačią reikšmę kaip ir 23 pav.

Tuo tarpu [Zr/Fe] gausa pasižymi teigiama koreliacija (PCC $\approx$ 0,32–0,36 visoje imtyje), stipriausiai išreikšta žvaigždėse milžinėse. Šis rezultatas nesutampa su anksčiau publikuotoms neigiamoms koreliacijoms Swastik et al. (2022), o toks neatitikimas gali būti susijęs su skirtingu naudotų spektrinių linijų rinkiniu arba Galaktikos cheminės evoliucijos ypatumais.

Bario gausos visoje imtyje pasižymi neigiamais polinkiais, ypač nykštukinėse žvaigždėse (PCC = $-0{,}21$), o tai dar kartą patvirtina anksčiau publikuotą Ba sumažėjimą planetas turinčiose žvaigždėse (da Silva et al. 2015; Mishenina et al. 2016; Delgado Mena et al. 2018). Priešingai, La ir Ce gausa rodo teigiamas koreliacijas, ypač žvaigždėse milžinėse (PCC = 0,41 La ir 0,38 Ce). Tai leidžia daryti prielaidą, kad praturtinimas sunkesniais *s*-proceso elementais gali būti labiau būdingas sistemoms, kuriose yra masyvių planetų.

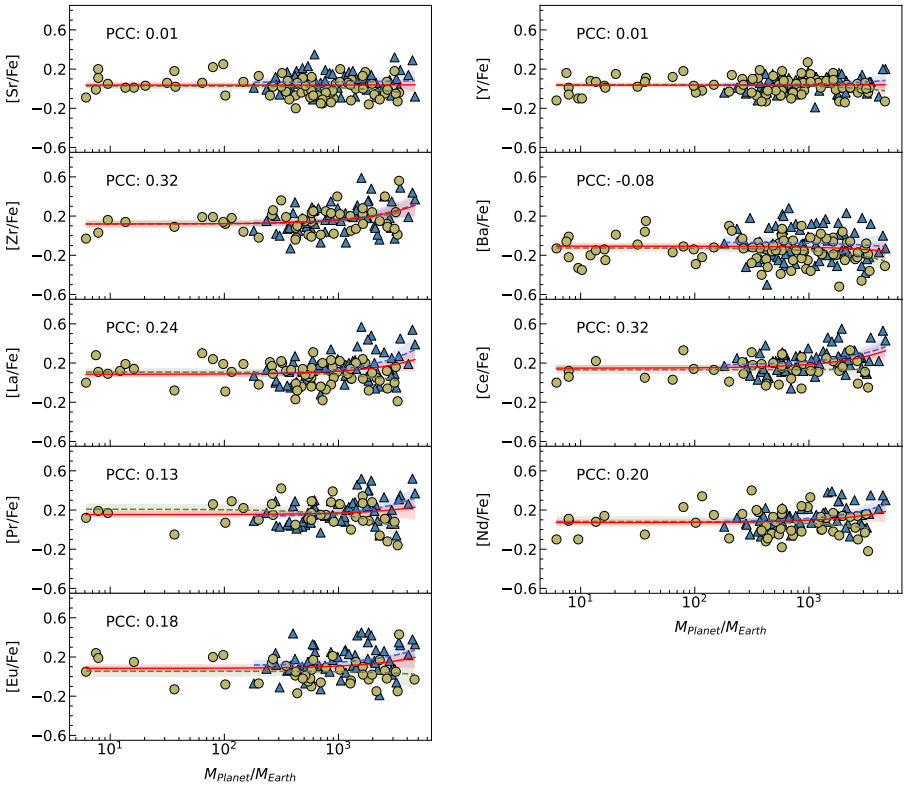

42 pav.: Neutronų pagavimo elementų santykinės gausos [El/Fe], pavaizduotos kaip funkcija nuo planetų masių žvaigždėse su viena planeta arba didžiausios masės planeta, kai sistemoje yra ne viena planeta. Visi simboliai turi tą pačią reikšmę kaip ir 36 pav. Daugiau informacijos pateikta tekste.

Žvaigždėse milžinėse Pr ir Nd gausos rodo panašias teigiamas koreliacijas kaip La ir Ce, tuo tarpu žvaigždėse nykštukėse Pr pasižymi neigiama koreliacija (PCC = $-0{,}41$), o Nd – silpna neigiama koreliacija (PCC = $-0{,}14$), taip galimai išryškindami evoliucinius skirtumus tarp nykštukių ir milžinių žvaigždžių. Europis žvaigždėse milžinėse rodo silpną teigiamą koreliaciją, o nykštukėse koreliacija tampa šiek tiek neigiama, kas atspindi platesnį rezultatų išsibarstymą, tačiau mažesnį šios priklausomybės stiprumą.

Apibendrinant atliktą analizę, matyti, kad dauguma neutronų pagavimo proceso elementų (Zr, La, Ce, Pr, Nd, Eu) gausos rodo teigiamas koreliacijas su planetų masėmis, ypač žvaigždžių milžinių atmosferose. Tai leidžia sieti praturtinimą sunkiaisiais elementais su žvaigždžių

evoliucija ir galimai planetų formavimosi procesais. Tuo tarpu Sr ir Ba pasižymi neigiama koreliacija visoje imtyje. Tai gali atspindėti skirtingus nukleosintezės kelius ir Galaktikos cheminės evoliucijos poveikį šių elementų gausoms.

8. Ateities perspektyvos

Šioje disertacijoje pateikti rezultatai prisideda prie žvaigždžių su planetomis sąsajos supratimo. Nustatytos koreliacijos tarp lengvųjų, α ir n-pagavimo elementų gausų ir žvaigždžių su planetomis parametrų išryškina naujas kryptis ateities tyrimams. Tolimesni darbai turėtų siekti tiksliau interpretuoti nustatytas priklausomybes, išplėsti tiriamų elementų spektrą ir analizuoti ryšius tarp žvaigždžių atmosferų cheminės sudėties ir planetinių sistemų formavimosi ypatybių.

Skirtumai tarp žvaigždžių su ir be atrastų planetų gali būti minimalūs, ir jų atsekimui reikėtų panaudoti pažangiausius analizės metodus. Visapusis 3D ir NLTE modeliavimas, ypač svarbus milžinėms ir nemetalingoms žvaigždėms, sumažintų sistemines paklaidas. Imties išplėtimas apimant įvairesnes Galaktikos žvaigždžių populiacijas leistų patikrinti, ar nustatytos cheminių elementų gausų pasiskirstymai yra universalūs, o gal priklauso nuo žvaigždės vietos Galaktikoje?

Ateities darbai taip pat turėtų apimti dar įvairesnį cheminių elementų rinkinį, įskaitant litį, sierą bei papildomus sunkesnius *s* ir *r*-proceso elementus. Tai padėtų tiksliau įvertinti maišymosi, praturtinimo ir galimos planetų akrecijos įtakos požymius. Išsamesnė geležies piko ir uolinių elementų analizė būtina norint nustatyti, ar Δ[El/H]–$T_{\rm cond}$ priklausomybes lemia uolinių elementų praturtinimas, ar vietiniai dulkių ir dujų santykio svyravimai žvaigždėdaros procese.

Stebėtos kai kurių sunkiųjų elementų gausų koreliacijos su planetų masėmis rodo galimą cheminių elementų gausų ryšį su planetų formavimosi efektyvumu. Šiai hipotezei patikrinti būtina integruoti vieningus egzoplanetų duomenis ir suderinti cheminę analizę su tiksliais planetų parametrais iš TESS, PLATO ir JWST misijų. Gausų apjungimas su *Gaia* kinematiniais duomenimis leistų vienu metu atsekti planetų turinčių žvaigždžių cheminės ir dinaminės raidos istorijas.

References

Abdurro'uf, Accetta, K., Aerts, C., et al. 2022, The Seventeenth Data Release of the Sloan Digital Sky Surveys: Complete Release of MaNGA, MaStar, and APOGEE-2 Data, Astrophys. J. Suppl. Ser., 259, 35

Adibekyan, V., Delgado-Mena, E., Figueira, P., et al. 2016, Abundance trend with condensation temperature for stars with different Galactic birth places, Astron. Astrophys., 592, A87

Adibekyan, V., Santos, N. C., Demangeon, O. D. S., et al. 2021, Stellar clustering and orbital architecture of planetary systems, Astron. Astrophys., 649, A111

Adibekyan, V. Z., González Hernández, J. I., Delgado Mena, E., et al. 2014, On the origin of stars with and without planets. T_c trends and clues to Galactic evolution, Astron. Astrophys., 564, L15

Adibekyan, V. Z., Santos, N. C., Sousa, S. G., et al. 2012a, Overabundance of α-elements in exoplanet-hosting stars, Astron. Astrophys., 543, A89

Adibekyan, V. Z., Sousa, S. G., Santos, N. C., et al. 2012b, Chemical abundances of 1111 FGK stars from the HARPS GTO planet search program. Galactic stellar populations and planets, Astron. Astrophys., 545, A32

Alexeeva, S., Wang, Y., Zhao, G., et al. 2023, NLTE Analysis of Y I and Y II in the Atmospheres of FGK Stars, Astrophys. J., 957, 10

Alvarez, R. & Plez, B. 1998, Near-infrared narrow-band photometry of M-giant and Mira stars: models meet observations, Astron. Astrophys., 330, 1109

Amarsi, A. M., Grevesse, N., Asplund, M., & Collet, R. 2021, The solar carbon, nitrogen, and oxygen abundances from a 3D LTE analysis of molecular lines, Astron. Astrophys., 656, A113

Amarsi, A. M., Liljegren, S., & Nissen, P. E. 2022, 3D non-LTE iron abundances in FG-type dwarfs, Astron. Astrophys., 668, A68

Asplund, M. 2005, New Light on Stellar Abundance Analyses: Departures from LTE and Homogeneity, Annu. Rev. Astron. Astrophys., 43, 481

Ayres, T. R. & Wiedemann, G. R. 1989, Non–LTE CO Revisited, Astrophys. J., 338, 1033

Bailer-Jones, C. A. L., Rybizki, J., Fouesneau, M., Demleitner, M., & Andrae, R. 2021, Estimating Distances from Parallaxes. V. Geometric and Photogeometric Distances to 1.47 Billion Stars in Gaia Early Data Release 3, Astron. J., 161, 147

Barnes, J. R., Standing, M. R., Haswell, C. A., et al. 2023, DMPP-4: candidate sub-Neptune mass planets orbiting a naked-eye star, Mon. Not. R. Astron. Soc., 524, 5196

Bashi, D. & Zucker, S. 2019, Small Planets in the Galactic Context: Host Star Kinematics, Iron, and Alpha-element Enhancement, Astron. J., 158, 61

Bensby, T., Feltzing, S., & Lundström, I. 2003, Elemental abundance trends in the Galactic thin and thick disks as traced by nearby F and G dwarf stars, Astron. Astrophys., 410, 527

Bensby, T., Feltzing, S., & Oey, M. S. 2014, Exploring the Milky Way stellar disk. A detailed elemental abundance study of 714 F and G dwarf stars in the solar neighbourhood, Astron. Astrophys., 562, A71

Bergemann, M., Hansen, C. J., Bautista, M., & Ruchti, G. 2012, NLTE analysis of Sr lines in spectra of late-type stars with new R-matrix atomic data, Astron. Astrophys., 546, A90

Bergemann, M. & Hoppe, R. 2025, 3D Non-LTE radiation transfer: theory and applications to stars, exoplanets, and kilonovae, arXiv e-prints, arXiv:2511.04254

Biazzo, K., D'Orazi, V., Desidera, S., et al. 2022, The GAPS Programme at TNG. XXXV. Fundamental properties of transiting exoplanet host stars, Astron. Astrophys., 664, A161

Bisterzo, S., Travaglio, C., Gallino, R., Wiescher, M., & Käppeler, F. 2014, Galactic Chemical Evolution and Solar s-process Abundances: Dependence on the ^{13}C-pocket Structure, Astrophys. J., 787, 10

Bitsch, B. & Battistini, C. 2020, Influence of sub- and super-solar metallicities on the composition of solid planetary building blocks, Astron. Astrophys., 633, A10

Bitsch, B. & Mah, J. 2023, Enriching inner discs and giant planets with heavy elements, Astron. Astrophys., 679, A11

Blanco-Cuaresma, S., Soubiran, C., Heiter, U., & Jofré, P. 2014, Determining stellar atmospheric parameters and chemical abundances of FGK stars with iSpec, Astron. Astrophys., 569, A111

Bond, I. A., Udalski, A., Jaroszyński, M., et al. 2004, OGLE 2003-BLG-235/MOA 2003-BLG-53: A Planetary Microlensing Event, Astrophys. J. Lett., 606, L155

Bond, J. C., Lauretta, D. S., Tinney, C. G., et al. 2008, Beyond the Iron Peak: r- and s-Process Elemental Abundances in Stars with Planets, Astrophys. J., 682, 1234

Bond, J. C., O'Brien, D. P., & Lauretta, D. S. 2010, The Compositional Diversity of Extrasolar Terrestrial Planets. I. In Situ Simulations, Astrophys. J., 715, 1050

Borucki, W. J., Koch, D., Basri, G., et al. 2010, Kepler Planet-Detection Mission: Introduction and First Results, Science, 327, 977

Boss, A. P. 1997, Giant planet formation by gravitational instability., Science, 276, 1836

Bovy, J. 2015, galpy: A python Library for Galactic Dynamics, Astrophys. J. Suppl. Ser., 216, 29

Bovy, J., Allende Prieto, C., Beers, T. C., et al. 2012, The Milky Way's Circular-velocity Curve between 4 and 14 kpc from APOGEE data, Astrophys. J., 759, 131

Bowler, B. P. 2016, Imaging Extrasolar Giant Planets, Publ. Astron. Soc. Pac., 128, 102001

Bressan, A., Marigo, P., Girardi, L., et al. 2012, PARSEC: stellar tracks and isochrones with the PAdova and TRieste Stellar Evolution Code, Mon. Not. R. Astron. Soc., 427, 127

Brewer, J. M. & Fischer, D. A. 2016, C/O and Mg/Si Ratios of Stars in the Solar Neighborhood, Astrophys. J., 831, 20

Brooke, J. S. A., Bernath, P. F., Schmidt, T. W., & Bacskay, G. B. 2013, Line strengths and updated molecular constants for the C_2 Swan system, J. Quant. Spectrosc. Radiat. Transf., 124, 11

Buchhave, L. A., Latham, D. W., Johansen, A., et al. 2012, An abundance of small exoplanets around stars with a wide range of metallicities, Nature, 486, 375

Burbidge, E. M., Burbidge, G. R., Fowler, W. A., & Hoyle, F. 1957, Synthesis of the Elements in Stars, Reviews of Modern Physics, 29, 547

Busso, M., Gallino, R., Lambert, D. L., Travaglio, C., & Smith, V. V. 2001, Nucleosynthesis and Mixing on the Asymptotic Giant Branch. III. Predicted and Observed s-Process Abundances, Astrophys. J., 557, 802

Busso, M., Gallino, R., & Wasserburg, G. J. 1999, Nucleosynthesis in Asymptotic Giant Branch Stars: Relevance for Galactic Enrichment and Solar System Formation, Annu. Rev. Astron. Astrophys., 37, 239

Butler, R. P., Marcy, G. W., Williams, E., et al. 1996, Attaining Doppler Precision of 3 M s-1, Publ. Astron. Soc. Pac., 108, 500

Chachan, Y., Knutson, H. A., Lothringer, J., & Blake, G. A. 2023, Breaking Degeneracies in Formation Histories by Measuring Refractory Content in Gas Giants, Astrophys. J., 943, 112

Charbonneau, D., Brown, T. M., Latham, D. W., & Mayor, M. 2000, Detection of Planetary Transits Across a Sun-like Star, Astrophys. J. Lett., 529, L45

Côté, B., Fryer, C. L., Belczynski, K., et al. 2018, The Origin of r-process Elements in the Milky Way, Astrophys. J., 855, 99

Cowan, J. J., Sneden, C., Lawler, J. E., et al. 2021, Origin of the heaviest elements: The rapid neutron-capture process, Reviews of Modern Physics, 93, 015002

Cseh, B., Világos, B., Roriz, M. P., et al. 2022, Barium stars as tracers of s-process nucleosynthesis in AGB stars. I. 28 stars with independently derived AGB mass, Astron. Astrophys., 660, A128

Cutri, R. M., Wright, E. L., Conrow, T., et al. 2021, VizieR Online Data Catalog: AllWISE Data Release (Cutri+ 2013), VizieR On-line Data Catalog: II/328. Originally published in: IPAC/Caltech (2013)

da Silva, R., Danielski, C., Delgado Mena, E., et al. 2024, Ariel stellar characterisation. II. Chemical abundances of carbon, nitrogen, and oxygen for 181 planet-host FGK dwarf stars, Astron. Astrophys., 688, A193

da Silva, R., Milone, A. d. C., & Rocha-Pinto, H. J. 2015, Homogeneous abundance analysis of FGK dwarf, subgiant, and giant stars with and without giant planets, Astron. Astrophys., 580, A24

Davidson, M. D., Snoek, L. C., Volten, H., & Doenszelmann, A. 1992, Oscillator strengths and branching ratios of transitions between low-lying levels in the barium II spectrum, Astron. Astrophys., 255, 457

de Zeeuw, T., Tamai, R., & Liske, J. 2014, Constructing the E-ELT, The Messenger, 158, 3

Dekker, H., D'Odorico, S., Kaufer, A., Delabre, B., & Kotzlowski, H. 2000, in Society of Photo-Optical Instrumentation Engineers (SPIE) Conference Series, Vol. 4008, Optical and IR Telescope Instrumentation and Detectors, ed. M. Iye & A. F. Moorwood, 534–545

Delgado Mena, E., Adibekyan, V., Santos, N. C., et al. 2021, Chemical abundances of 1111 FGK stars from the HARPS GTO planet search program. IV. Carbon and C/O ratios for Galactic stellar populations and planet hosts, Astron. Astrophys., 655, A99

Delgado Mena, E., Adibekyan, V. Z., Figueira, P., et al. 2018, Chemical Abundances of Neutron-capture Elements in Exoplanet-hosting Stars, Publ. Astron. Soc. Pac., 130, 094202

Delgado Mena, E., Israelian, G., González Hernández, J. I., et al. 2010, Chemical Clues on the Formation of Planetary Systems: C/O Versus Mg/Si for HARPS GTO Sample, Astrophys. J., 725, 2349

Den Hartog, E. A., Lawler, J. E., Sneden, C., & Cowan, J. J. 2003, Improved Laboratory Transition Probabilities for Nd II and Application to the Neodymium Abundances of the Sun and Three Metal-poor Stars, Astrophys. J. Suppl. Ser., 148, 543

Dodson-Robinson, S. E., Bodenheimer, P., Laughlin, G., et al. 2008, Saturn Forms by Core Accretion in 3.4 Myr, Astrophys. J. Lett., 688, L99

Dorn, C., Harrison, J. H. D., Bonsor, A., & Hands, T. O. 2019, A new class of Super-Earths formed from high-temperature condensates: HD219134 b, 55 Cnc e, WASP-47 e, Mon. Not. R. Astron. Soc., 484, 712

Durisen, R. H., Boss, A. P., Mayer, L., et al. 2007, in Protostars and Planets V, ed. B. Reipurth, D. Jewitt, & K. Keil, 607

Ecuvillon, A., Israelian, G., Santos, N. C., et al. 2004a, Nitrogen abundances in planet-harbouring stars, Astron. Astrophys., 418, 703

Ecuvillon, A., Israelian, G., Santos, N. C., et al. 2004b, C, S, Zn and Cu abundances in planet-harbouring stars, Astron. Astrophys., 426, 619

Ecuvillon, A., Israelian, G., Santos, N. C., et al. 2006, Oxygen abundances in planet-harbouring stars. Comparison of different abundance indicators, Astron. Astrophys., 445, 633

Eitner, P., Bergemann, M., & Larsen, S. 2019, NLTE modelling of integrated light spectra. Abundances of barium, magnesium, and manganese in a metal-poor globular cluster, Astron. Astrophys., 627, A40

Feltzing, S., Howes, L. M., McMillan, P. J., & Stonkutė, E. 2017, On the metallicity dependence of the [Y/Mg]-age relation for solar-type stars, Mon. Not. R. Astron. Soc., 465, L109

Feng, F., Butler, R. P., Vogt, S. S., et al. 2022, 3D Selection of 167 Substellar Companions to Nearby Stars, Astrophys. J. Suppl. Ser., 262, 21

Fischer, D. A., Howard, A. W., Laughlin, G. P., et al. 2014, in Protostars and Planets VI, ed. H. Beuther, R. S. Klessen, C. P. Dullemond, & T. Henning, 715–737

Fischer, D. A. & Valenti, J. 2005, The Planet-Metallicity Correlation, Astrophys. J., 622, 1102

Gaia Collaboration, Brown, A. G. A., Vallenari, A., et al. 2021, Gaia Early Data Release 3. Summary of the contents and survey properties, Astron. Astrophys., 649, A1

Gaia Collaboration, Prusti, T., de Bruijne, J. H. J., et al. 2016, The Gaia mission, Astron. Astrophys., 595, A1

Gammie, C. F. 2001, Nonlinear Outcome of Gravitational Instability in Cooling, Gaseous Disks, Astrophys. J., 553, 174

Gaudi, B. S. 2012, Microlensing Surveys for Exoplanets, Annu. Rev. Astron. Astrophys., 50, 411

Gerber, J. M., Magg, E., Plez, B., et al. 2023, Non-LTE radiative transfer with Turbospectrum, Astron. Astrophys., 669, A43

Ghezzi, L., Cunha, K., Smith, V. V., et al. 2010, Stellar Parameters and Metallicities of Stars Hosting Jovian and Neptunian Mass Planets: A Possible Dependence of Planetary Mass on Metallicity, Astrophys. J., 720, 1290

Gilmore, G. & Wyse, R. F. G. 1985, The abundance distribution in the inner spheroid., Astron. J., 90, 2015

Gonzalez, G. 1997, The stellar metallicity-giant planet connection, Mon. Not. R. Astron. Soc., 285, 403

Gonzalez, G. 2009, Stars with planets and the thick disc, Mon. Not. R. Astron. Soc., 399, L103

González Hernández, J. I., Delgado-Mena, E., Sousa, S. G., et al. 2013, Searching for the signatures of terrestrial planets in F-, G-type main-sequence stars, Astron. Astrophys., 552, A6

Gray, D. F. 2005, The Observation and Analysis of Stellar Photospheres (Cambridge University Press)

Grevesse, N., Asplund, M., & Sauval, A. J. 2007, The Solar Chemical Composition, Space Sci. Rev., 130, 105

Guo, Y., Storm, N., Bergemann, M., et al. 2025, Non-local thermodynamic equilibrium (NLTE) abundances of europium (Eu) for a sample of metal-poor stars in the galactic halo and metal-poor disk with 1D and <3D> models, Astron. Astrophys., 693, A211

Gustafsson, B., Edvardsson, B., Eriksson, K., et al. 2008, A grid of MARCS model atmospheres for late-type stars. I. Methods and general properties, Astron. Astrophys., 486, 951

Haywood, M. 2008, A peculiarity of metal-poor stars with planets?, Astron. Astrophys., 482, 673

Heiter, U., Lind, K., Bergemann, M., et al. 2021, Atomic data for the Gaia-ESO Survey, Astron. Astrophys., 645, A106

Henry, G. W., Marcy, G. W., Butler, R. P., & Vogt, S. S. 2000, A Transiting "51 Peg-like" Planet, Astrophys. J. Lett., 529, L41

Hrudková, M., Hatzes, A., Karjalainen, R., et al. 2017, The discovery of a planetary candidate around the evolved low-mass Kepler giant star HD 175370, Mon. Not. R. Astron. Soc., 464, 1018

Husser, T. O., Wende-von Berg, S., Dreizler, S., et al. 2013, A new extensive library of PHOENIX stellar atmospheres and synthetic spectra, Astron. Astrophys., 553, A6

Jeong, G., Han, I., Park, M.-G., et al. 2018, A Search for Exoplanets around Northern Circumpolar Stars. IV. Six Planet Candidates to the K Giants, HD 44385, HD 97619, HD 106574, HD 118904, HD 164428, and HD 202432, Astron. J., 156, 64

Jeong, G., Lee, B. C., Park, M. G., Bang, T. Y., & Han, I. 2022, Search for exoplanets around northern circumpolar stars. V. Three likely planetary companions to the giant stars HD 19615, HD 150010, and HD 174205, Astron. Astrophys., 662, A12

Johansson, S., Litzén, U., Lundberg, H., & Zhang, Z. 2003, Experimental f-Value and Isotopic Structure for the Ni I Line Blended with [O I] at 6300 Å, Astrophys. J. Lett., 584, L107

Johnson, J. A., Aller, K. M., Howard, A. W., & Crepp, J. R. 2010, Giant Planet Occurrence in the Stellar Mass-Metallicity Plane, Publ. Astron. Soc. Pac., 122, 905

Joshi, Y. C. 2007, Displacement of the Sun from the Galactic plane, Mon. Not. R. Astron. Soc., 378, 768

Jurgenson, C., Fischer, D., McCracken, T., et al. 2016, Design and Construction of VUES: The Vilnius University Echelle Spectrograph, Journal of Astronomical Instrumentation, 5, 1650003

Karakas, A. I. & Lattanzio, J. C. 2014, The Dawes Review 2: Nucleosynthesis and Stellar Yields of Low- and Intermediate-Mass Single Stars, Publ. Astron. Soc. Aust., 31, e030

Kobayashi, C., Karakas, A. I., & Lugaro, M. 2020, The Origin of Elements from Carbon to Uranium, Astrophys. J., 900, 179

Kokubo, E. & Ida, S. 1998, Oligarchic Growth of Protoplanets, Icarus, 131, 171

Korotin, S. A., Andrievsky, S. M., Hansen, C. J., et al. 2015, Grid of theoretical NLTE equivalent widths of four Ba ii lines and barium abundance in cool stars, Astron. Astrophys., 581, A70

Kramida, A., Ralchenko, Y., Reader, J., & Team, N. A. 2023, NIST Atomic Spectra Database (version 5.9), https://physics.nist.gov/asd

Kurucz, R. 1993, ATLAS9 Stellar Atmosphere Programs and 2 km/s grid., Robert Kurucz CD-ROM, 13

Kurucz, R. L. 2005, New atlases for solar flux, irradiance, central intensity, and limb intensity, Memorie della Societa Astronomica Italiana Supplementi, 8, 189

Lagarde, N., Reylé, C., Robin, A. C., et al. 2019, The Gaia-ESO Survey: impact of extra mixing on C and N abundances of giant stars, Astron. Astrophys., 621, A24

Lambrechts, M. & Johansen, A. 2012, Rapid growth of gas-giant cores by pebble accretion, Astron. Astrophys., 544, A32

Lawler, J. E., Bonvallet, G., & Sneden, C. 2001a, Experimental Radiative Lifetimes, Branching Fractions, and Oscillator Strengths for La II and a New Determination of the Solar Lanthanum Abundance, Astrophys. J., 556, 452

Lawler, J. E., Wickliffe, M. E., den Hartog, E. A., & Sneden, C. 2001b, Improved Laboratory Transition Parameters forEu II and Application to the Solar Europium Elemental and Isotopic Composition, Astrophys. J., 563, 1075

Lind, K. & Amarsi, A. M. 2024, Three-Dimensional Nonlocal Thermodynamic Equilibrium Abundance Analyses of Late-Type Stars, Annu. Rev. Astron. Astrophys., 62, 475

Lind, K., Bergemann, M., & Asplund, M. 2012, Non-LTE line formation of Fe in late-type stars - II. 1D spectroscopic stellar parameters, Mon. Not. R. Astron. Soc., 427, 50

Lindegren, L., Klioner, S. A., Hernández, J., et al. 2021, Gaia Early Data Release 3. The astrometric solution, Astron. Astrophys., 649, A2

Liu, F., Yong, D., Asplund, M., et al. 2020, Detailed chemical compositions of planet-hosting stars - I. Exploration of possible planet signatures, Mon. Not. R. Astron. Soc., 495, 3961

Lodders, K. 2003, Solar System Abundances and Condensation Temperatures of the Elements, Astrophys. J., 591, 1220

Mack, III, C. E., Schuler, S. C., Stassun, K. G., & Norris, J. 2014, Detailed Abundances of Planet-hosting Wide Binaries. I. Did Planet Formation Imprint Chemical Signatures in the Atmospheres of HD 20782/81?, Astrophys. J., 787, 98

Madhusudhan, N., Lee, K. K. M., & Mousis, O. 2012, A Possible Carbon-rich Interior in Super-Earth 55 Cancri e, Astrophys. J. Lett., 759, L40

Mah, J. & Bitsch, B. 2023, Forming super-Mercuries: Role of stellar abundances, Astron. Astrophys., 673, A17

Marois, C., Macintosh, B., Barman, T., et al. 2008, Direct Imaging of Multiple Planets Orbiting the Star HR 8799, Science, 322, 1348

Mashonkina, L. & Gehren, T. 2000, Barium and europium abundances in cool dwarf stars and nucleosynthesis of heavy elements, Astron. Astrophys., 364, 249

Mashonkina, L., Gehren, T., Shi, J. R., Korn, A. J., & Grupp, F. 2011, A non-LTE study of neutral and singly-ionized iron line spectra in 1D models of the Sun and selected late-type stars, Astron. Astrophys., 528, A87

Mashonkina, L., Ryabchikova, T., & Ryabtsev, A. 2005, NLTE ionization equilibrium of Nd II and Nd III in cool A and Ap stars, Astron. Astrophys., 441, 309

Matteucci, F. 2021, Modelling the chemical evolution of the Milky Way, Astron. Astrophys. Rev., 29, 5

Mayor, M., Pepe, F., Queloz, D., et al. 2003, Setting New Standards with HARPS, The Messenger, 114, 20

Mayor, M. & Queloz, D. 1995, A Jupiter-mass companion to a solar-type star, Nature, 378, 355

McWilliam, A. 1998, Barium Abundances in Extremely Metal-poor Stars, Astron. J., 115, 1640

Meggers, W. F., Corliss, C. H., & Scribner, B. F. 1975, Tables of spectral-line intensities. Part I, II_- arranged by elements.

Meléndez, J., Asplund, M., Gustafsson, B., & Yong, D. 2009, The Peculiar Solar Composition and Its Possible Relation to Planet Formation, Astrophys. J. Lett., 704, L66

Mihalas, D. 1978, Stellar atmospheres (W.H. Freeman and Company)

Mikolaitis, Š., Drazdauskas, A., Minkevičiūtė, R., et al. 2019, High-resolution spectroscopic study of dwarf stars in the northern sky. Na to Zn abundances in two fields with radii of 20 degrees, Astron. Astrophys., 628, A49

Mikolaitis, Š., Tautvaišienė, G., Drazdauskas, A., et al. 2018, Spectroscopy of Dwarf Stars Around the North Celestial Pole, Publ. Astron. Soc. Pac., 130, 074202

Miles, B. M. & Wiese, W. L. 1969, Critical Evaluation of Transition Probabilities for Ba I and Ba II, Atomic Data, 1, 1

Mints, A. & Hekker, S. 2017, A Unified tool to estimate Distances, Ages, and Masses (UniDAM) from spectrophotometric data, Astron. Astrophys., 604, A108

Mints, A. & Hekker, S. 2018, Isochrone fitting in the Gaia era, Astron. Astrophys., 618, A54

Mishenina, T., Basak, N., Adibekyan, V., Soubiran, C., & Kovtyukh, V. 2021, Chemical composition of stars with massive planets, Mon. Not. R. Astron. Soc., 504, 4252

Mishenina, T., Kovtyukh, V., Soubiran, C., & Adibekyan, V. Z. 2016, Behaviour of elements from lithium to europium in stars with and without planets, Mon. Not. R. Astron. Soc., 462, 1563

Mordasini, C., Alibert, Y., & Benz, W. 2009, Extrasolar planet population synthesis. I. Method, formation tracks, and mass-distance distribution, Astron. Astrophys., 501, 1139

Nayakshin, S. 2017, Dawes Review 7: The Tidal Downsizing Hypothesis of Planet Formation, Publ. Astron. Soc. Aust., 34, e002

Nissen, P. E. 2015, High-precision abundances of elements in solar twin stars. Trends with stellar age and elemental condensation temperature, Astron. Astrophys., 579, A52

Nissen, P. E., Chen, Y. Q., Carigi, L., Schuster, W. J., & Zhao, G. 2014, Carbon and oxygen abundances in stellar populations, Astron. Astrophys., 568, A25

Öberg, K. I., Murray-Clay, R., & Bergin, E. A. 2011, The Effects of Snowlines on C/O in Planetary Atmospheres, Astrophys. J. Lett., 743, L16

Ohno, K. & Fortney, J. J. 2023, Nitrogen as a Tracer of Giant Planet Formation. I. A Universal Deep Adiabatic Profile and Semianalytical Predictions of Disequilibrium Ammonia Abundances in Warm Exoplanetary Atmospheres, Astrophys. J., 946, 18

Ormel, C. W. & Klahr, H. H. 2010, The effect of gas drag on the growth of protoplanets. Analytical expressions for the accretion of small bodies in laminar disks, Astron. Astrophys., 520, A43

Pepe, F., Cristiani, S., Rebolo, R., et al. 2021, ESPRESSO at VLT. On-sky performance and first results, Astron. Astrophys., 645, A96

Pepe, F., Mayor, M., Delabre, B., et al. 2000, in Society of Photo-Optical Instrumentation Engineers (SPIE) Conference Series, Vol. 4008, Optical and IR Telescope Instrumentation and Detectors, ed. M. Iye & A. F. Moorwood, 582–592

Pepe, F., Molaro, P., Cristiani, S., et al. 2014, ESPRESSO: The next European exoplanet hunter, Astronomische Nachrichten, 335, 8

Perryman, M., Hartman, J., Bakos, G. Á., & Lindegren, L. 2014, Astrometric Exoplanet Detection with Gaia, Astrophys. J., 797, 14

Pian, E., D'Avanzo, P., Benetti, S., et al. 2017, Spectroscopic identification of r-process nucleosynthesis in a double neutron-star merger, Nature, 551, 67

Piskunov, N. E., Kupka, F., Ryabchikova, T. A., Weiss, W. W., & Jeffery, C. S. 1995, VALD: The Vienna Atomic Line Data Base., Astron. Astrophys. Suppl., 112, 525

Pollack, J. B., Hubickyj, O., Bodenheimer, P., et al. 1996, Formation of the Giant Planets by Concurrent Accretion of Solids and Gas, Icarus, 124, 62

Prantzos, N., Abia, C., Cristallo, S., Limongi, M., & Chieffi, A. 2020, Chemical evolution with rotating massive star yields II. A new assessment of the solar s- and r-process components, Mon. Not. R. Astron. Soc., 491, 1832

Rafikov, R. R. 2005, Can Giant Planets Form by Direct Gravitational Instability?, Astrophys. J. Lett., 621, L69

Ram, R. S., Brooke, J. S. A., Bernath, P. F., Sneden, C., & Lucatello, S. 2014, Improved Line Data for the Swan System $^{12}C^{13}C$ Isotopologue, Astrophys. J. Suppl. Ser., 211, 5

Ramírez, I., Asplund, M., Baumann, P., Meléndez, J., & Bensby, T. 2010, A possible signature of terrestrial planet formation in the chemical composition of solar analogs, Astron. Astrophys., 521, A33

Rauer, H., Aerts, C., Cabrera, J., et al. 2024, The PLATO Mission, arXiv e-prints, arXiv:2406.05447

Reddy, A. B. S. & Lambert, D. L. 2017, Solar Twins and the Barium Puzzle, Astrophys. J., 845, 151

Ricker, G. R., Winn, J. N., Vanderspek, R., et al. 2015, Transiting Exoplanet Survey Satellite (TESS), Journal of Astronomical Telescopes, Instruments, and Systems, 1, 014003

Rinehart, S., Clampin, M., Ricker, G. R., et al. 2015, in AAS/Division for Extreme Solar Systems Abstracts, Vol. 47, AAS/Division for Extreme Solar Systems Abstracts, 106.06

Rosenthal, L. J., Fulton, B. J., Hirsch, L. A., et al. 2021, The California Legacy Survey. I. A Catalog of 178 Planets from Precision Radial Velocity Monitoring of 719 Nearby Stars over Three Decades, Astrophys. J. Suppl. Ser., 255, 8

Ryabchikova, T., Piskunov, N., Kurucz, R. L., et al. 2015, A major upgrade of the VALD database, , 90, 054005

Ryabchikova, T., Piskunov, N., & Pakhomov, Y. 2022, Using Molecular Lines to Determine Carbon and Nitrogen Abundances in the Atmospheres of Cool Stars, Atoms, 10, 103

Sahu, S., Gänsicke, B. T., Williams, J. T., et al. 2025, Discovery of an icy and nitrogen-rich extrasolar planetesimal, Mon. Not. R. Astron. Soc., 543, 223

Santos, N. C., Adibekyan, V., Mordasini, C., et al. 2015, Constraining planet structure from stellar chemistry: the cases of CoRoT-7, Kepler-10, and Kepler-93, Astron. Astrophys., 580, L13

Santos, N. C., Israelian, G., & Mayor, M. 2001, The metal-rich nature of stars with planets, Astron. Astrophys., 373, 1019

Schneider, A. D. & Bitsch, B. 2021, How drifting and evaporating pebbles shape giant planets. I. Heavy element content and atmospheric C/O, Astron. Astrophys., 654, A71

Schönrich, R., Binney, J., & Dehnen, W. 2010, Local kinematics and the local standard of rest, Mon. Not. R. Astron. Soc., 403, 1829

Seabroke, G. M., Fabricius, C., Teyssier, D., et al. 2021, Gaia Early Data Release 3. Updated radial velocities from Gaia DR2, Astron. Astrophys., 653, A160

Shaltout, A. M. K., Abdelkawy, A. G. A., & Beheary, M. M. 2020, Non-local thermodynamical equilibrium abundance analysis of singly ionized praseodymium for the Sun, Mon. Not. R. Astron. Soc., 496, 5361

Sharma, A., Stonkutė, E., Drazdauska, A., et al. 2024, Chemical composition of planetary hosts: C, N, and α-element abundances, Astron. Astrophys., 691, A160

Sharma, A., Stonkutė, E., Drazdauskas, A., et al. 2025, Chemical composition of planetary hosts: II. Abundances of neutron-capture elements, Astron. Astrophys., 701, A153

Shejeelammal, J., Meléndez, J., Rathsam, A., & Martos, G. 2024, The [Y/Mg] chemical clock in the Galactic disk: The influence of metallicity and the Galactic population in the solar neighbourhood, Astron. Astrophys., 690, A107

Skrutskie, M. F., Cutri, R. M., Stiening, R., et al. 2006, The Two Micron All Sky Survey (2MASS), Astron. J., 131, 1163

Slumstrup, D., Grundahl, F., Brogaard, K., et al. 2017, The [Y/Mg] clock works for evolved solar metallicity stars, Astron. Astrophys., 604, L8

Smiljanic, R., Korn, A. J., Bergemann, M., et al. 2014, The Gaia-ESO Survey: The analysis of high-resolution UVES spectra of FGK-type stars, Astron. Astrophys., 570, A122

Sneden, C. 1973, The nitrogen abundance of the very metal-poor star HD 122563., Astrophys. J., 184, 839

Sneden, C., Cowan, J. J., Lawler, J. E., et al. 2002, Europium Isotopic Abundances in Very Metal Poor Stars, Astrophys. J. Lett., 566, L25

Sneden, C., Lawler, J. E., Cowan, J. J., Ivans, I. I., & Den Hartog, E. A. 2009, New Rare Earth Element Abundance Distributions for the Sun and Five r-Process-Rich Very Metal-Poor Stars, Astrophys. J. Suppl. Ser., 182, 80

Sneden, C., Lucatello, S., Ram, R. S., Brooke, J. S. A., & Bernath, P. 2014, Line Lists for the A $^2\Pi$-X $^2\Sigma^+$ (Red) and B $^2\Sigma^+$-X $^2\Sigma^+$ (Violet) Systems of CN, $^{13}C^{14}N$, and $^{12}C^{15}N$, and Application to Astronomical Spectra, Astrophys. J. Suppl. Ser., 214, 26

Soliman, N. H. & Hopkins, P. F. 2025, Are Stars Really Ingesting Their Planets? Examining an Alternative Explanation, Astrophys. J., 979, 98

Sousa, S. G., Santos, N. C., Israelian, G., Mayor, M., & Udry, S. 2011, Spectroscopic stellar parameters for 582 FGK stars in the HARPS volume-limited sample. Revising the metallicity-planet correlation, Astron. Astrophys., 533, A141

Stetson, P. B. & Pancino, E. 2008, DAOSPEC: An Automatic Code for Measuring Equivalent Widths in High-Resolution Stellar Spectra, Publ. Astron. Soc. Pac., 120, 1332

Stonkutė, E., Chorniy, Y., Tautvaišienė, G., et al. 2020, High-resolution Spectroscopic Study of Dwarf Stars in the Northern Sky: Lithium, Carbon, and Oxygen Abundances, Astron. J., 159, 90

Storm, N., Barklem, P. S., Yakovleva, S. A., et al. 2024, 3D NLTE modelling of Y and Eu. Centre-to-limb variation and solar abundances, Astron. Astrophys., 683, A200

Suárez-Andrés, L., Israelian, G., González Hernández, J. I., et al. 2016, CNO behaviour in planet-harbouring stars. I. Nitrogen abundances in stars with planets, Astron. Astrophys., 591, A69

Suárez-Andrés, L., Israelian, G., González Hernández, J. I., et al. 2017, CNO behaviour in planet-harbouring stars. II. Carbon abundances in stars with and without planets using the CH band, Astron. Astrophys., 599, A96

Suárez-Andrés, L., Israelian, G., González Hernández, J. I., et al. 2018, C/O vs. Mg/Si ratios in solar type stars: The HARPS sample, Astron. Astrophys., 614, A84

Swastik, C., Banyal, R. K., Narang, M., et al. 2022, Galactic Chemical Evolution of Exoplanet Hosting Stars: Are High-mass Planetary Systems Young?, Astron. J., 164, 60

Swastik, C., Banyal, R. K., Narang, M., Unni, A., & Sivarani, T. 2024, Age Analysis of Extrasolar Planets: Insight from Stellar Isochrone Models, Astron. J., 167, 270

Tautvaišienė, G., Mikolaitis, Š., Drazdauskas, A., et al. 2022, Chemical Composition of Bright Stars in the Northern Hemisphere: Star-Planet Connection, Astrophys. J. Suppl. Ser., 259, 45

Tautvaišienė, G., Viscasillas Vázquez, C., Mikolaitis, Š., et al. 2021, Abundances of neutron-capture elements in thin- and thick-disc stars in the solar neighbourhood, Astron. Astrophys., 649, A126

Teng, H.-Y., Sato, B., Takarada, T., et al. 2022, Regular radial velocity variations in nine G- and K-type giant stars: Eight planets and one planet candidate, Publ. Astron. Soc. Jpn, 74, 92

Thiabaud, A., Marboeuf, U., Alibert, Y., Leya, I., & Mezger, K. 2015, Elemental ratios in stars vs planets, Astron. Astrophys., 580, A30

Tinetti, G., Eccleston, P., Lueftinger, T., et al. 2022, in European Planetary Science Congress, EPSC2022–1114

Travaglio, C., Galli, D., Gallino, R., et al. 1999, Galactic Chemical Evolution of Heavy Elements: From Barium to Europium, Astrophys. J., 521, 691

Udry, S. & Santos, N. C. 2007, Statistical Properties of Exoplanets, Annu. Rev. Astron. Astrophys., 45, 397

Unni, A., Narang, M., Sivarani, T., et al. 2022, Carbon Abundance of Stars in the LAMOST-Kepler Field, Astron. J., 164, 181

Unterborn, C. T. & Panero, W. R. 2019, The Pressure and Temperature Limits of Likely Rocky Exoplanets, Journal of Geophysical Research (Planets), 124, 1704

Valenti, J. A. & Piskunov, N. 1996, Spectroscopy made easy: A new tool for fitting observations with synthetic spectra., Astron. Astrophys. Suppl., 118, 595

van Leeuwen, F. 2007, Validation of the new Hipparcos reduction, Astron. Astrophys., 474, 653

Vogt, S. S., Allen, S. L., Bigelow, B. C., et al. 1994, in Society of Photo-Optical Instrumentation Engineers (SPIE) Conference Series, Vol. 2198, Instrumentation in Astronomy VIII, ed. D. L. Crawford & E. R. Craine, 362

Šubjak, J., Lodieu, N., Kabáth, P., et al. 2023, Search for planets around stars with wide brown dwarfs, Astron. Astrophys., 671, A10

Winn, J. N. & Fabrycky, D. C. 2015, The Occurrence and Architecture of Exoplanetary Systems, Annu. Rev. Astron. Astrophys., 53, 409

Wolszczan, A. & Frail, D. A. 1992, A planetary system around the millisecond pulsar PSR1257 + 12, Nature, 355, 145

Xiao, G.-Y., Teng, H.-Y., Zhou, J., et al. 2024, Two Long-period Giant Planets around Two Giant Stars: HD 112570 and HD 154391, Astron. J., 167, 59

Yun, S., Lee, Y. S., Kim, Y. K., et al. 2024, Connections between Planetary Populations and Chemical Characteristics of Their Host Stars, Astrophys. J., 971, 35

A Appendix

Table A1: Contents of the machine-readable table available online at CDS.

Col	Label	Units	Explanations
1	Host TYC ID	—	Tycho-2 catalogue identification
2	Teff	K	Effective temperature
3	e_Teff	K	Error in effective temperature
4	Logg	[cm/s^2]	Stellar surface gravity
5	e_Logg	[cm/s^2]	Error in stellar surface gravity
6	[Fe/H]	dex	Metallicity
7	e_[Fe/H]	dex	Error in metallicity
8	Vt	km/s	Microturbulence velocity
9	e_Vt	km/s	Uncertainty in microturbulence velocity
10	Vrad	km/s	Radial velocity
11	e_Vrad	km/s	Uncertainty in radial velocity
12	Age	Gyr	Stellar age
13	e_Age	Gyr	Uncertainty in stellar age
14	U	km/s	Heliocentric space velocity U
15	e_U	km/s	Uncertainty in heliocentric space velocity U
16	V	km/s	Heliocentric space velocity V
17	e_V	km/s	Uncertainty in Heliocentric space velocity V
18	W	km/s	Heliocentric space velocity W
19	e_W	km/s	Uncertainty in Heliocentric space velocity W
20	d	kpc	Stellar distance
21	R_{mean}	kpc	Mean Galactocentric distance
22	e_R_{mean}	kpc	Uncertainty in mean Galactrocentric distance
23	z_{max}	kpc	Maximum distance from Galactic plane
24	e_z_{max}	kpc	Uncertainty in maximum distance from Galactic plane
25	e	—	Orbital eccentricity
26	e_e	—	Uncertainty in orbital eccentricity
27	[C/H]	dex	Carbon abundance
28	e_[C/H]	dex	Uncertainty in carbon abundance
29	[N/H]	dex	Nitrogen abundance
30	e_[N/H]	dex	Uncertainty in nitrogen abundance
31	[O/H]	dex	Oxygen abundance
32	e_[O/H]	dex	Uncertainty in oxygen abundance
33	[Mg/H]	dex	Magnesium abundance
34	e_[Mg/H]	dex	Uncertainty in magnesium abundance

35	[Si/H]	dex	Silicon abundance
36	e_[Si/H]	dex	Uncertainty in silicon abundance
37	C/O	dex	Carbon to Oxygen abundance ratio
38	N/O	dex	Nitrogen to Oxygen abundance ratio
39	Mg/Si	dex	Magnesium to Silicon abundance ratio
40	TD/D	—	Thick disk-to-thin disk probability ratio
41	Thin | Thick	—	Chemical attribution to the Galactic subcomponent

Table A2: Contents of the machine-readable table available at the CDS.

Col	Label	Units	Explanations
1	Host TYC ID	—	Tycho-2 catalogue identification
2	Teff	K	Effective temperature
3	e_Teff	K	Uncertainty in effective temperature
4	Logg	[cm/s^2]	Stellar surface gravity
5	e_Logg	[cm/s^2]	Uncertainty in stellar surface gravity
6	[Fe/H]	dex	Metallicity
7	e_[Fe/H]	dex	Uncertainty in metallicity
8	Vt	km s^{-1}	Microturbulence velocity
9	e_Vt	km s^{-1}	Uncertainty in microturbulence velocity
10	$[\mathrm{Sr/H}]_{NLTE}$	dex	Strontium abundance
11	e_[Sr/H]	dex	Uncertainty in strontium abundance
12	$[\mathrm{Y/H}]_{NLTE}$	dex	Yttrium abundance
13	e_[Y/H]	dex	Uncertainty in yttrium abundance
14	[Zr I/H]	dex	Zirconium abundance
15	e_[Zr I/H]	dex	Uncertainty in zirconium abundance
16	[Zr II/H]	dex	Zirconium abundance
17	e_[Zr II/H]	dex	Uncertainty in zirconium abundance
18	$[\mathrm{Ba/H}]_{NLTE}$	dex	Barium abundance
19	e_[Ba/H]	dex	Uncertainty in barium abundance
20	[La/H]	dex	Lanthanum abundance
21	e_[La/H]	dex	Uncertainty in lanthanum abundance
22	[Ce/H]	dex	Cerium abundance
23	e_[Ce/H]	dex	Uncertainty in cerium abundance
24	[Pr/H]	dex	Praseodymium abundance
25	e_[Pr/H]	dex	Uncertainty in praseodymium abundance
26	[Nd/H]	dex	Neodymium abundance
27	e_[Nd/H]	dex	Uncertainty in neodymium abundance
28	$[\mathrm{Eu/H}]_{NLTE}$	dex	Europium abundance
29	e_[Eu/H]	dex	Uncertainty in europium abundance

Note: Symbols I and II denote the neutral and ionised state of elements, respectively.

Curriculum Vitae

Name: Ashutosh
Surname: Sharma

Ashutosh Sharma is an early-career astrophysicist specialising in stellar spectral analysis. His research interests include the determination of stellar atmospheric parameters, precise chemical abundance analysis, and the investigation of the star-planet connection in the context of exoplanet formation and evolution.

Employment Details:

- **Junior Researcher** (Nov 2024–)
  Vilnius University, Lithuania

  Current Field of Research:
  - Chemical composition of planet-host stars
  - High-resolution spectroscopy
  - Stellar spectral analysis

Education:

- **Ph.D. in Physics (Astrophysics)** (2020–2025)
  Vilnius University, Lithuania
- **M.Sc. in Electronics Engineering** (2018–2020)
  Vilnius Gediminas Technical University, Lithuania
- **M.Sc. in Physics (Electronics)** (2014–2016)
  Chaudhary Charan Singh University, India
- **B.Sc. (Hons.) Physics** (2011–2014)
  University of Delhi, India

Vilnius University Press
9 Saulėtekio Ave., Building III, LT-10222 Vilnius
Email: info@leidykla.vu.lt, www.leidykla.vu.lt
bookshop.vu.lt, journals.vu.lt
Print run 15